# Geology of the Western Part of the Date Creek Mountains, Yavapai County, Arizona

by

David Eddy

A Thesis Presented in Partial Fulfillment
of the Requirements for the Degree
Master of Science

Approved April 2012 by the
Graduate Supervisory Committee:

Stephen Reynolds, Chair
Steven Semken
Ramon Arrowsmith

ARIZONA STATE UNIVERSITY

May 2012

ABSTRACT

New quadrangle-scale geologic mapping of the western part of the Date Creek Mountains (DCM) in west-central Arizona has revealed new insights into the geologic units, structures, and geologic history. Three U-Pb dates also provide surprising new information about the age and spatial relationships of the DCM as well as implications for the tectonics of the area.

Paleoproterozoic metamorphic rocks in the central part of the DCM are presumably correlative with the Yavapai schist exposed in other parts of the Arizona Transition Zone. A granite formerly assigned to the Paleoproterozoic was subdivided into megacrystic and fine-grained units and hosts a set of previously undescribed subvertical felsic dikes. A new U-Pb date of the fine-grained phase has shown that unit to be Jurassic.

The Mesoproterozoic Granite of Joshua Tree Parkway (Bryant, 1995), which also has fine-grained and megacrystic phases, displays a subhorizontal interunit contact suggestive of vertical stacking of individual intrusions.

The age of another granitic pluton previously thought to be Laramide has been revised to Jurassic with the new U-Pb dates. Multiple noncontinuous sections of Tertiary volcanic rocks cover parts of the western end of the range with a combined thickness of at least 500 m. Tertiary basin fill abuts the northern and western edges of the range and perched remnants of the fill in the mountains suggest a former thickness

of at least 100 m more than today. Quaternary alluvium is present in the drainages and covers the slopes south of the mountains. In addition to the felsic dikes, mafic and pegmatite dikes are also present.

Two major structures are exposed in the study area: a roughly north-trending graben at the western end of the range and a probable normal fault which cuts northwest-southeast across the DCM and displays a zone of brittle deformation up to a few hundred meters wide. The orientation of the normal fault mirrors that of other similar faults in the area and is considered to be the result of regional tectonics activity, while the graben may owe its existence to movement on an underlying low-angle detachment fault.

ACKNOWLEDGMENTS

The author wishes to thank the faculty of the SESE for their assistance and support, especially his advisor, Prof. Stephen Reynolds and committee members Profs. J Ramón Arrowsmith and Steven Semken. Thanks are also due the SESE staff for their assistance in navigating the unfamiliar academic bureaucracy. Two days spent with Ed DeWitt in the field were very illuminating and are much appreciated. The author is grateful for the three U-Pb zircon age dates, provided by Dr. Jon Spencer of the Arizona Geological Survey and the University of Arizona, that produced such unexpected results. The author's employer, the Bureau of Land Management, is thanked for allowing considerable flexibility in work schedule during the several years this endeavor has consumed. Special thanks is due Dr. Charles Ferguson of the Arizona Geological Survey who allowed me to attend his "Whole Lava Love" field camp in the spring of 2004, an event where his enthusiasm and breadth of knowledge reignited my interest in the geological sciences and led me to pursue this advanced degree.

TABLE OF CONTENTS

LIST OF FIGURES

Plate

## INTRODUCTION

The Date Creek Mountains (DCM) in west-central Arizona have been little studied despite their proximity to major population areas and relative lack of isolation. The purpose of this study was to conduct detailed geologic mapping on terrain that had previously only been examined on a reconnaissance basis and gather information that would provide new details into the history of the range and its regional geologic and tectonic relationships.

The DCM lies in the southwestern corner of Yavapai County (Figure 1) approximately 113 km (70 miles) northwest of Phoenix. The range is bounded by the Date Creek valley on the north and west, Martinez Creek valley on the east, and the alluvial plains of the Congress and Date Creek Basins to the south (Figure 2). The area of bedrock outcrop comprises an area approximately 21 km (13 miles) from east to west and 8 km (5 miles) north to south. The range is within the Arizona Transition Zone physiographic province, but is located at its southern edge with the southern border of the DCM also being the boundary between the Transition Zone and the Basin and Range province to the south. Elevations range from about 2700 ft (823 m) in the Date Creek Valley at the west end to a high point at an unnamed and unbenchmarked peak of 4920+ ft (1500 m) in the east-central part of the range. The majority of the lands are owned by the State of Arizona, with some lands, mainly in the eastern areas, owned by the Federal Government and managed by the

Bureau of Land Management. What little private land is present is concentrated in ranches along Date Creek and around the old mining town of Congress at the east end of the DCM. Primary access to the area is via: (1) U.S. Highway (US) 93, which cuts across the westernmost end of the DCM, (2) US 89, which skirts the southeastern corner of the range at Congress, and (3) State Route 71, which extends southwesterly from Congress to connect to US 93. A primitive county-maintained dirt road branches northwest from US 89 and follows the Martinez Creek drainage northeast of the DCM. Several jeep roads and four-wheel drive trails penetrate parts of the mountains, while much of the area is accessible only by non-motorized travel.

The study area comprises approximately the western half of the DCM (Figures 1 & 2). Field work was conducted during numerous trips, typically only a few days long, between 2007 and 2012, but totaling over 50 days. Twenty thin sections were produced from collected hand samples and three new U-Pb dates were obtained from samples provided to Dr. Jon Spencer of the Arizona Geological Survey and analyzed by the University of Arizona in Tucson.

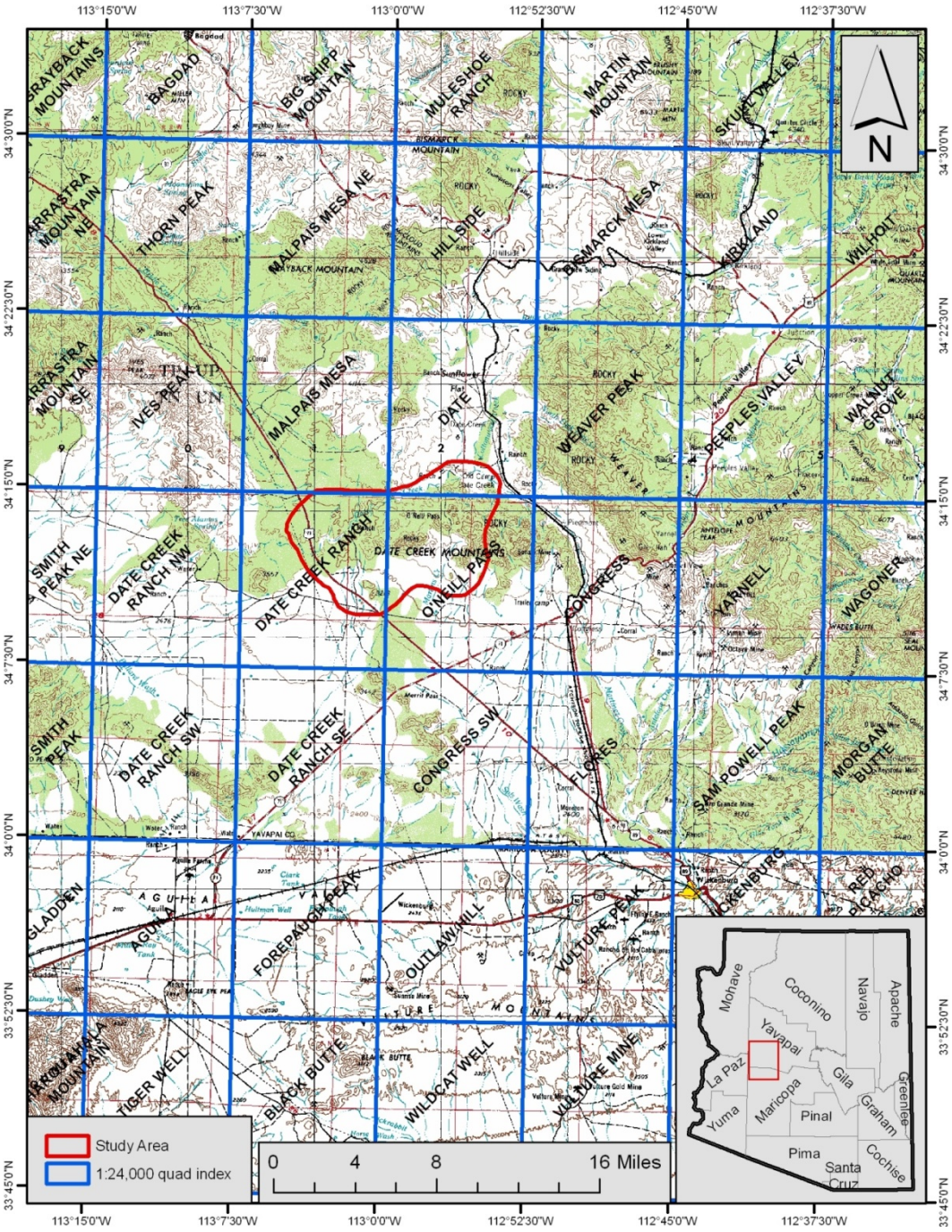


Figure 1 – Geography of the area. 1:250,000 scale topographic map of west-central Arizona showing location of study area and names of 1:24,000 scale quadrangles for the area.

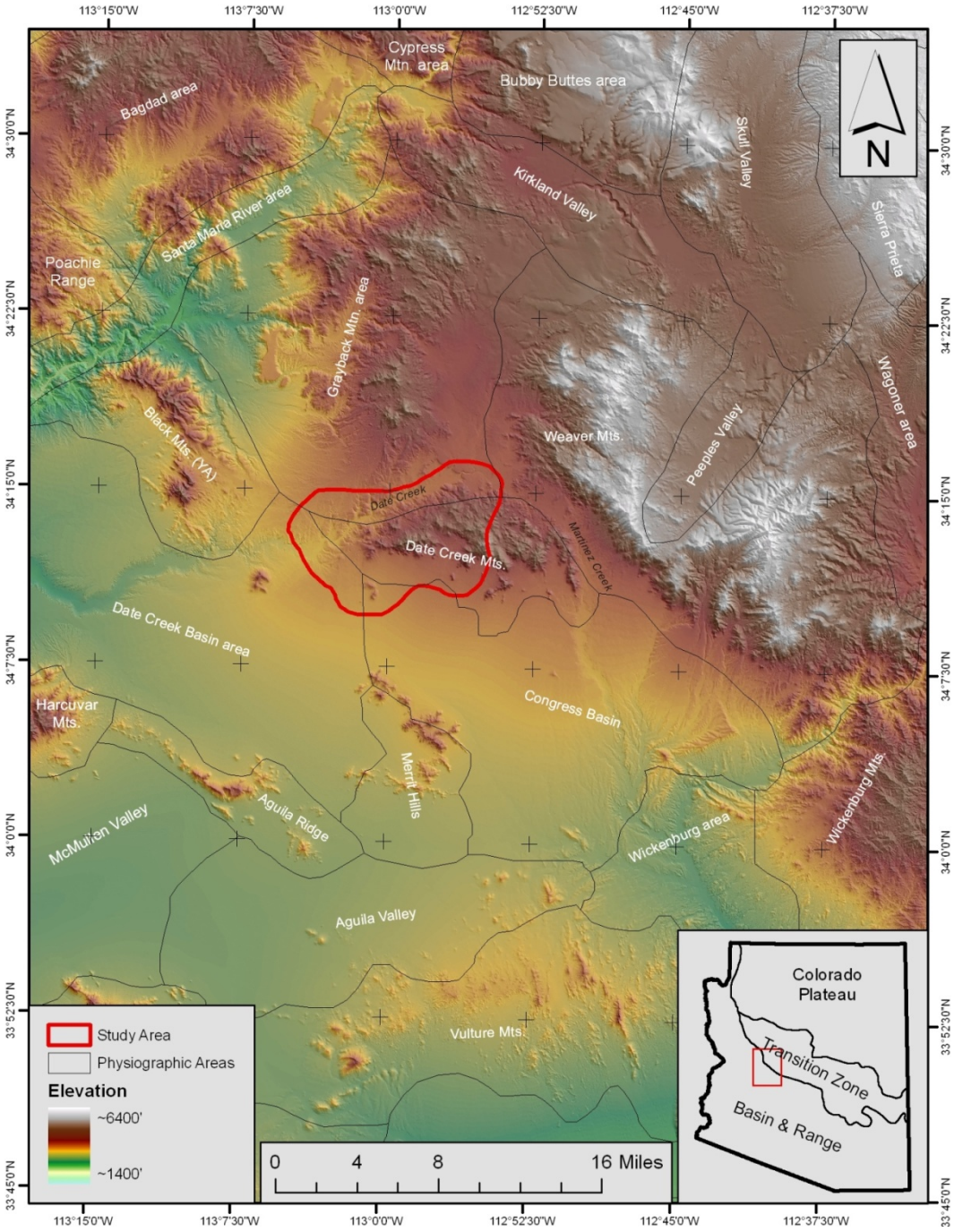


Figure 2 – Physiographic map of west-central Arizona showing location of study area and named physiographic areas as delineated by the Arizona Geological Survey (Trapp and Reynolds, 1998).

## REGIONAL GEOLOGIC AND TECTONIC SETTING

Arizona is divided into three physiographic provinces (Figure 2): the Colorado Plateau (CP) in the north, the Basin and Range (BR) in the south, and cutting across the state between them, the northwest-southeast belt of the Transition Zone (TZ).

The CP is a largely stable region having escaped any strong deformation since the Proterozoic though it has undergone periods of broad uplift and subsidence and also some compression during the Laramide orogeny (Anderson, 1989). The boundary between the CP and the TZ is considered to be the Mogollon Rim, which generally marks the southern limit of the mostly flat lying thick Phanerozoic sequence, south of where it has been removed revealing the Proterozoic basement. That basement extends north under the CP and its younger cover with the result that the boundary is more geomorphic than structural (Spencer et al, 2001).

The boundary between the TZ and the BR is not only physiographic but also tectonic. The style of deformation in the BR reflects the generally northeast-southwest to east-west extension it has undergone in the latter half of the Cenozoic that, in most areas, resulted in the long, parallel, alternating mountains and valleys of a graben-and-horst terrain.

In contrast, the structure of much of the TZ is a series of fault blocks that down step to the south and half-grabens that are thought to have resulted from the thinning of underlying crust. This thinning is

considered to have occurred prior to BR formation and resulted from the movement to the southwest of ductile crust from beneath the TZ through extensive low-angle northeast-dipping detachment faulting (Spencer et al, 2001). As the crust thinned and cooled, this ductility was reduced causing the movement to cease. High areas of long-wavelength corrugations in these lower plates were later exhumed through erosion and created the linear mountain ranges now defined as metamorphic core complexes (Spencer and Reynolds, 1989).

Based on origin and age of accretion, the Proterozoic crust of Arizona is divided into three provinces: Mojave, Yavapai, and Mazatzal (Figure 3). The Mojave province is composed of Paleoproterozoic crust with an Archean heritage, reworked Archean crust, and 2.0-1.8 Ga juvenile arcs, whereas the Yavapai is 1.8-1.7 Ga juvenile crust that was accreted onto the eastern margin of the continent (Whitmeyer and Karlstrom, 2007). The boundary between the Mojave and the Yavapai has been placed at various locations by different researchers over the years with one of the latest studies putting it in the immediate vicinity of the DCM (Bryant et al, 2001). Previously, the DCM was considered to be in the middle of the Yavapai province.

These provinces are further broken down into tectonostratigraphic blocks bounded by major shear zones. The DCM is located in the southeastern corner of the Hualapai block, next to the known southern end of the Mesa Butte shear zone (Figure 3).

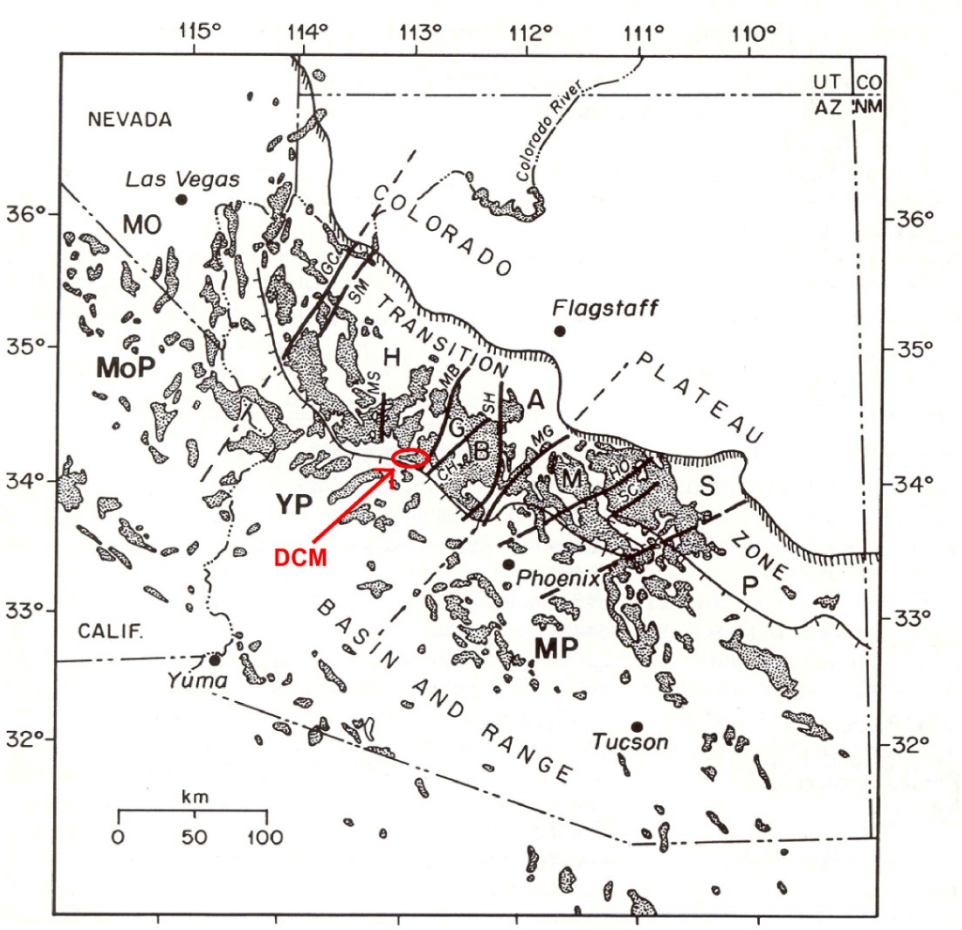


Figure 3 – Map of Arizona showing physiographic provinces and Proterozoic crustal provinces and tectonostratigraphic blocks. Provinces: MoP – Mojave, YP – Yavapai, MP – Mazatzal. Blocks: MO – Mojave, H – Hualapai, G - Green Gulch, B - Big Bug, A - Ash Creek, M – Mazatzal, S – Sunflower, P - Pinal. Shear zones (thick lines): GC - Gneiss Canyon, SM - Slate Mountain, MS - Mountain Spring, MB - Mesa Butte, CH – Chaparral, SH – Shylock, MG - Moore Gulch, SC - Slate Creek. Shaded areas represent Proterozoic outcrops. The location of the study area is indicated (adapted from Williams, 1991, Figure 2).

During the Paleozoic, most of Arizona underwent periods of subsidence, deposition, and uplift producing in a thick sequence of sedimentary rocks. South of the Colorado Plateau and especially in the southwestern part of the state, most of those units have subsequently

been removed by erosion, leaving only remnants of the once more continuous layers.

In the Jurassic, subduction of the Kula and/or Farallon oceanic plates beneath the southwestern edge of the continent produced a magmatic arc. All exposures of Jurassic volcanic and plutonic rock previously known in Arizona are in the BR (Tosdal et al, 1989; Ludington et al, 2005).

## PREVIOUS STUDIES

No known detailed mapping has been done previously in the DCM, though reconnaissance level mapping has been done by Wilson (1958) and DeWitt (pers. comm.) and in the western part of the range by Bryant (1995). Surrounding areas in which detailed mapping has been conducted include (Figures 2 and 4) the Merritt Hills (Reynolds and Spencer, 1985) to the south, Aguila Ridge (Reynolds and Spencer, 1984) to the southwest, the Black Hills (YA) (Brooks, 1985) to the west, the Poachie Range (Bryant, 1992) to the northwest, and part of the Bagdad area (Anderson et al, 1992) farther northwest. To the south and southeast the Vulture Mountains, Wickenburg area, and Wickenburg Mountains (Grubensky et al, 1987; Grubensky and Reynolds, 1988, Grubensky, 1989; Reynolds et al, 1988; Stimac et al, 1987) have also been mapped at quadrangle-scale. Published intermediate scale geologic mapping of the area is available for the Phoenix North 30' x 60' quadrangle (Demsey,

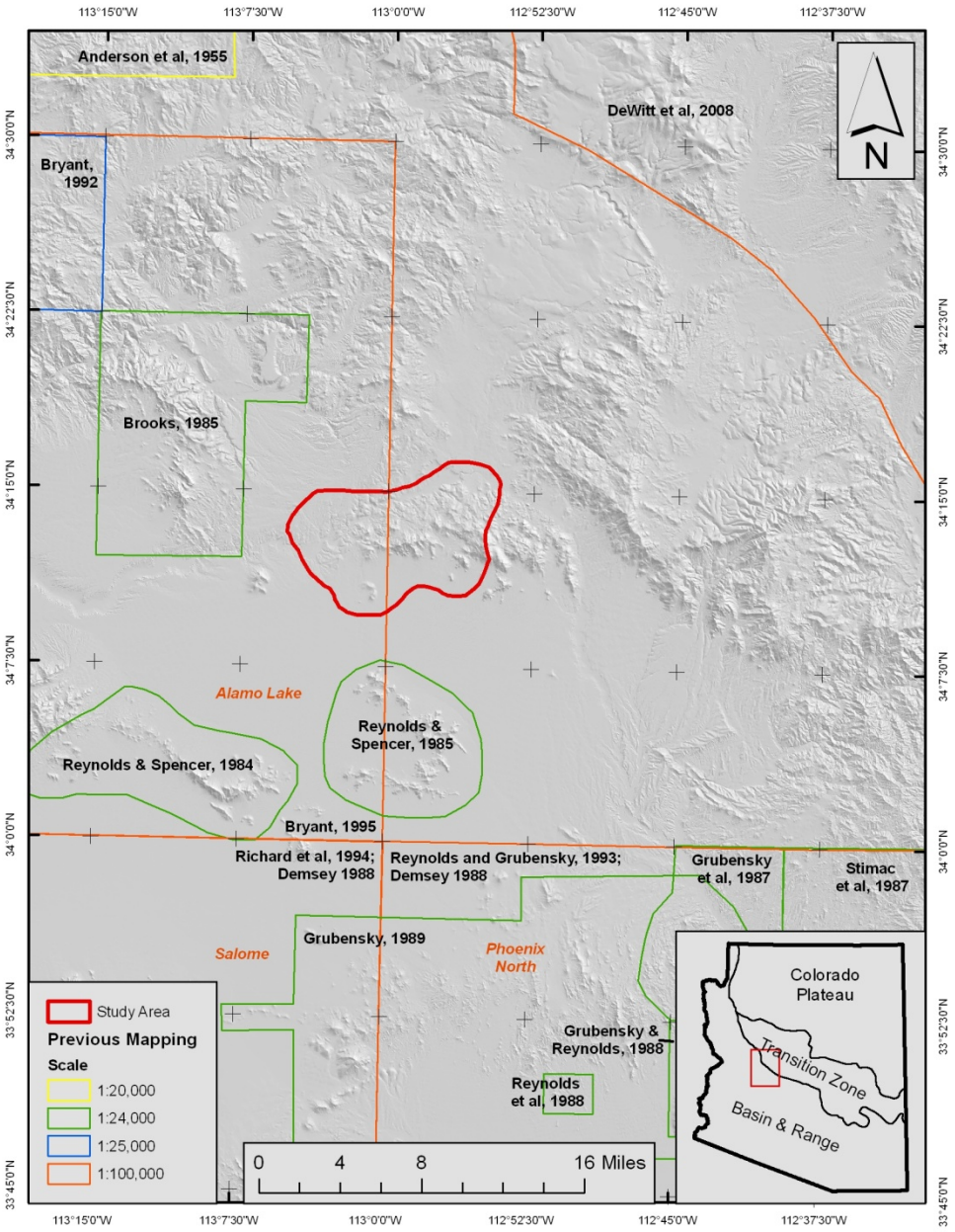


Figure 4 – Physiographic map of west-central Arizona showing study area and areas of existing geologic mapping at scales of 1:100,000 and larger.

1988; Reynolds and Grubensky, 1993), the Salome 30' x 60' quadrangle (Demsey, 1988; Richard et al, 1994), the Prescott National Forest area (DeWitt et al, 2008), and the Alamo Lake 30' x 60' quadrangle (Bryant, 1995), which includes the western end of the DCM.

## MAP UNIT DESCRIPTIONS FOR PLATE 1

### Cenozoic Units

*Qal – Quaternary alluvium.*

Unit consists of young alluvial deposits of sand, gravel, and silt within major active fluvial drainages. Thickness ranges from a few cm to several m.

*Qoa – Quaternary older alluvium.*

Sediments comprised of various older alluvial materials derived from inactive or intermittently active fluvial, weathering, and erosional processes. Includes pediment deposits on slopes south of the DCM and other areas of soil or other residium development covering bedrock. Thickness ranges from several cm to several m.

*Qc – Quaternary colluvium.*

Occurs as apron or fan-like deposits located at the base of slopes and consisting of mostly broken rock ranging in size from cobbles to boulders. Results predominately from physical weathering of relatively resistant rock. Thickness ranges from several cm to a few m.

Figure 5 – Quaternary-Tertiary older alluvium (QToa). Normally brown, silty, and with a generally horizontal surface. Found only as remnants in small drainage heads and other protected locations along the DCM's south slope. Length of hammer in upper right for scale is approximately 33 cm. Exposure is located in the SE¼ of Sec. 17, T. 10 N., R. 7 W.

*TQoa – Tertiary or Quaternary older alluvium.*

Comprises deposits presumed to be remnants of a previously more extensive alluvial layer. Preserved only in protected alcoves and at the heads of small drainages along the southern mountain front. Brown, lightly to moderately indurated, mostly silty, and normally forms a conspicuous horizontal surface (Figure 5) which contrasts with the slope of the adjacent pediment. Thickness ranges from few cm to a few m.

*Tbf – Tertiary basin-fill deposits of Bryant (1995).*

Unit includes conglomerate, sandstone, siltstone, and other alluvial deposits along with a few interfingered lava flows. Occurs only on the

northern and western sides of the DCM and is part of a regionally more extensive deposit. Characterized in the study area by a surface with 25%-50% subangular to rounded cobble to boulder size clasts composed of intrusive and extrusive igneous rocks and resistant metamorphic units (Figure 6). Thickness of unit along Date Creek at least 150 m but Bryant (1995) places the entire unit's thickness at up to 1,000 m.

Figure 6 – Typical view of surface of Tertiary basin fill (Tbf) exhibiting prevalence of subangular to rounded cobble- to boulder-sized material and lithologic heterogeneity. Exposure located in the SE¼ of Sec. 2, T. 10 N., R. 8 W.

*Ta – Tertiary trachyandesite of Bryant (1995).*

Within the DCM this unit includes red to reddish-brown vesicular trachyandesite, basaltic trachyandesite, or basaltic lava flows, and mud-flow breccias (Bryant, 1995). Term used by author only where flows are

not part of a thicker defined volcanic sequence, specifically, at a small isolated exposure on western Date Creek and on the two hills lying south of the western end of the mountains just north of US 93, where the lavas sit directly on Proterozoic rocks.

*Tb – Tertiary basalt.*

Vesicular black basalt, present only in a small area within the northern edge of the study area where it is part of larger, extensive valley-filling basaltic lava flows (Figure 7). A few meters thick in the study area but part of a thicker sequence of multiple flows to the north.

*Tv2 – Tertiary volcanic rocks.*

Subdivision of Ta of Bryant (1995) within the Date Creek Ranch graben (DCRG). Exposure thickness in the DCM is about 180 m with the top approximately 40 m being several andesitic or basaltic lava flows of varying thickness and the remainder composed of ash-fall tuffs with a minor thin (< 1 m) rhyolite welded tuff and a few brown and black vitrophyres. Lavas, some of which display autobreccias, cap all of the hills within the Tv2 areas of the DCRG. It is assumed that Tv2, which has no bottom visible and no correlative layers with Tv1, is the younger since Tv1 rests directly on Proterozoic rock to the southwest of the graben. Bryant (1995) gives a K-Ar apparent age of 23.2 ± 0.8 Ma for a Ta sample (that appears to be within the area of Tv2) from hill 3583' in the northeastern DCRG (Appendix Figure B-1). Thin section sample photographs for unit are in Appendix A as Figures A-35, A-36, A-41, and A-42.

Figure 7 – Tertiary basalt flow capping Tertiary sediments. View looking north of the southern end of extensive basalt flows filling valley north of the DCM. Nature of the termination of the flow is indeterminate. Paleoproterozoic schists and gneisses in foreground. Grayback Mountains in left middle distance and Bubby Buttes area in right distance (see Figure 2). Viewpoint is from the SE¼ of Sec. 36, T. 11 N., R. 7 W.

*Tv1 – Tertiary volcanic rocks.*

Subdivision of Ta of Bryant (1995) and includes areas previously mapped as Trl and Trb. Unit described from the exposures in the low hills in the southwest part of the study area. Base of sequence rests on Mesoproterozoic plutonic rocks (Yjm). Lower part of unit consists of approximately 200 m of interlayered ash-fall tuff (Figure 11) with minor poorly sorted sandstone (Figure 10) and conglomerate layers containing some reworked volcanic materials. In sequence above the tuffs is a black vitrophyre approximately 1 m thick (Figure 12), a rhyolitic welded tuff

Figure 8 – View looking northwest of hill 3583' in north end of DCRG displaying section of Tv2. Obvious ledge about one-quarter of the way down the slope is a resistant tuff and marks the division between the capping lavas and the underlying tuffs. Date Creek is visible in the middle distance with slopes of Tbf behind. Stream along right edge of photo generally follows the northern part of the DCRG's eastern fault. Jgf in foreground. Flat, lava capped plateau in distance is Malpais Mesa with Black Hills (YA) on the left. Viewpoint in NW¼ of Sec. 17, T. 10 N., R. 7 W.

about 2 m thick, and a lava flow of basaltic or andesitic composition at least 3-4 m thick. The tuffs are tan to pinkish in color, contain 10%-20% crystal and lithic fragments to 2 mm, and commonly include pumice fragments up to 2 cm. The vitrophyre has a glassy matrix with 20% crystal fragments, primarily plagioclase and quartz with minor opaque minerals. The rhyolite tuff is brownish-red to grayish-purple with about 20% crystals, mainly quartz and biotite, and commonly exhibits what appear to be flattened lithophysae. Both the vitrophyre and the rhyolite tuff form

prominent ledges (Figure 9). The presence of the vitrophyre and rhyolite tuff in the NW fault blocks within the DCRG indicate those areas to be Tv1. Bryant (1995) reports a K-Ar apparent age of 24.3 ± 0.9 Ma from a rhyolite welded tuff in the north-central part of the DCRG. Thin section sample photographs for unit are in Appendix A as Figures A-37 through A-40.

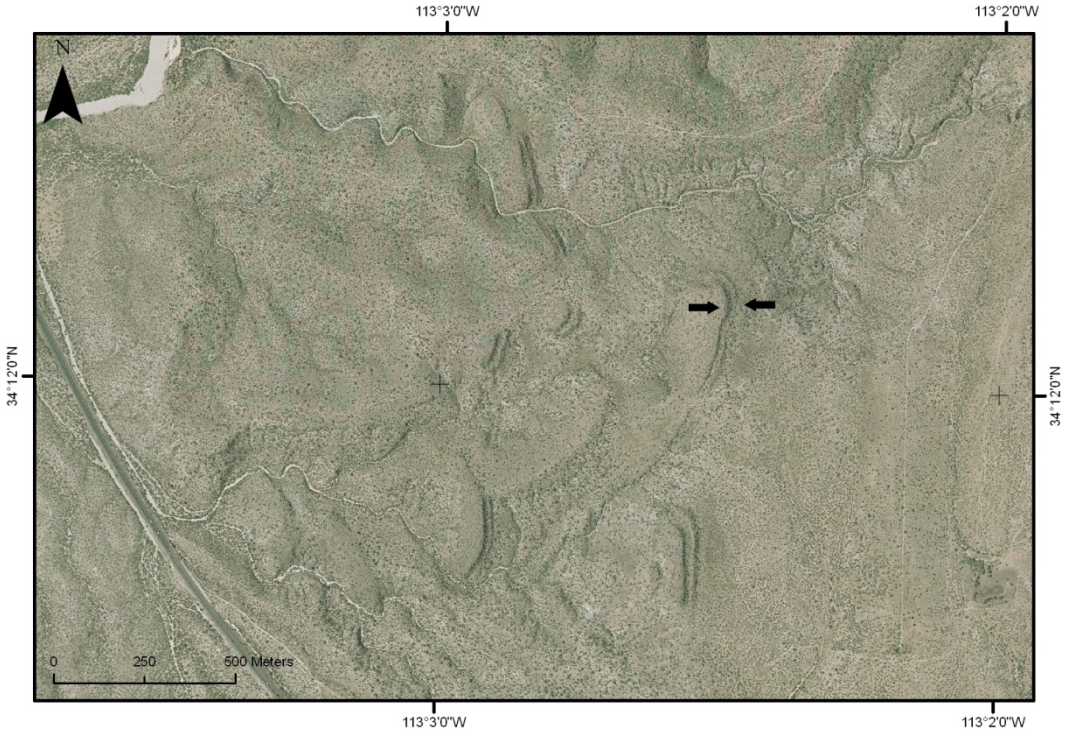


Figure 9 – Portion of 2005 color DOQQ (Digital Orthophoto Quarter Quad) for the NE quadrant of the Date Creek Ranch 7½′ quadrangle showing area of low volcanic hills in the SW part of the study area. Arrows point to the prominent lower and upper ledges formed respectively by the vitrophyre and the rhyolite welded tuff of Tv1.

Figure 10 – Poorly sorted sandstone within ash-fall tuff of Tv1. Note lithologically heterogeneous angular to subangular clasts. Exposure from the streambed section of unit within the SW½ of Sec. 13, T. 10 N., R. 8 W.

Figure 11 – Ash fall tuff of Tv1 with visible pumice clasts. Exposure from the streambed section of unit within the SW½ of Sec. 13, T. 10 N., R. 8 W.

Figure 12 – Exposure of vitrophyre (center) and welded rhyolite tuff (right) units of Tv1. Location of outcrop is in SE¼ of Sec. 13, T. 10 N., R. 8 W.

*Tvu – Tertiary volcanic rocks undifferentiated.*

Used for exposures too small to be confidently assigned to specific units.

## Mesozoic Units

*Jg – Jurassic granite.*

Leucocratic granite, readily forms resistant blocky outcrops due to sets of intersecting vertical joints (Figures 13-15). Medium- to coarse-grained, granular, friable, with approximately 50% white feldspar (mostly K-feldspar with minor plagioclase), 30% quartz, and 20% biotite. Unit originally thought to be Laramide in age (E. DeWitt, pers. comm.), but new

Figure 13 – Jurassic granite (Jg) pluton displaying blocky nature of outcrops resulting from intersecting vertical joint sets. View looking northwest from the south side of pluton in the SW¼ of Sec. 16, T. 10 N., R. 7 W.

U-Pb zircon dating places it in the Jurassic (174.0 ± 2.5 Ma). Contacts with surrounding units generally sharp and well defined. Thin section sample photographs for unit are in Appendix A as Figures A-33 and A-34.

*Jgf – Jurassic granite, fine-grained.*

Originally part of "X?g" of Bryant (1995), which was subdivided by mapping into fine-grained Xgf and megacrystic Xgm. A new U-Pb date of the fine-grained phase produced an age of 184.2 ± 1.8 Ma. Unit generally forms scattered low-relief outcrops usually no taller than a few meters (Figure 16). Weathered rock color varies from pink to red to brown

with fresh surfaces displaying a dark gray appearance. Granular with approximately 50% feldspar (mostly K-feldspar), 30% quartz, and 20% biotite. Feldspars and quartz are typically 1-2 mm with biotite being 0.2-0.5 mm but commonly in clots to 2 mm. Thin section sample photographs for unit are in Appendix A as Figures A-5 and A-6.

*Jgd – Jurassic felsic dikes (shown only as felsic dikes on map).*

Dense, fine-grained, crystalline dikes, cutting predominately Jgf and to a lesser extent, XJgm (Figure 17). Though not dated, are considered to be Jurassic because of spatial relationships. Groundmass of rock is approximately 50% each K-feldspar and quartz with intimately intergrown crystal grains. Biotite and other mafic minerals are present but have been mostly segregated into schlieren (Figure 18). All of the dikes have an orientation of north to north-northeast. Shown on Plate 1 as felsic dikes. Thin section sample photographs for unit are in Appendix A as Figures A-13 and A-14.

Figure 14 – Close-up view of Jg showing medium- to coarse-grained, granular nature of unit. Outcrop located in SW¼ of Sec. 16, T. 10 N., R. 7 W.

Figure 15 – View of northwest side Jg pluton looking to the northeast. Contact of leucocratic granite pluton with darker megacrystic granite (XJgm) obvious in middle of photo. Weaver Mountains in left background. Viewpoint located in NE¼ of Sec. 17, T. 10 N., R. 7 W.

Figure 16 – Fine-grained Jurassic granite Jgf. View of typical scattered low-relief outcrop terrain formed on unit. Looking northwest from viewpoint in the NE¼ of Sec. 17, T. 10 N., R. 7 W.

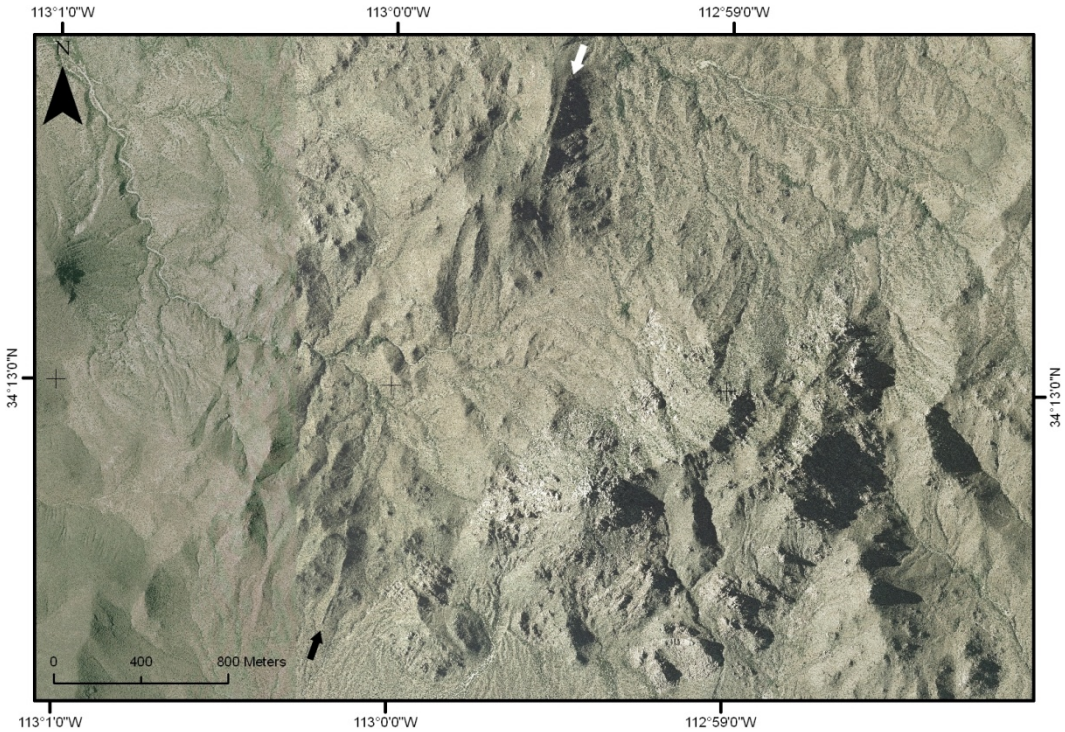

Figure 17 – Part of the 2005 color DOQQs of the NW quadrant of the O'Neill Pass and NE quadrant of the Date Creek Ranch quadrangles showing some of the Jurassic felsic dikes (arrows). The obvious light colored mass in the southeastern part of the picture is the Jg pluton.


Figure 18 – Block of Jurassic felsic dike displaying segregation of mafic minerals into schlieren. Location is in north-central part of Sec. 17, T. 10 N., R. 7 W.

## Proterozoic Units

*Yjf – Mesoproterozoic Granite of Joshua Tree Parkway (Bryant, 1995), fine-grained unit.*

A dense, fine-grained, resistant granite that forms blocky outcrops varying in color from beige to dark gray (Figure 19). Fresh surface is light gray. Approximately 50% feldspar, mostly potassic, 30% quartz, and 20% mafic minerals including biotite, magnetite, and hornblende. Many of the exposures, especially in the area west of US 93, display a subhorizontal

Figure 19 – View showing contrast between Yjf outcrop in foreground displaying blocky, sub-angular, smooth surfaced rock and Yjm on the left and left background with its rounded boulders and rough textured surfaces. This exposure is one example of linear ridges of Yjf that protrude upward from the subhorizontal contact between the two units into the overlying Yjm. Outcrop located in the SE¼ of Sec. 10, T. 10 N., R. 8 W.

contact between Yjf and the overlying Yjm. Thin section sample photographs for unit are in Appendix A as Figures A-25 and A-26.

*Yjm – Mesoproterozoic Granite of Joshua Tree Parkway (Bryant, 1995), megacrystic unit.*

Unit is a porphyritic, coarse-grained granite, with megacrysts of K-feldspar to 4 cm (Figure 20). Outcrops are gray to light reddish-brown and form rounded boulder landscapes (Figure 19). Fresh surfaces appear darker due to the quantity of mafic minerals. Percentage of megacrysts in rock frequently about 50% (Figure 20) but can vary from near 0% to near

Figure 20 – Typical outcrop of Yjm showing white potassic feldspar megacrysts weathering in relief and dark shade of the groundmass resulting from the high percentage of mafic minerals. Outcrop located in the NE¼ of Sec. 10, T. 10 N., R. 8 W.

100% where the rock becomes crystal-supported and has the appearance of a cumulate. Groundmass is about 40% potassic feldspar crystals to 1 cm, 20% quartz, and 40% mafic minerals including biotite and magnetite. A sample of this unit from the Grayback Mountains to the north has been U-Pb dated at 1415.3 ± 6 Ma (Bryant, 1995, 2001). Thin section sample photographs for unit are in Appendix A as Figures A-23 and A-24.

Figure 21 – Example of outcrop of Yjz showing fine-grained, mafic mineral-rich nature with inclusion of even more mafic material exhibiting flow alignment. Outcrop located in the NW¼ of Sec. 5, T. 10 N., R. 7 W.

*Yjz – Mesoproterozoic Granite of Joshua Tree Parkway (Bryant, 1995), mafic unit (new subdivision).*

Numerous enclaves of a silica poor unit are present within Yj. Composition is variable but appears to fall within the range of a gabbro or monzogabbro. Grain size is medium to very fine-grained. Most masses

are too small to map at quadrangle scale, commonly have a pod-like appearance, and usually contain smaller enclaves of an even more mafic material typically displaying some degree of flow alignment (Figure 21). Feldspars are almost entirely plagioclase and as a percentage of rock vary from about 5% to 50%. Quartz is rare. Mafic minerals appear to be mostly biotite and hornblende. Boundaries with host rock locally show evidence of magma mixing. Thin section sample photographs for unit are in Appendix A as Figures A-19 through A-22 and Figures A-27 through A-30.

*Yg – Mesoproterozoic porphyritic granite.*

Present only in the northeastern part of the study area east of the belt of metamorphic rocks. Frequently forms terrains of scattered tan to gray to light-brownish-red outcrops and boulders. White to salmon colored potassic feldspar phenocrysts to 2 cm approximately 20%-30% of rock, groundmass 50% potassic feldspar, 10% plagioclase, 30% quartz, and 10% biotite. Enclaves of Xm in areas proximal to the contact with that unit are common. Thin section sample photographs for unit are in Appendix A as Figures A-31 and A-32.

*XJgm – Paleoproterozoic or Jurassic megacrystic granite.*

Originally part of “X?g” of Bryant (1995) which was subdivided by mapping into the fine-grained Xgf and megacrystic Xgm. U-Pb age dating of Xgf revealed it to be Jurassic and it has been redesignated Jgf. The megacrystic phase was not dated but it is suspected that it may also be

Jurassic based on observations of field relationships. Indications include the typically poorly defined contact between Jgf and XJgm and that XJgm is adjacent to two other intrusive bodies which new data has now shown to be Jurassic, thus possibly making XJgm part of a suite of similar aged plutons.

Areas of XJgm frequently produce large continuous outcrop exposures and tan to reddish-orange boulder covered slopes (Figure 22). At outcrop scale, the rock may appear much darker (Figure 23) because of the high percentage of mafic minerals in the groundmass. Percentage of rock composed of K-feldspar phenocrysts to about 2 cm is commonly about 40%-50%, quartz about 20%-30%, and mafic minerals including biotite and magnetite about 20%-40%. Includes numerous inclusions and sheets of Xm in areas proximal to that contact. Thin section sample photographs for unit are in Appendix A as Figures A-7 through A-12.

Figure 22 – Hill of XJgm showing its rugged, bouldery nature. In contrast to Jg, no ordered vertical joint sets are present which gives irregular shapes of most boulders and outcrops. View to the southeast of hill on the line between Secs. 13 and 24, T. 10 N., R. 7 W.

Figure 23 – Outcrop of XJgm showing well-formed, rectangular K-feldspar phenocrysts exhibiting flow alignment and dark, mafic mineral-rich groundmass. Outcrop located in the SW¼ of Sec. 13, T. 10 N., R. 7 W.

*Xd – Paleoproterozoic diorite porphyry.*

Single exposure in study area is small hill south of US 93 in the NE¼ of Sec. 31, T. 10 N., R. 7 W. Unit weathers into large blocks giving hill the appearance of a boulder pile. Surface weathers to a deep brown with fresh surfaces being brown to lavender. Phenocrysts of hornblende to 2 cm compose 10%-30% of rock. Groundmass is 60% plagioclase, 20% hornblende, 10% potassic feldspar, and 10% other minerals. Previously suspected to be Mesoproteroic, a new U-Pb date has revealed it to be Paleoproterozoic with an age of 1681.4 ± 8.0 Ma. Thin section sample photographs for unit are in Appendix A as Figures A-15 through A-18.

*Xm – Paleoproterozoic metasedimentary and metavolcanic rocks, undivided.*

Similar to other exposures within the TZ that are referred to as the Yavapai schist (Ysc) by the U.S. Geological Survey (Geolex database, accessed March 31, 2012) or the proposed Yavapai Supergroup (Anderson, 1989a; Anderson, 1989b). Metamorphic rocks were not shown on maps of the Date Creek Mountains at the time of Anderson's original exhaustive study (1986) and thus were not included in his work on metamorphic rocks within the TZ. Later reconnaissance mapping by Ed DeWitt (pers. comm.) resulted in their recognition and subsequent designation on geologic maps of the area.

Figure 24 – Outcrop of granofels within Xm. Outcrop location is NE¼ of Sec. 14, T. 10 N., R. 7 W.

Figure 25 – Outcrop of schists and gneisses of Xm looking generally northeast, parallel to foliation. Located in the NW¼ of Sec. 1, T. 10 N., R. 7 W.

The north-northeast strike of foliation generally parallels that measured in other regional exposures of the Ysc. Various sources give different ages which generally range from 1660–1800 Ma. In the DCM, the unit forms a roughly north-northeast-trending belt across the central part of the range. Rock types include feldspar-quartz granofels (Figure 24), quartz-hornblende-feldspar gneiss, quartz-biotite gneiss, muscovite-quartz-feldspar schist, biotite-quartz schist, quartz-biotite schist, migmatite, amphibolite, and epidotite. The unit falls within the amphibolite metamorphic facies. Spatially schists seem to predominate in the eastern part of the belt (Figure 25) while granofels is more common on the western side. Thickness not measured. Thin section sample photographs for unit are in Appendix A as Figures A-1 through A-4.

## Dikes and Veins

*Pegmatite dikes*

Age unknown, possible Proterozoic. Pegmatite dikes up to about 1 m wide. Several exist in the study area but only one is large enough to map at quadrangle scale. Observed in situ exposures only cut Xm. Contain only quartz and feldspar in very large crystals (Figure 26).

*Mafic dikes*

Ages unknown, could be Proterozoic to Cenozoic. Mafic dikes and masses are common within the study area but their exposures are too

Figure 26 – Pegmatite dike cutting Xm in the NE¼ of Sec. 11, T. 10 N., R. 7 W.

Figure 27 – Outcrop of massive quartz vein cutting Xm. Located in the SE¼ of Sec. 2, T. 10 N., R. 7 W.

small to be mapped at quadrangle scale. Dikes have highly variable appearance and orientation and have been observed cutting units of all ages. Thin section sample photographs for unit are in Appendix A as Figures A-43 and A-44.

*Massive quartz veins*

Ages unknown, probably Proterozoic and Cenozoic. Massive quartz veins are common in the study area and are of two types—massive solid quartz veins to 3 m thick cutting Xm (Figure 27) and veins to about 2 m thick within and parallel to the O'Neill Pass Fault Zone (OPFZ). The large quartz veins cutting Xm are largely parallel the foliation and since restricted to that unit are likely also Paleoproterozoic. The quartz veins emplaced along the OPFZ are obviously related to that structure and are therefore Cenozoic.

## DISCUSSION

Several unexpected and interesting features and relationships were observed within the study area. This section will describe those occurrences and where possible, try to provide an explanation for their genesis and the implications for the DCM as it relates to the regional geologic and tectonic setting.

### Contact between Yjf and Yjm

Granitic plutons are generally considered to have been emplaced through the diapir-like vertical rise of magma masses. One result of this

mechanism is that the majority of the pluton's contact with adjacent units is high-angle in nature. In contrast, the contact between the fine-grained unit of the Granite of Joshua Tree Parkway (Bryant, 1995) and its overlying megacrystic unit is subhorizontal over large areas. The contact surface undulates and varies laterally but only on the order of a few meters over short distances (Figure 29). In some areas, narrow, linear masses of the Yjf have pushed upwards as much as a few meters into the overlying Yjm (Figures 19). There is no obvious intermixing of the adjacent units and generally the contact surface of the Yjf appears to have a chilled margin. Although visible in all areas of Yj outcrop, these characteristics are especially pronounced in the area west of US 93. These relationships have led the author to conclude that they represent a mode of emplacement characterized by vertical stacking of horizontal, possibly tabular plutons or sills, similar to the scenario proposed by Farina et al (2010)(Figure 28).

There are four groups of Yj outcrops: west of US 93, on the west side of the DCRG, on the east side of the DCRG, and on the east side of the metamorphic belt. The general elevation of the contact in these areas is respectively, 2900' (884 m), 2900' (884 m), 3000' (915 m), and 3400' (1037 m). If these are all the same contact, which requires a relatively narrow vertical section of the same few hundred meters to be exposed laterally over a distance of 13 kilometers, then the slope may represent either tilting during emplacement or regional tilting to the west post-

emplacement. It is possible, perhaps even likely, that they are not all the same contact, but to verify that, additional detailed mapping, probably aided by geochemical and thin section analysis, would be required.

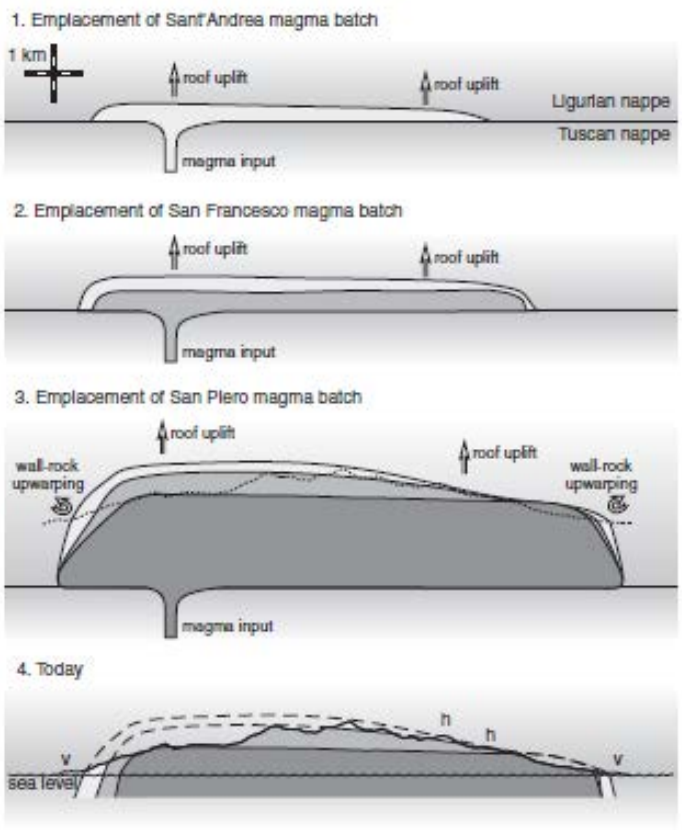


Figure 28 – Figure 15 from Farina et al (2010) illustrating vertical stacking of individual horizontal plutons (sills). This mode of emplacement is a possible explanation for the observed sub-horizontal contact between Yjf and Yjm.

Figure 29 – Contact between Yjm and Yjf. Smooth, flat ground is contact surface of Yjf with remnants of Yjm overlying. Exposure is in the NE¼ of Sec. 10, T. 10 N., R. 8 W.

Additional evidence for the horizontal mode of emplacement hypothesis is also present in the style of contact between the metamorphic unit and its three surrounding plutons. Both XJgm and Yg contain entrained sheets and enclaves of the older metamorphic rock within the igneous unit proximal to the contact, a relationship which would be expected from diapiric magma impingement on the underside of Xm. However, the area of Yj which is adjacent to the southeastern part of the metamorphic belt contains no enclaves and the contact, where visible, is sharp, a relationship that would result from horizontal impingement.

## Jurassic plutons

Three U-Pb zircon age analyses were provided by Dr. Jon Spencer of the Arizona Geological Survey and the University of Arizona for plutons within the study area. Two of these, granites thought to be Paleoproterozoic and Laramide, turned out to both be Jurassic with ages of 184.2 ± 1.8 and 174.0 ± 2.5 Ma. These dates were unexpected as the TZ is north of the area (Figure 30) thought to be occupied by the Jurassic arc (Tosdal et al, 1989). It has been suggested by Dr. Stephen Reynolds that these upper plate plutons may be the tops of intrusive bodies that could match up with their roots exposed in the lower plate to the southwest. Using geologic data from the state map produced by Ludington et al (2005) and plate movement direction from Spencer and Reynolds (1991), it would appear that the most likely candidates for this match occur within the Granite Wash Mountains (Figure 31). However, the distance between the plutons is measured at 78 km, about 20% greater than the crustal extension of 66 km calculated by Spencer and Reynolds (1991). Additional studies utilizing detailed mapping, geochemical methods, or more age dates will be needed to confirm or refute this hypothesis.

## Date Creek Ranch Graben

At the west end of the DCM is a single graben that trends generally NNW and varies in width from about 0.8-1.5 km (Plate 1). The graben is bordered on the east and west by Paleoproterozoic and Jurassic plutonic

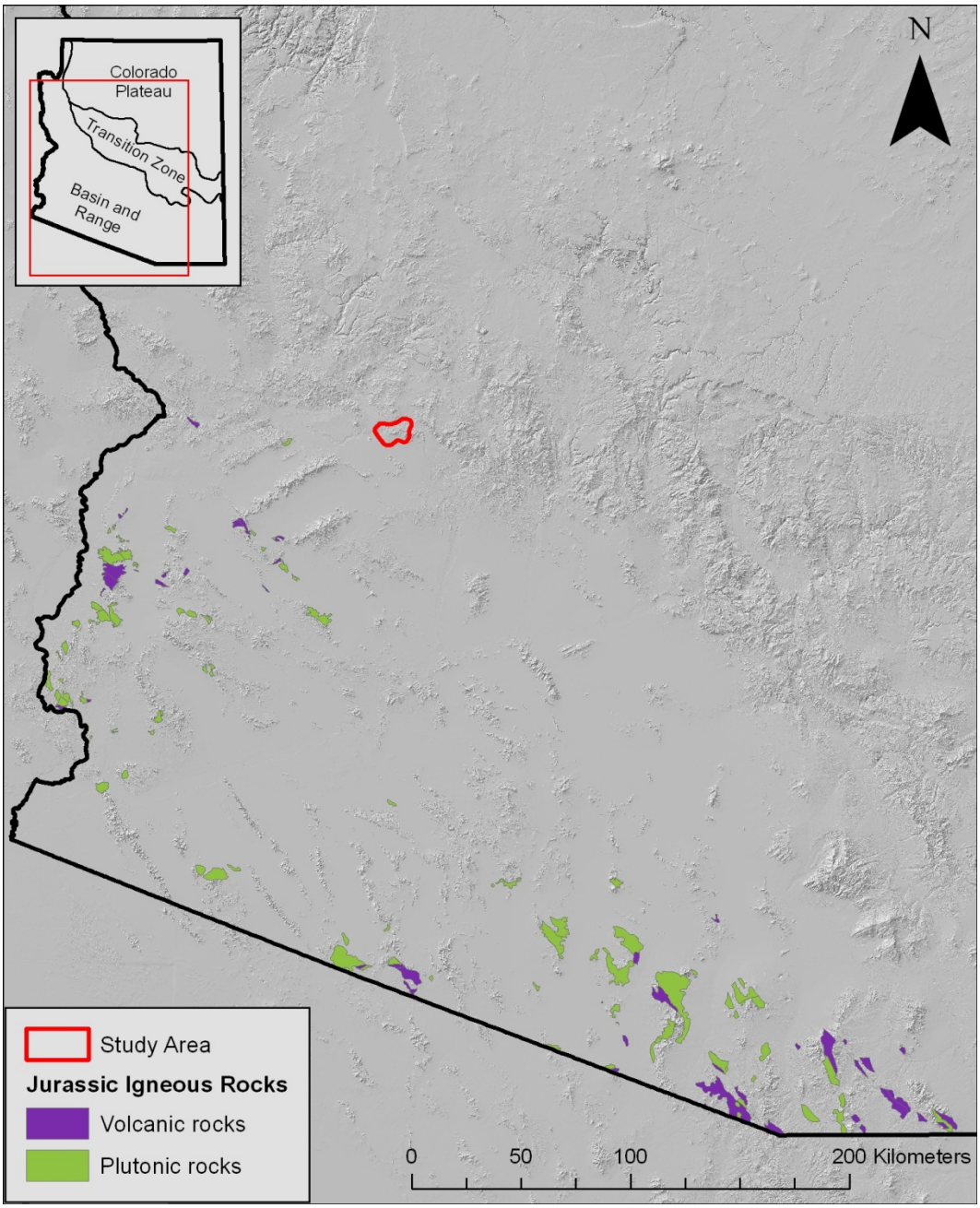


Figure 30 – Physiographic map of southwestern Arizona showing locations of Jurassic igneous rock outcrops. Geologic data from Ludington et al, 2005.

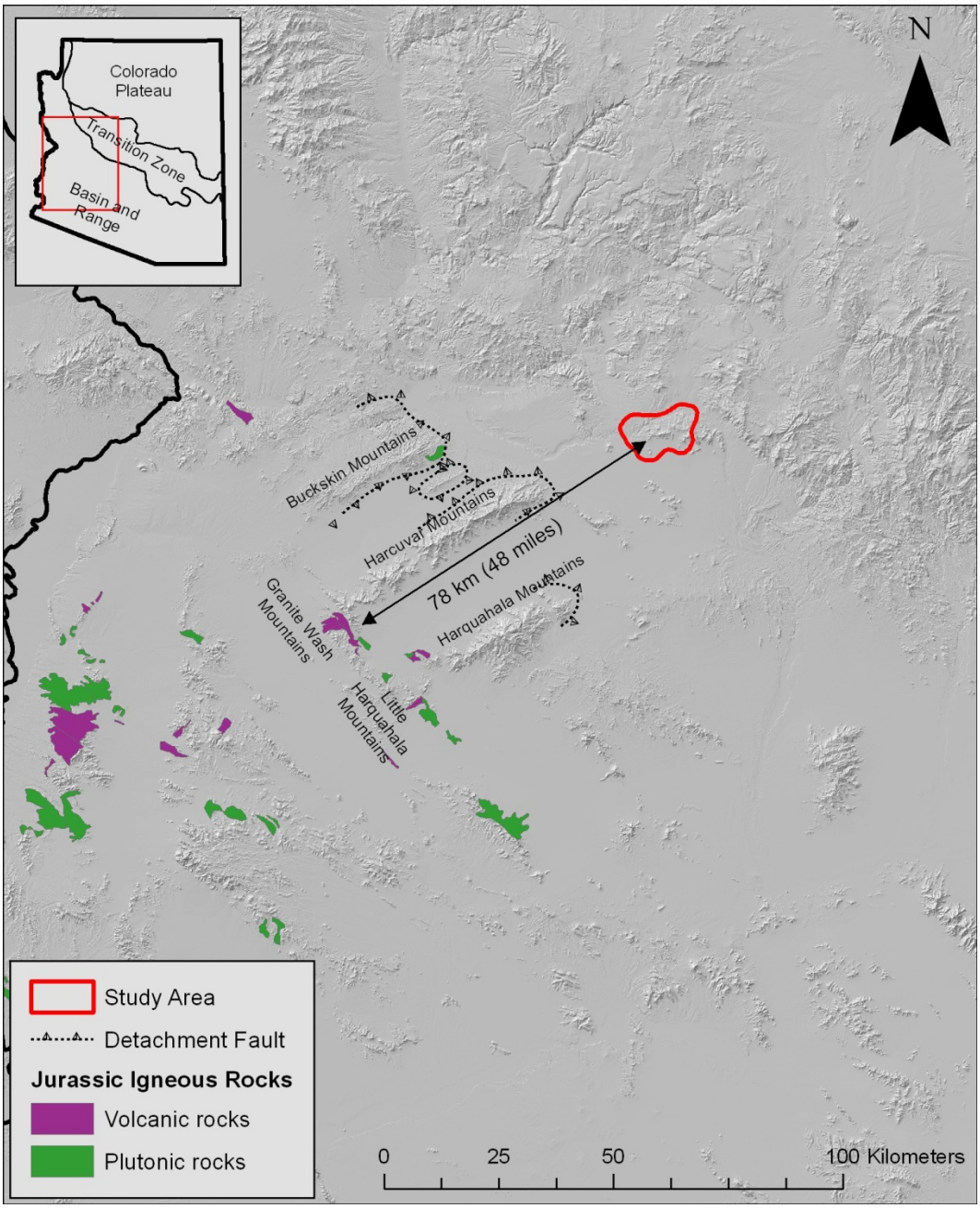


Figure 31 – Physiographic map of west-central Arizona showing location of Jurassic igneous rocks which may be related to the newly dated Jurassic plutons in the Date Creek Mountains. Geologic data from Ludington et al, 2005. The proximity of Jurassic intrusive and volcanic rocks to each other in areas of lower plate exposures, such as in the Granite Wash Mountains (Reynolds et al, 1989), is the result of thrust faults.

rocks and is filled by Tertiary volcanic rocks. Two noncorrelative sequences, Tv1 and Tv2, occupy the graben with a total thickness of at least 400 m suggesting a throw of at least that much. The name Date Creek Ranch Graben (DCRG) is suggested by the author because that segment of Date Creek which crosses the less resistant volcanic rocks in the graben has produced a wider stream channel than where it crosses the adjacent plutonic rocks and thus provided suitable ground for the establishment of the ranch.

Since the graben is a result of extensional forces, the direction of extension should be normal to the graben's orientation. There are no other known structures in this part of the TZ with a similarly oriented stress field. However, if one looks at the metamorphic core complexes to the southwest, a potential cause for the graben and its orientation becomes apparent (Figure 32). The azimuth of the direction of movement of the lower plate below the regional detachment fault was 235º (Spencer and Reynolds, 1991). This places the extension direction essentially normal to the DCRG and gives a path for the extraction of the Harcuvar Mountains core complex that originally lay beneath the DCM. If the trailing (southwest) edge of the upper plate was thin enough in this area, drag on or disruption in the upper plate from the movement along the detachment fault could have created the DCRG.

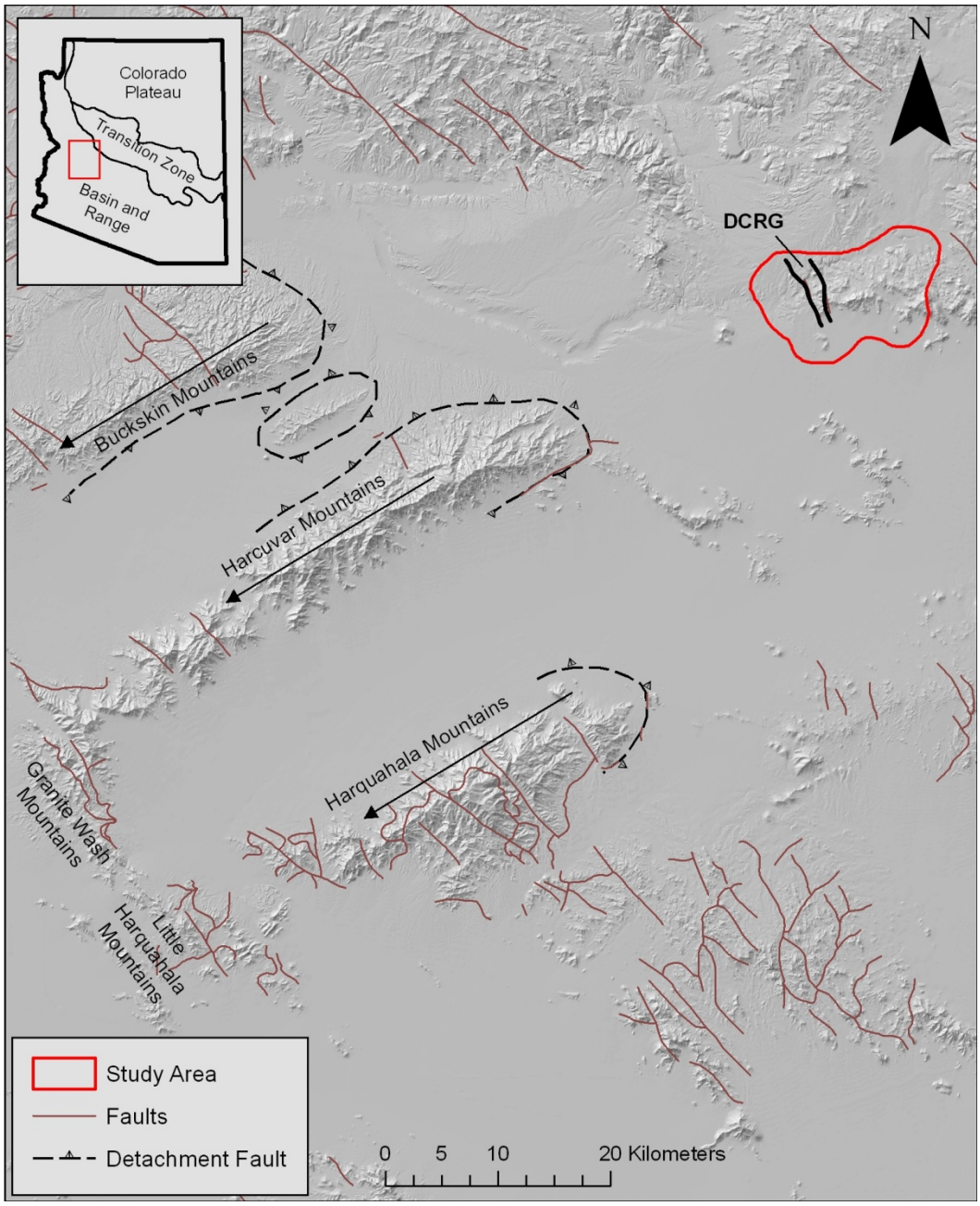


Figure 32 – Physiographic map of part of west-central Arizona. Faults are from Ludington et al (2005). Arrows show direction of shear-indicated movement of the lower plate relative to the upper plate in metamorphic core complexes (Spencer and Reynolds, 1991). DCRG is Date Creek Ranch Graben. Teeth are on upper plate of detachment fault.

## O’Neill Pass Fault Zone (OPFZ)

A linear feature, visible both on aerial imagery and physiographic maps, which traverses the study area from southeast to northwest, has been determined to be a fault zone (Plate 1). The name O’Neill Pass Fault Zone is herein suggested by the author because the weathering and erosion of the zone has created that pass in the mountains which carries one of the few geographic names shown on maps of the DCM. No indicators of relative motion of the fault blocks have been observed, but the author suspects that it is a normal fault with a down-thrown southern block which would make its style consistent with other parallel faults in the TZ to the north (Figure 33).

Rather than being a single fault plane, the OPFZ is a zone of brittle deformation ranging in width from 100-600 m. Though the surface is mainly weathered alluvium, fault breccias and other deformed rock are commonly found both in the loose surface material and exposed in outcrops visible in cross-cutting erosional gullies within the zone (Figure 34). Also common are slickenlines (Figure 35) both on outcrops and on epidote fracture fillings. Although the zone bounding faults have not been observed, their general surface location is thought to be constrained by the lines where large coherent outcrops are replaced by the alluvial weathered materials. A few smaller coherent outcrops are present within the fault zone but are considered to be slabs from the adjoining walls

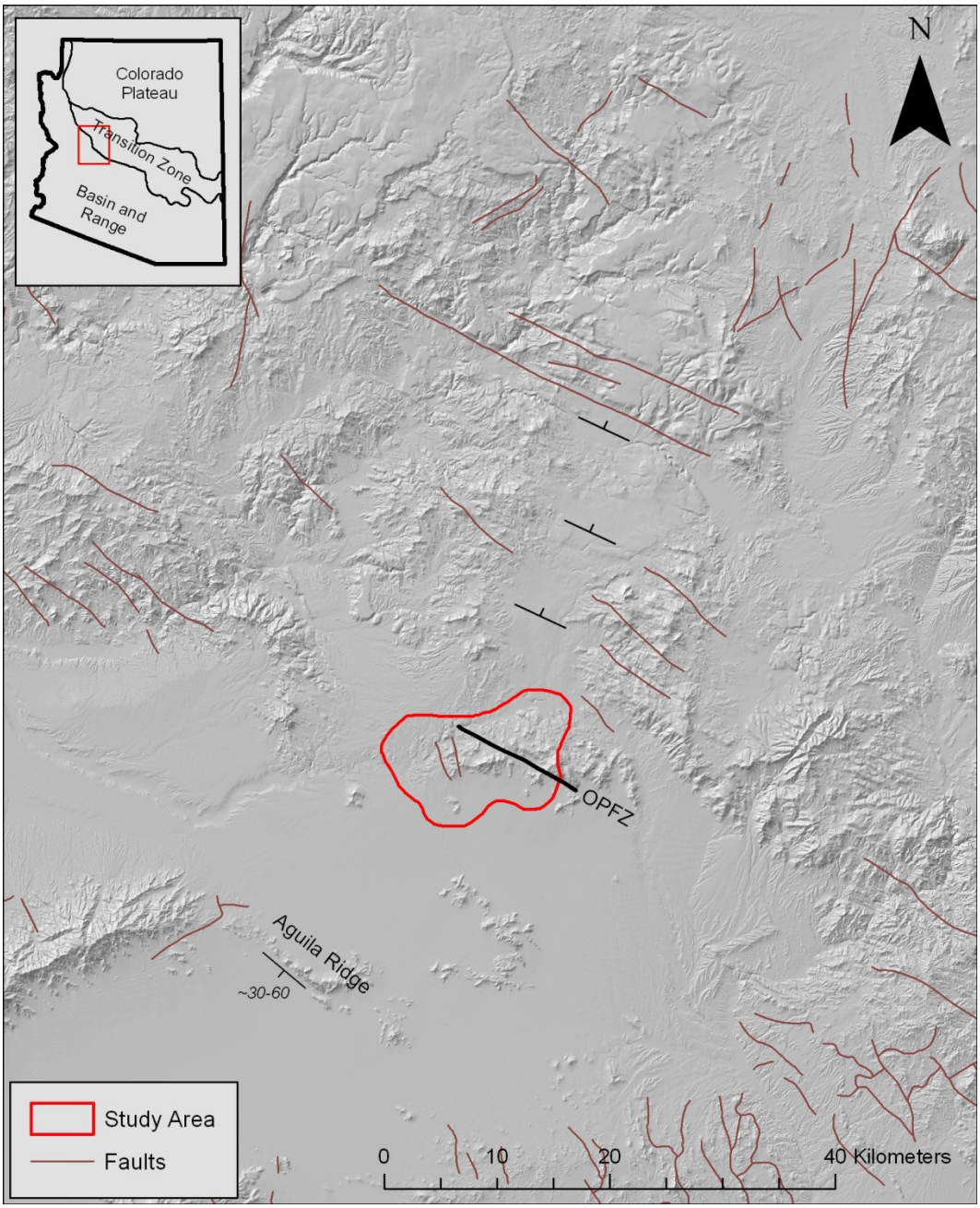


Figure 33 – Physiographic map of part of west-central Arizona. Faults are from Ludington et al (2005); dips at Aguila Ridge are from Reynolds and Spencer (1984). OPFZ is O'Neill Pass Fault Zone. Note the pervasive nature of the northwest-southeast fabric within the TZ.

entrained within the zone that have escaped significant deformation.

Massive quartz veins that parallel the zone are present in the eastern part of the OPFZ, some up to 2 m thick and displaying a boxwork-like internal fabric. Farther to the east, outside of the study area, a mafic dike has been observed, which also appears to have been emplaced within the fault zone.

The OPFZ is the southwesternmost visible fault in this part of the TZ (Figure 33). The next observed subparallel fault to the southwest is at Aguila Ridge, approximately 27 km (17 miles) away in the BR, where the block tilts to the southwest and the fault presumably dips to the northeast (Figure 31). Fault blocks within the TZ generally have a northward tilt as illustrated by the map and cross-section of Stimac et al (1987) for the Wickenburg Mountains southeast of the DCM. Tilt-block domains within the adjoining BR can have either a northeast or southwest tilt (Spencer and Reynolds, 1989). Based on the dips at Aguila Ridge and the map in Spencer and Reynolds (1989), it appears that the southwest tilted Whipple Domain is adjacent to the DCM.

Thin section photographs for a fault breccia sample from the OPFZ are in Appendix A as Figures A-45 and A-46.

Figure 34 – Block of fault breccia within the OPFZ exposed in an erosional gully located in the SW¼ of Sec. 11, T. 10 N., R. 7 W.

Figure 35 – Small block with fault surface exhibiting slickenlines within the OPFZ. Up is to the left. Outcrop located in the SW¼ of Sec. 11, T. 10 N., R. 7 W.

### Tertiary basin-fill (Tbf)

North and west of the DCM, basins and valleys are filled with Tbf, Bryant's (1995) Miocene-Pliocene basin-fill deposits. He places the thickness of the unit at perhaps as much as 1,000 m.

Evidence from the northeastern corner of the study area and surrounding terrain indicates that the unit in that area was previously at least 100 m thicker than today. Perched remnants of Tbf remain in the Weaver Mountains, Grayback Mountains, and DCM with a thickness of about 100 m and a base about 30 m above the nearest current edge of the deposit (Figure 36). This thickness represents only what is now remaining so it is possible that the original thickness was considerably greater.

A depositional surface in the Date Creek drainage at least 130 m higher than present has implications for the amount of bedrock covered as well as the amount of materials that has been transported from the area within the last approximately 15 million years, the age Bryant assigns to Tbf in this region.

## GEOLOGIC HISTORY OF THE DATE CREEK MOUNTAINS AREA

According to Whitmeyer and Karlstrom (2007), history of the area began over 2.5 Ga as a small plate of Archean crust they call Mojavia. At approximately 2.0-1.8 Ga, a juvenile arc formed to the east, the intervening space was filled with reworked Archean crust, and the whole

landmass began moving to the relative northeast toward the growing North American craton. The large juvenile crust terrain that makes up the Yavapai Province accreted to the relative southeast of the continent at about 1.76-1.72 Ga and shortly thereafter at 1.72-1.68 Ga, widespread granitoid intrusions were emplaced in the area, represented in the study area by units Xd and possibly XJgm, that would become much of the southwestern United States. More juvenile crust terrain accreted to the relative southeast edge of the continent at 1.69-1.65 Ga to form the Mazatzal Province and these too were intruded by granitoids during the period 1.65-1.60 Ga. From 1.48-1.35 Ga, A-type plutons intruded much of the southern part of the continent, represented by the Yj granites in the study area. For the remainder of the Proterozoic, accretion and rifting continued to occur at the continental margins, but apparently there was no tectonic activity taking place in the region of the study area.

During the Paleozoic, the region underwent periods of broad subsidence, deposition, and uplift (Blakey and Ranney, 2008). However, little evidence of this activity remains in southwestern Arizona as the thick sedimentary sequences that are present elsewhere, especially on the Colorado Plateau, have largely been removed through erosion, with the exception of the occasional remnant such as within the thrust sheets in the Harquahala Mountains.

In the Mesozoic, plate collision and accretion occurred along the continental margin southwest of the study area, resulting in significant

uplift and thrust faulting. At the same time, the Farallon and/or Kula oceanic plates were subducting beneath the region and during the Jurassic, an island arc system formed in southwestern Arizona (Tosdal et al, 1989) producing much igneous intrusive and extrusive activity, of which the J units in the study area were part.

During much of the Cenozoic, collisional forces continued to thicken the crust of the region, but when the trailing edge of the subducting plate was pulled beneath the continent, relative plate motions caused a change from a compressional regime to one of extension. This allowed for the graben-and-horst terrain of the BR to form and for the ductile (at the time) lower crust beneath the TZ to be forced up and to the southwest, beneath northeast dipping detachment surfaces, creating what would be known, following exposure, as metamorphic core complexes.

Also during the Cenozoic, significant volcanism was occurring throughout Arizona. Degraded volcanic edifices, vents, and large areas of lava flows exist in proximity to the DCM. Remnants of once more extensive blankets of volcanic rocks are present within the study area as represented by units Ta and Tv. In concert with the tectonic and volcanic activity of the period, much terrestrial sedimentation has taken place, especially over the grabens, where alluvial thicknesses can reach thousands of meters (Richard et al, 2007).

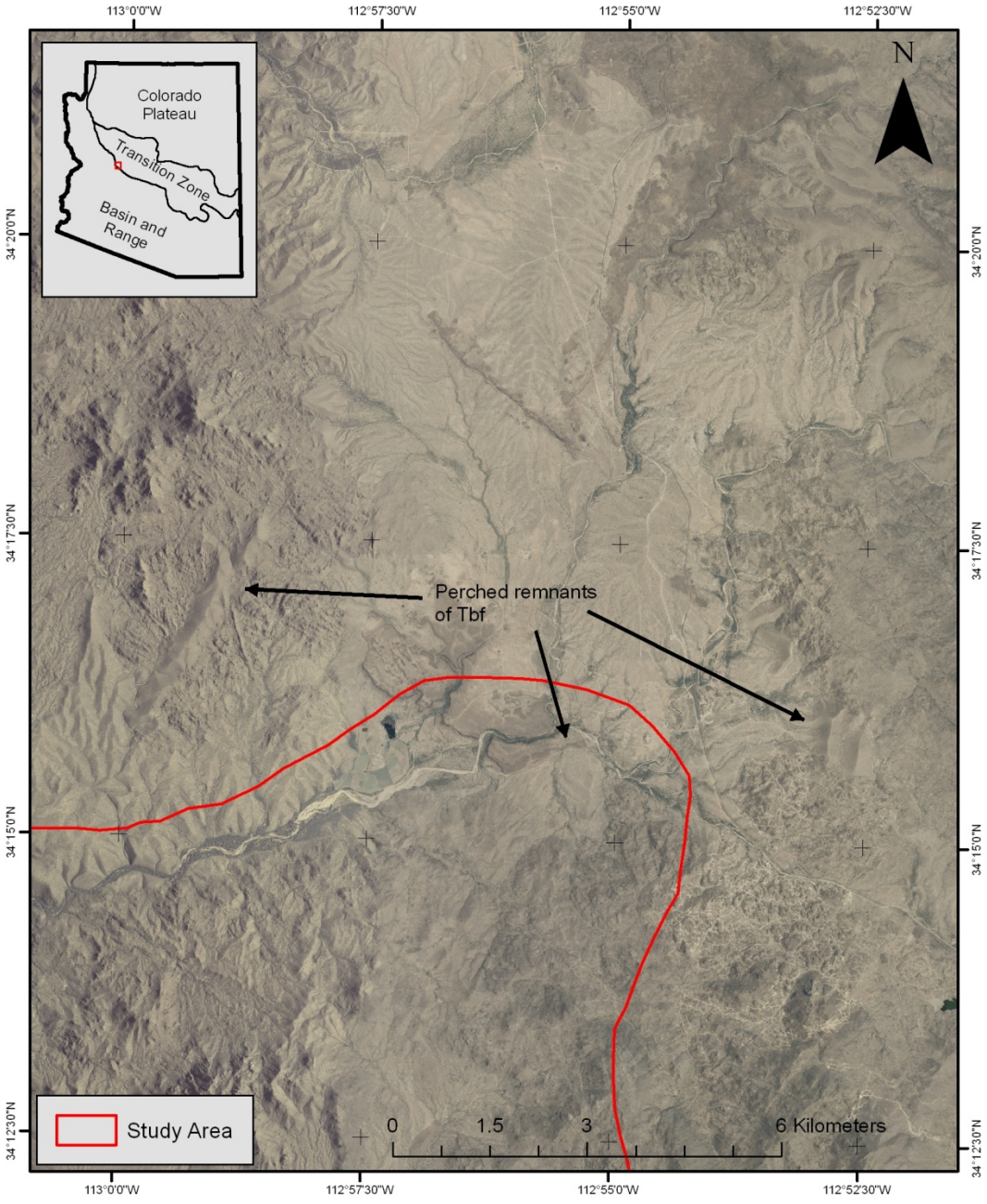


Figure 36 – DOQQs of northeastern part of study area and surrounding terrain showing locations of perched remnants of Tbf.

## CONVENTIONS

Numbers used in quantification and measurement are metric with the exception of elevation which is in feet, the same unit as the base map, followed by the approximate metric equivalent in parentheses.

The author has attempted to adhere to the latest naming conventions for igneous and metamorphic rocks as outlined in the most recent classification publications of the International Union of Geological Sciences (Fettes and Desmons, 2007; Le Maitre, 2002).

## REFERENCES


Anderson, C.A., Scholz, E.A., and Strobell, Jr., J.D. 1955, Geology and Ore Deposits of the Bagdad Area, Yavapai County, Arizona: U.S. Geological Survey Professional Paper 278, 103p, map scale 1:20,000.

Anderson, P., 1986, The Proterozoic tectonic evolution of Arizona: Tucson, University of Arizona, unpublished Ph.D. dissertation, 416 p.

Anderson, P., 1989a, Proterozoic plate tectonic evolution of Arizona: *in* Jenney, J.P., and Reynolds, S.J., editors, Geologic evolution of Arizona, Arizona Geological Society Digest 17, p. 17-55.

Anderson, P., 1989b, Stratigraphic framework, volcanic-plutonic evolution, and vertical deformation of the Proterozoic volcanic belts of central Arizona: *in* Jenney, J.P., and Reynolds, S.J., editors, Geologic evolution of Arizona, Arizona Geological Society Digest 17, p. 57-147.

Anderson, R.E., 1989, Tectonic evolution of the Intermontane System: Basin and Range, Colorado Plateau, and High Lava Plains, Chapter 10 *in* Pakiser, L.C., and W.D. Mooney, editors, Geophysical Framework of the Continental United States: Geological Society of America Memoir 172, p. 163-176.

Blakey, R., and Ranney, W., 2008, Ancient Landscapes of the Colorado Plateau: Grand Canyon Association, 156 p.

Brooks, W.E., 1985, Reconnaissance geologic map of part of McLendon Volcano, Yavapai County, Arizona: U.S. Geological Survey, Miscellaneous Field Studies Map MF-1783, scale 1:24,000.

Bryant, B., 1992, Geologic map of the Poachie Range, Mohave and Yavapai Counties, Arizona: U.S. Geological Survey, Miscellaneous Investigations Series Map I-2198, scale 1:25,000.

Bryant, B., 1995, Geologic map, cross sections, isotopic dates, and mineral deposits of the Alamo Lake 30' x 60' quadrangle, west-central Arizona: U.S. Geological Survey, Miscellaneous Investigations Series Map I-2489, scale 1:100,000.

Bryant, B., Wooden, J.L. and Nealey, L.D., 2001, Geology, Geochronology, geochemistry, and Pb-isotopic compositions of

Proterozoic rocks, Poachie region, west-central Arizona—A study of the east boundary of the Proterozoic Mojave crustal province: U.S. Geological Survey Professional Paper 1639, 54 p.

Demsey, K.A., 1988, Geologic map of Quaternary and upper Tertiary alluvium in the Phoenix North 30' x 60' quadrangle, Arizona (revised August 1990): Arizona Geological Survey, Open-File Report 88-17, scale 1:100,000.

Demsey, K.A., 1988, Quaternary geologic map of the Salome 30 x 60 minute quadrangle, west-central Arizona: Arizona Geological Survey, Open-File Report 88-04, scale 1:100,000.

DeWitt, E., Langenheim, V., Force, E., Vance, R.K., Lindberg, P.A., and Driscoll, R.I., 2008, Geologic map of the Prescott National Forest and the headwaters of the Verde River, Yavapai and Coconino Counties, Arizona: U.S. Geological Survey, Scientific Investigations Map SIM-2996, scale 1:100,000.

Farina, F., Dini, A., Innocenti, F., Rocchi, S., and Westerman, D.S., 2010, Rapid incremental assembly of the Monte Capanne pluton (Elba Island, Tuscany) by downward stacking of magma sheets: GSA Bulletin, v. 122, no. 9/10, p. 1463-1479.

Feddes, D., and Desmons, J., editors, 2007, Metamorphic rocks: a classification and glossary of terms: Cambridge University Press, 244 p.

Grubensky, M.J., 1989, Geologic map of the Vulture Mountains, west-central Arizona: Arizona Geological Survey, Map M-27, scale 1:24,000.

Grubensky, M.J. and Reynolds, S.J., 1988, Geologic map of the southeastern Vulture Mountains, west-central Arizona: Arizona Geological Survey, Open-File Report 88-09, scale 1:24,000.

Grubensky, M.J., Stimac, J.A., Reynolds, S.J., and Richard, S.M., 1987, Geologic map of the northeastern Vulture Mountains and vicinity, central Arizona: Arizona Geological Survey, Open-File Report 87-10, scale 1:24,000.

Le Maitre, R.W., 2002, Igneous rocks: a classification and glossary of terms, 2nd edition: Cambridge University Press, 236 p.

Ludington, S., Moring, B.C., Miller, R.J., Flynn, K.S., Hopkins, M.J., and Haxel, G.A., 2005, Preliminary integrated databases for the United States – Western States: California, Nevada, Arizona, and Washington: U.S. Geological Survey Open-File Report 2005-1305, digital data.

Reynolds, S.J. and Grubensky, M.J., 1993, Geologic map of the Phoenix North 30' x 60' quadrangle, central Arizona: Arizona Geological Survey, Open-File Report 93-17, scale 1:100,000.

Reynolds, S.J. and Spencer, J.E., 1984, Geologic map of the Aguila Ridge – Bullard Peak area, eastern Harcuvar Mountains, west-central Arizona: Arizona Geological Survey, Open-File Report 84-4, scale 1:24,000.

Reynolds, S.J., Spencer, J.E., DeWitt, E., White, D.C., and Grubensky, M.J., 1988, Geologic map of the Vulture Mine area, Vulture Mountains, west-central Arizona: Arizona Geological Survey Open-File Report 88-10, scale 1:24,000.

Reynolds, S.J., Spencer, J.E., Laubach, S.E., Cunningham, D, and Richard, S.M., 1993, Geologic map, geologic evolution, and mineral deposits of the Granite Wash Mountains, west-central Arizona: Arizona Geological Survey Open-File Report 89-04, 52 p., scale 1:24,000.

Reynolds, S.J., and Spencer, J.E., 1985, Reconnaissance geologic map of the Merritt Hills, Southwestern Yavapai County, Arizona: Arizona Geological Survey, Open-File Report 85-5, scale 1:24,000.

Richard, S.M., Shipman, T.C., Greene, L.C., and Harris, R.C., 2007, Estimated depth to bedrock in Arizona: Arizona Geological Survey, Digital Geologic Map Series DGM-52, v. 1.0, 9 p., map scale 1:1,000,000.

Richard, S.M., Spencer, J.E., and Reynolds, S.J., 1994, Geologic map of the Salome 30' x 60' quadrangle, west-central Arizona: Arizona Geological Survey, Open-File Report 94-17, scale 1:100,000.

Spencer, J.E., Richard, S.M., and Ferguson, C.A., 2001, Cenozoic structure and evolution of the boundary between the Basin and Range and Transition Zone provinces in Arizona *in* Erskine, M.C., J.E. Faulds, J.M. Bartley, and P.D. Rowley, editors, The Geologic Transition, High Plateaus to Great Basin – A Symposium and Field Guide, The Macklin Volume, Utah Geological Association

Publication 30 and Pacific Section, American Association of Petroleum Geologists Publication GB 78, p. 273-289.

Spencer, J.E., and Reynolds, S.J., 1989, Middle Tertiary tectonics of Arizona and adjacent areas *in* Jenney, J.P., and S.J. Reynolds, editors, Geologic evolution of Arizona: Arizona Geological Society Digest 17, p. 539-574.

Spencer, J.E., and Reynolds, S.J., 1991, Tectonics of mid-Tertiary extension along a transect through west central Arizona: Tectonics, vol. 10, no. 6, p. 1204-1221.

Stimac, J.A., Fryxell, J.E., Reynolds, S.J., Richard, S.M., Grubensky, M.J., and Scott, E.A., 1987, Geologic map of the Wickenburg, southern Buckhorn, and northwestern Hieroglyphic Mountains, central Arizona: Arizona Geological Survey Open-File Report 87-09, scale 1:24,000.

Tosdal, R.M., Haxel, G.B., and Wright, J.E., 1989, Jurassic geology of the Sonoran Desert region, southern Arizona, southeastern California, and northernmost Sonora: Construction of a continental-margin magmatic arc *in* Jenney, J.P., and S.J. Reynolds, 1989, Geologic evolution of Arizona: Arizona Geological Society Digest 17, p. 397-434.

Trapp, R.A., and Reynolds, S.J., 1998, Physiographic areas in Arizona used by the Arizona Geological Survey: Arizona Geological Survey, Digital Information Series DI-10, 4 p., 1 disk.

Whitmeyer, S.J., and Karlstrom, K.E., 2007, Tectonic model for the Proterozoic growth of North America: Geosphere, v. 3, no. 4, p. 220-259.

Williams, M.L., 1991, Overview of Proterozoic metamorphism in Arizona, *in* Karlstrom, K.E., editor, Proterozoic geology and ore deposits of Arizona: Arizona Geological Society Digest 19, p. 11-26.

Wilson, E.D., 1958, Geologic map of Yavapai County, Arizona: Arizona Bureau of Mines, University of Arizona, Tucson, scale 1:375,000.

# APPENDIX A

## SELECTED THIN SECTION PHOTOGRAPHS OF GEOLOGIC UNITS

All photos are in sets of two of the same view on a single page with the odd-numbered (top) photos taken under crossed-polars and the even-numbered (bottom) photos taken with plane-polarized light. Width of field-of-view of all photos is approximately 2mm.

Figures A-1 and A-2 – Hornblende-quartz-plagioclase gneiss from unit Xm. Two twinned plagioclase crystals in lower left, gray to cream colored quartz crystals scattered about, and green, brown, and dark brown amphibole, probably hornblende as indicated by 120º cleavage visible in some crystals, filling most of view.

Figures A-3 and A-4 – Feldspar-quartz granofels from unit Xm. Microcline crystals in upper right displaying cross-hatched twinning, white to cream to dark gray quartz crystals fill most of view.

Figures A-5 and A-6 – Fine-grained granite from unit Jgf. Large yellow-stained K-feldspar crystal in center, white to gray crystals of quartz, euhedral brown hornblende crystal above left of center, small square plagioclase crystal below right of center, and small biotite at top edge of view left of center.

Figures A-7 and A-8 – Megacrystic granite from unit XJgm. Large twinned plagioclase filling much of top half of view with brown biotite in lower half and gray quartz on right and left.

Figures A-9 and A-10 – Megacrystic granite from unit XJgm. Myrmekite (intergrowth of quartz and plagioclase) in center of view, plagioclase on left and quartz on right.

Figures A-11 and A-12 – Megacrystic granite from unit XJgm. Yellow-stained K-feldspar filling most of view including large twinned crystal in upper left, white to gray areas in right half mostly quartz, and brown biotite in lower right.

Figures A-13 and A-14 – Felsic dike. Large microcline crystal in center displaying cross-hatched twinning, with gray to cream colored quartz in rest of view.

Figures A-15 and A-16 – Diorite porphyry from unit Xd. Large twinned hornblende phenocryst with included plagioclase crystals fills most of view, groundmass in upper right and lower left mostly plagioclase few small quartz crystals.

Figures A-17 and A-18 – Diorite porphyry from unit Xd. Twinned and zoned plagioclase crystal in middle with brown biotite to the right and bottom, with groundmass of mostly plagioclase.

Figures A-19 and A-20 – Monzogabbro from unit Yjz. Mostly twinned crystals of plagioclase with few small crystals of brown biotite, and hornblende in bottom right.

Figures A-21 and A-22 – Monzonite from unit Yjz. Twinned plagioclase crystals with brown biotite crystals in groundmass of yellow-stained K-feldspar.

Figures A-23 and A-24 – Megacrystic granite from unit Yjm. Large twinned K-feldspar crystal fills view with cross-hatched twinning visible in top half, small brown biotite crystal in upper left and a few very small gray plagioclase crystals scattered about.

Figures A-25 and A-26 – Fine-grained granite from unit Yjf. Mostly yellow-stained K-feldspar with line of brown biotite crystals across upper half, and a few gray to white quartz crystals.

Figures A-27 and A-28 – Monzonite from unit Yjz. Twinned plagioclase crystals with brown and green hornblende crystals, some of groundmass probably yellow-stained K-feldspar, square opaque possibly pyrite.

Figures A-29 and A-30 – Monzonite from unit Yjz. Unknown mineral (chlorite?) vein diagonally across view, minor gray plagioclase and brown to green hornblende, much of mineral assemblage unidentified.

Figures A-31 and A-32 – Granite porphyry from unit Yg. Yellow-stained K-feldspar with gray quartz on right and upper and lower left corners, unknown euhedral opaque on left edge.

Figures A-33 and A-34 – Medium-grained granite from unit Jg. Yellow-stained K-feldspar on right, brown biotite on left, and quartz in middle.

Figures A-35 and A-36 – Basaltic lava from unit Tv2. Olivine (?) crystals and small plagioclase lathes in a microcrystalline groundmass.

Figures A-37 and A-38 – Vitrophyre from unit Tv1. Olivine (?) crystal in center with plagioclase in lower left, in glassy groundmass.

Figures A-39 and A-40 – Rhyolite welded tuff from unit Tv1. Gray quartz crystals in lower right with glassy groundmass.

Figures A-41 and A-42 – Ash-fall tuff from unit Tv2. Crystals of twinned-plagioclase and biotite in center and quartz in upper left in groundmass of glassy shards.

Figures A-43 and A-44 – Mafic dike. Hornblende (?).

Figures A-45 and A-46 – Fault breccia from O'Neill Pass fault zone.

References Used in Mineral Identification

Delvigne, J.E., 1998, Atlas of micromorphology of mineral alteration and weathering: The Canadian Mineralogist, Special Publication 3, 494 p.

MacKenzie, W.S., and Adams, A.E., 1994, A colour atlas of rocks and minerals in thin section: London, UK, Manson Publishing, 192 p.

MacKenzie, W.S., Donaldson, C.H., and Guilford, C., 1982, Atlas of igneous rocks and their texture: London, UK, Pearson Prentice Hall, 148 p.

MacKenzie, W.S., and Guilford, C., 1980, Atlas of rock-forming minerals in thin section: London, UK, Pearson Prentice Hall, 98 p.

Melgarejo, J.C., and Martin, R.F., 2011, Atlas of non-silicate minerals in thin section: The Canadian Mineralogist, Special Publication 7, 522 p.

Perkins, D., and Henke, K.R., 2004, Minerals in thin section, second edition: Upper Saddle River, New Jersey, Pearson Prentice Hall, 163 p.

Philpotts, A.R., 2003, Petrography of igneous and metamorphic rocks: Prospect Heights, Illinois, Waveland Press, Inc., 178 p.

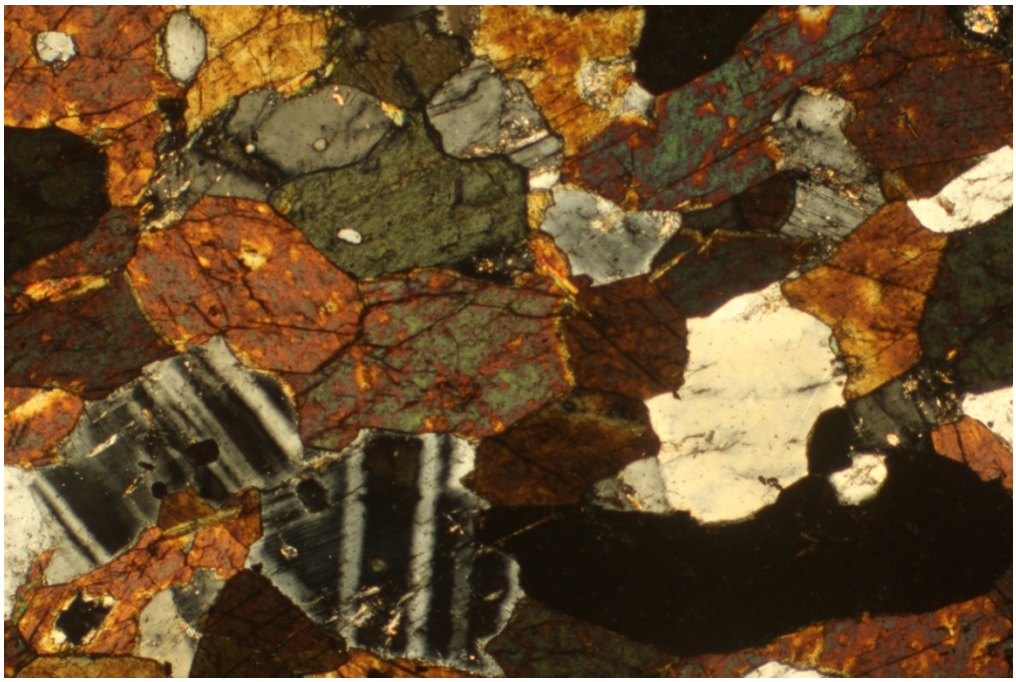

Figure A-1 – See caption at beginning of Appendix A.

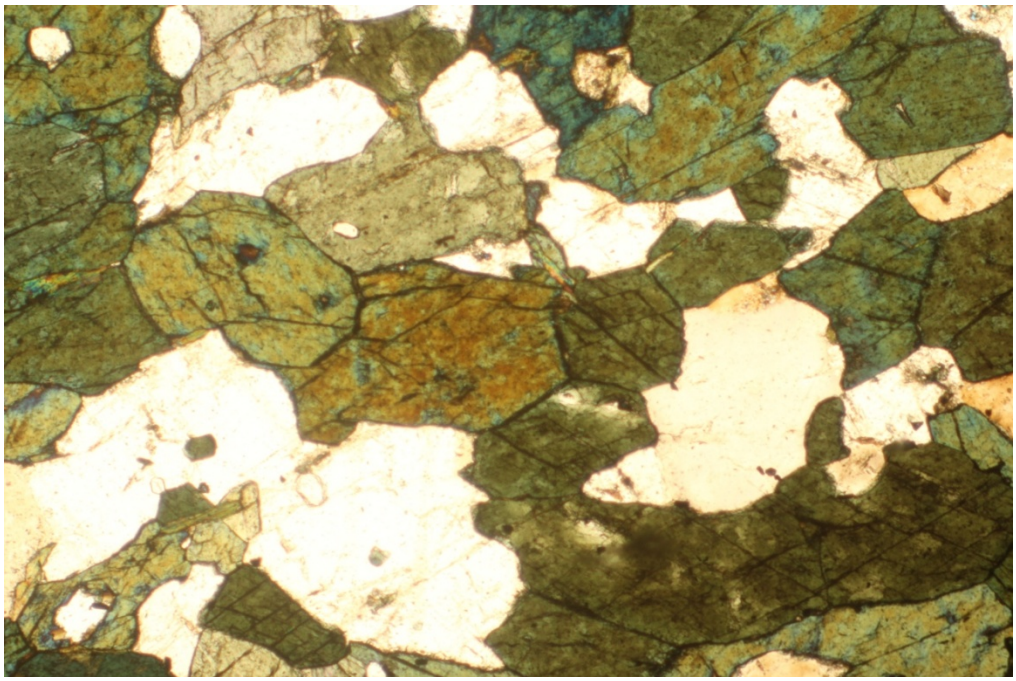

Figure A-2 – See caption at beginning of Appendix A.

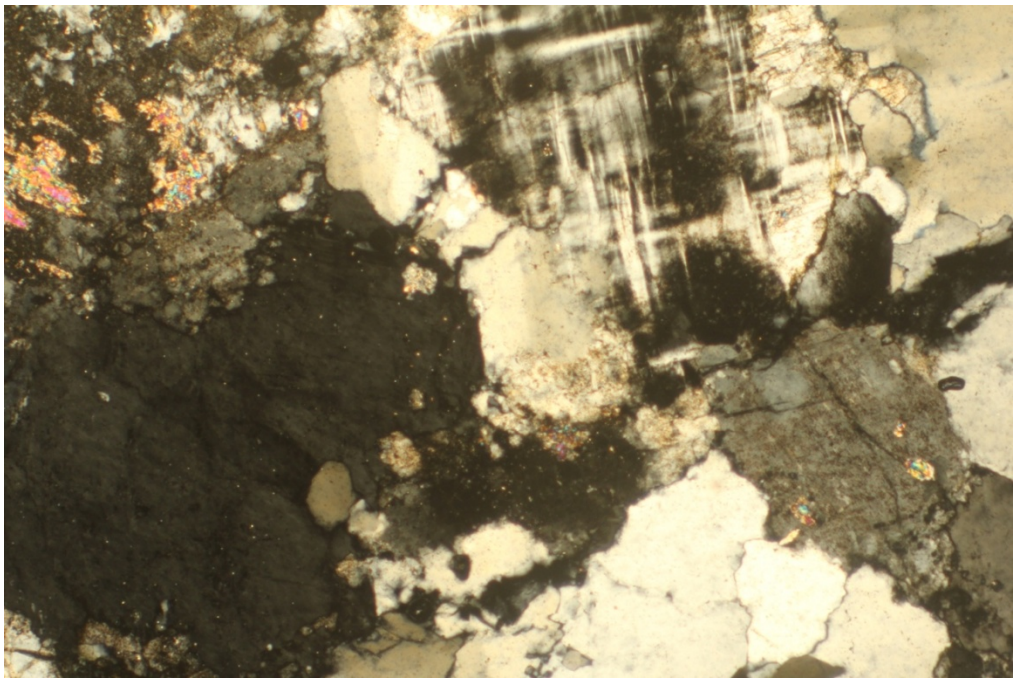

Figure A-3 – See caption at beginning of Appendix A.

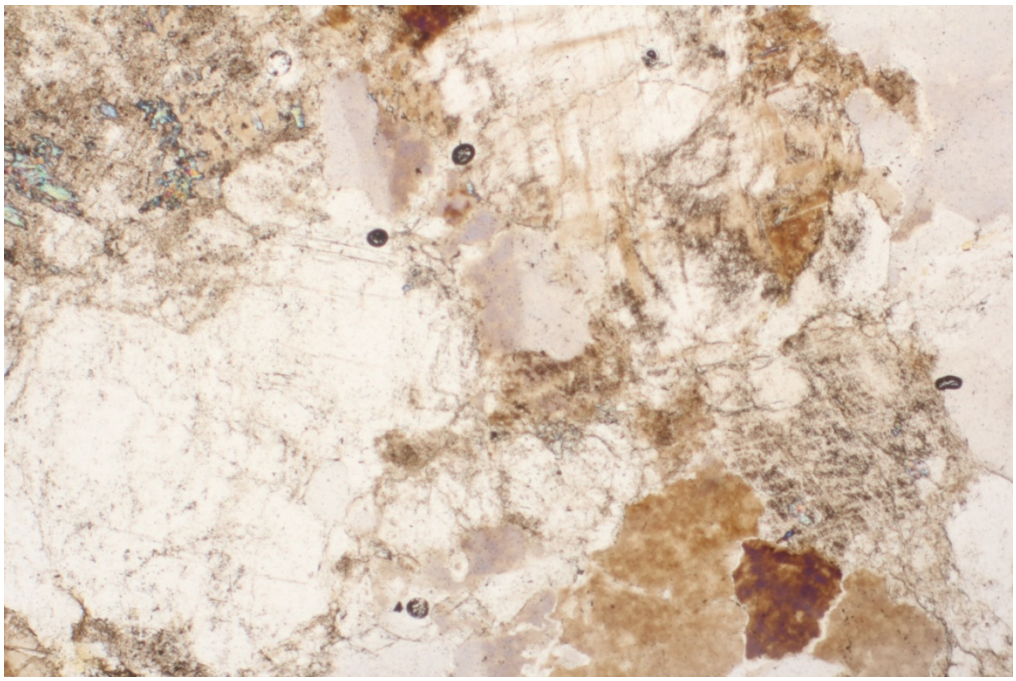

Figure A-4 – See caption at beginning of Appendix A.

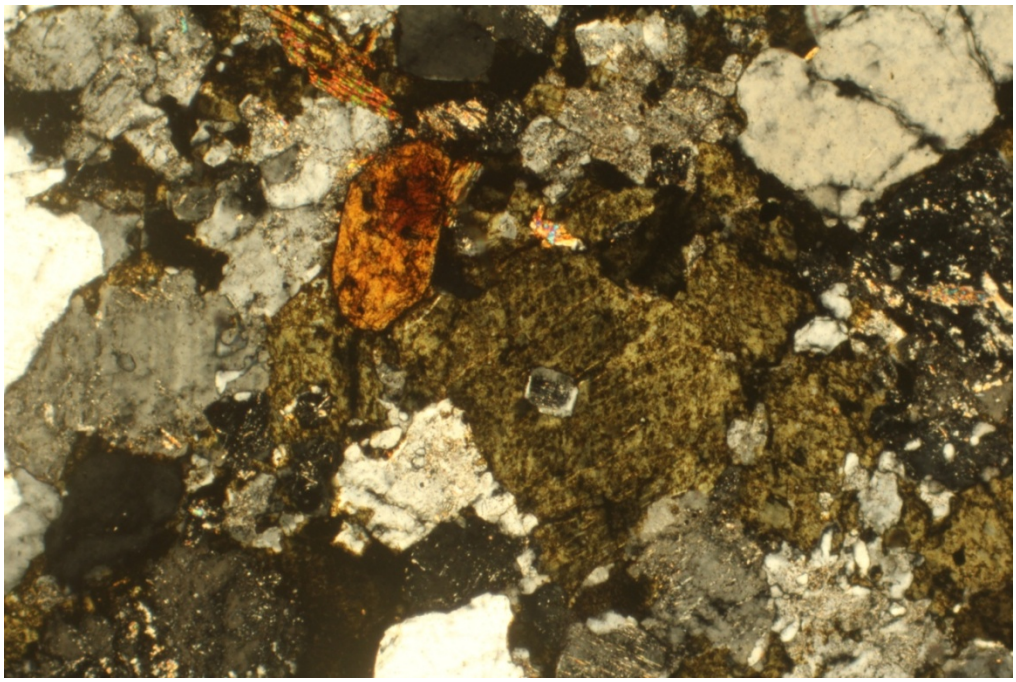

Figure A-5 – See caption at beginning of Appendix A.

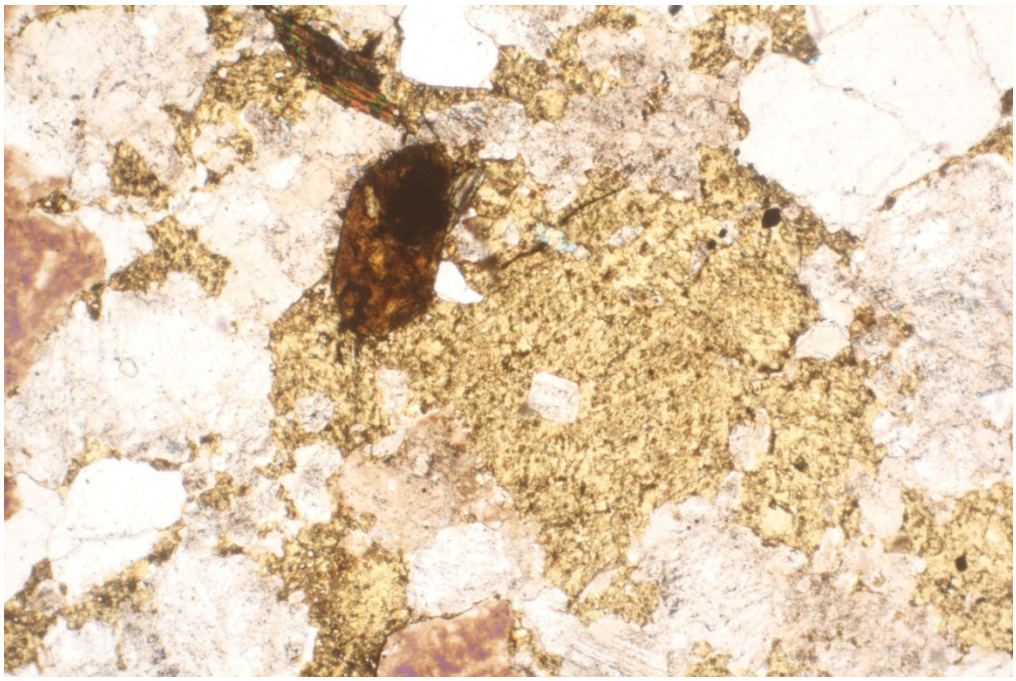

Figure A-6 – See caption at beginning of Appendix A.

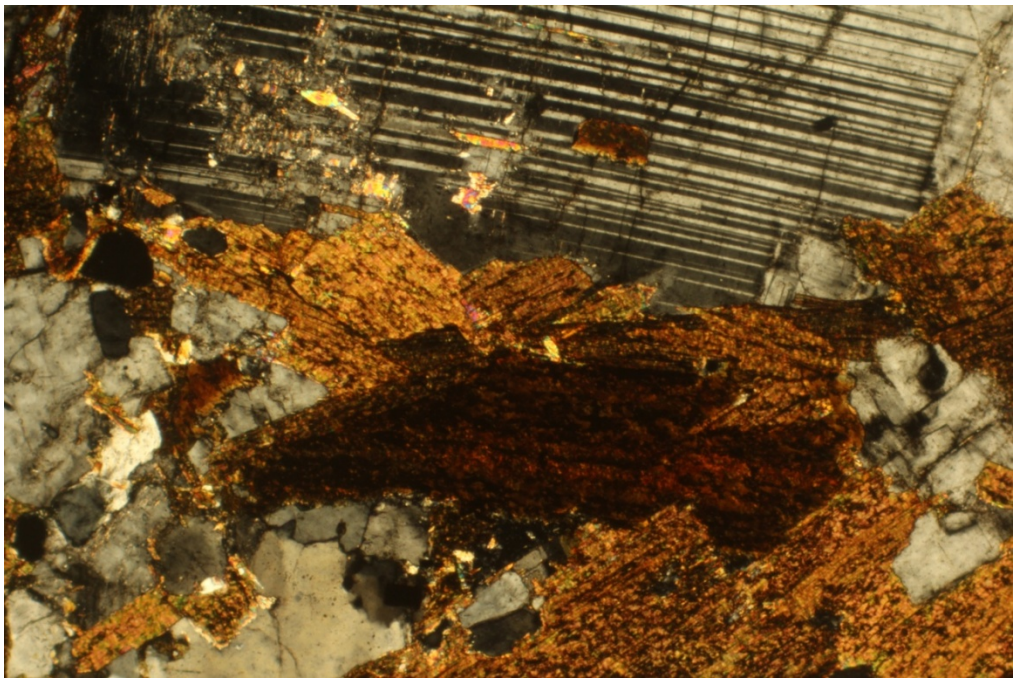

Figure A-7 – See caption at beginning of Appendix A.

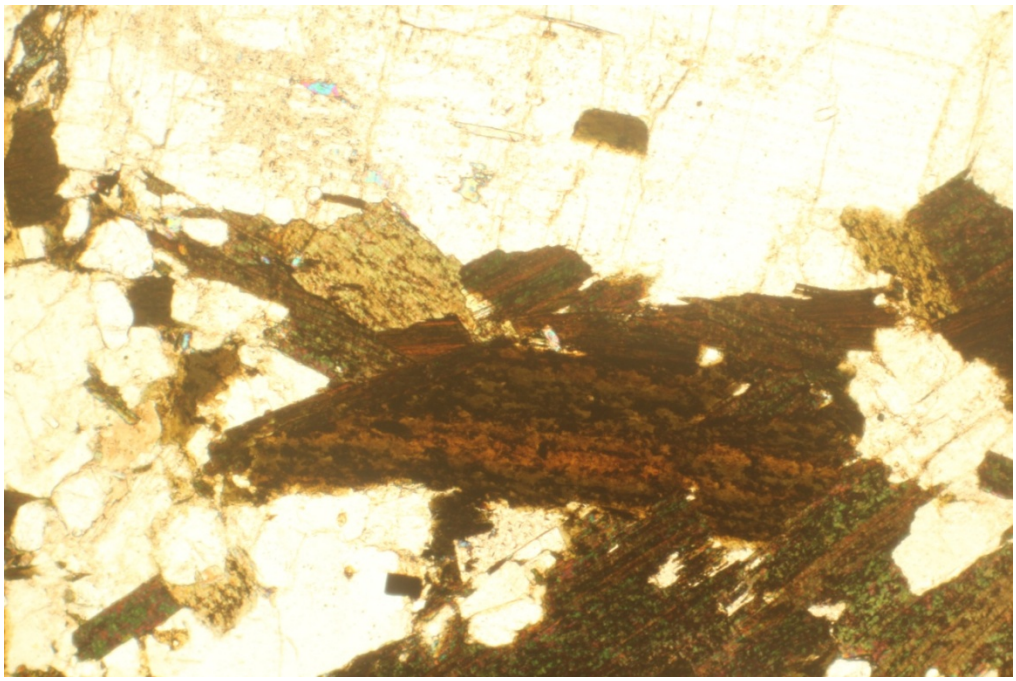

Figure A-8 – See caption at beginning of Appendix A.

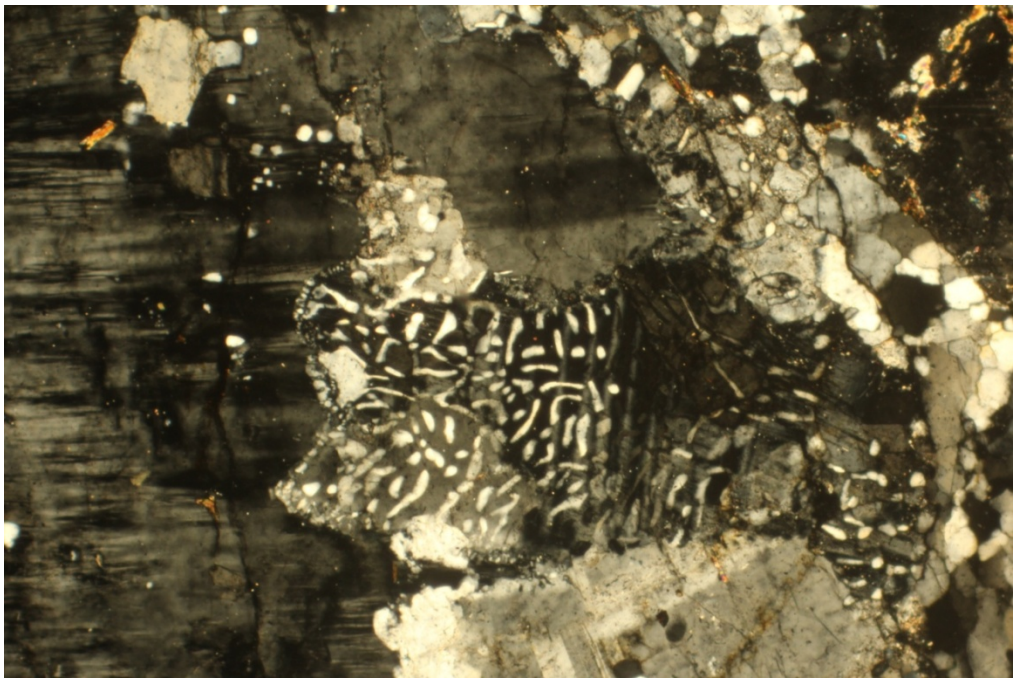

Figure A-9 – See caption at beginning of Appendix A.

Figure A-10 – See caption at beginning of Appendix A.

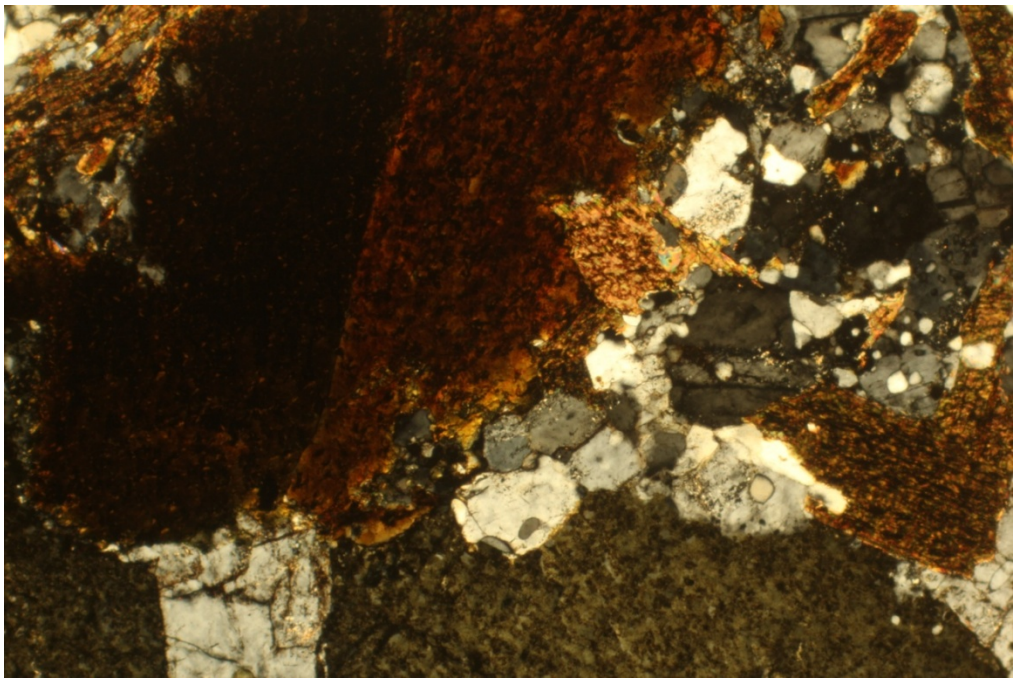

Figure A-11 – See caption at beginning of Appendix A.

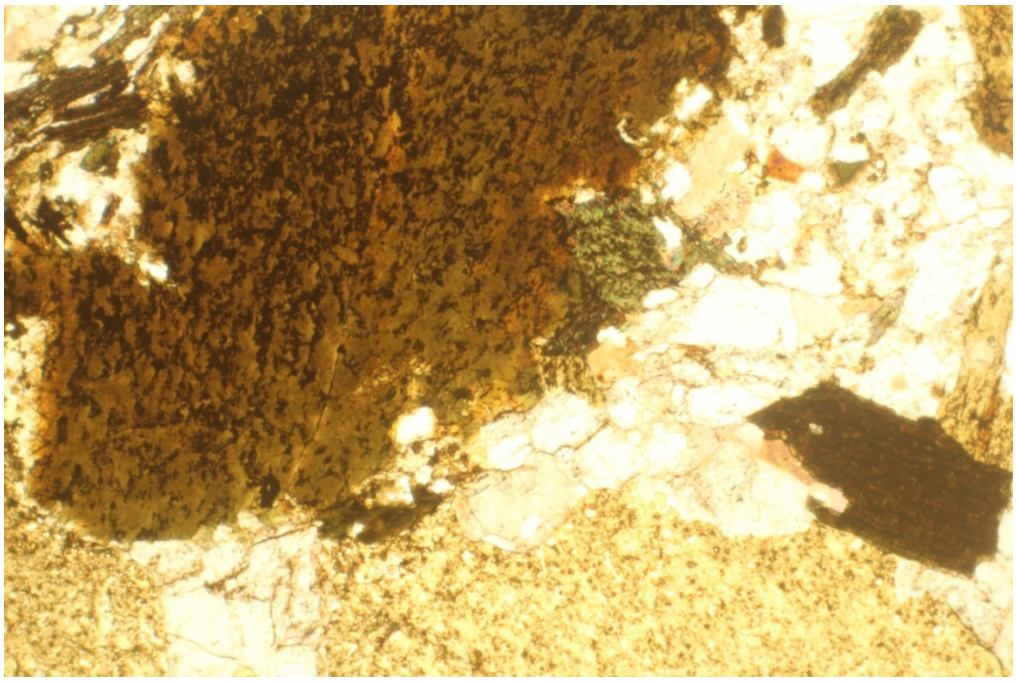

Figure A-12 – See caption at beginning of Appendix A.

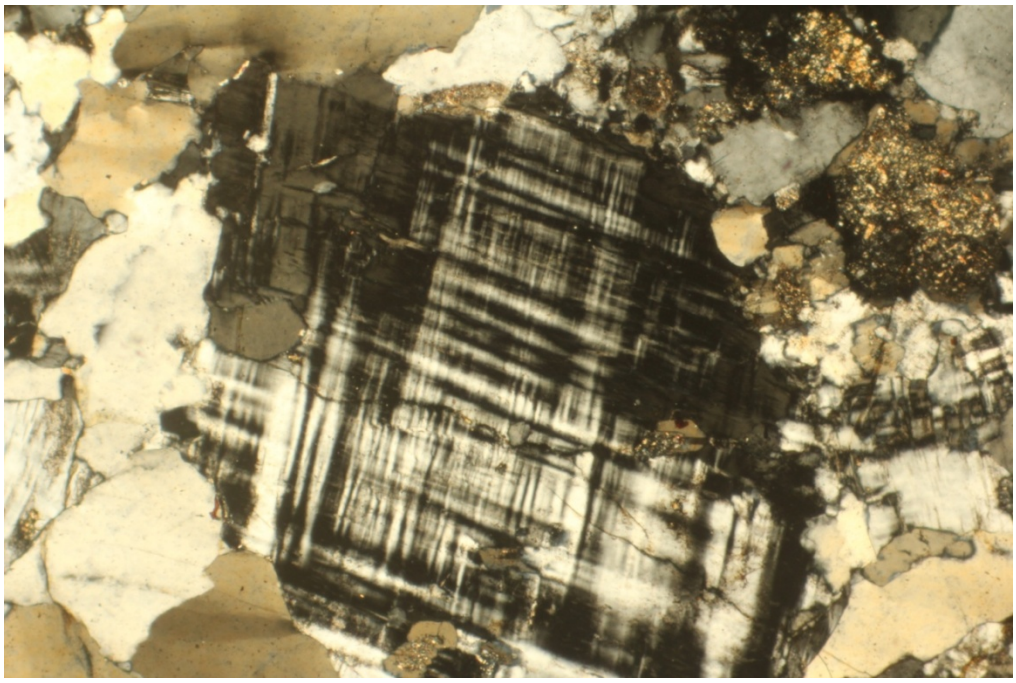

Figure A-13 – See caption at beginning of Appendix A.

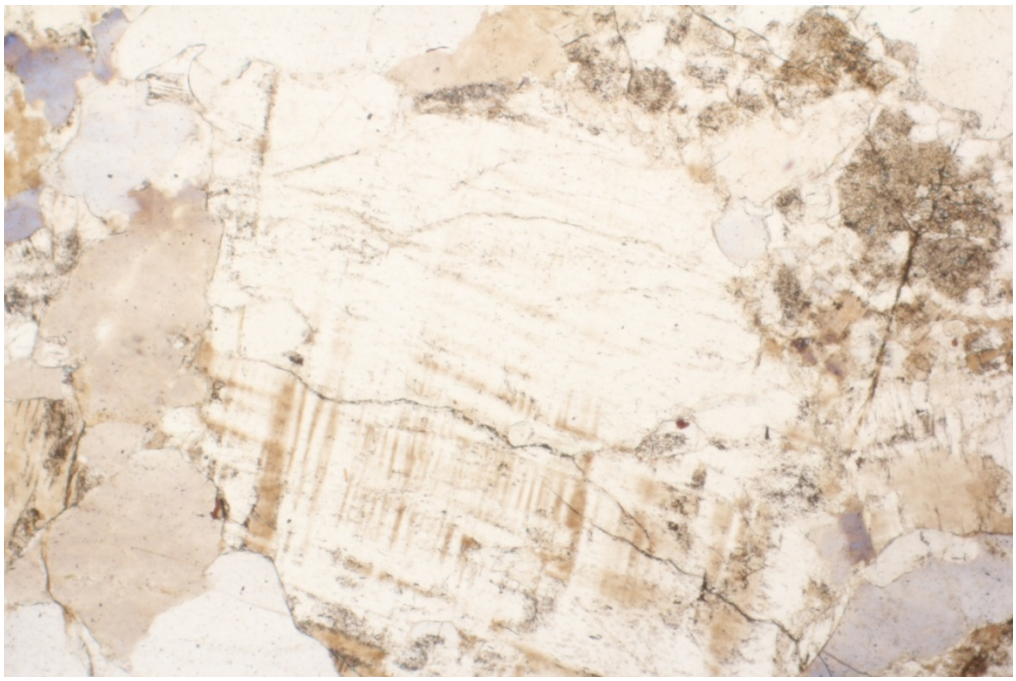

Figure A-14 – See caption at beginning of Appendix A.

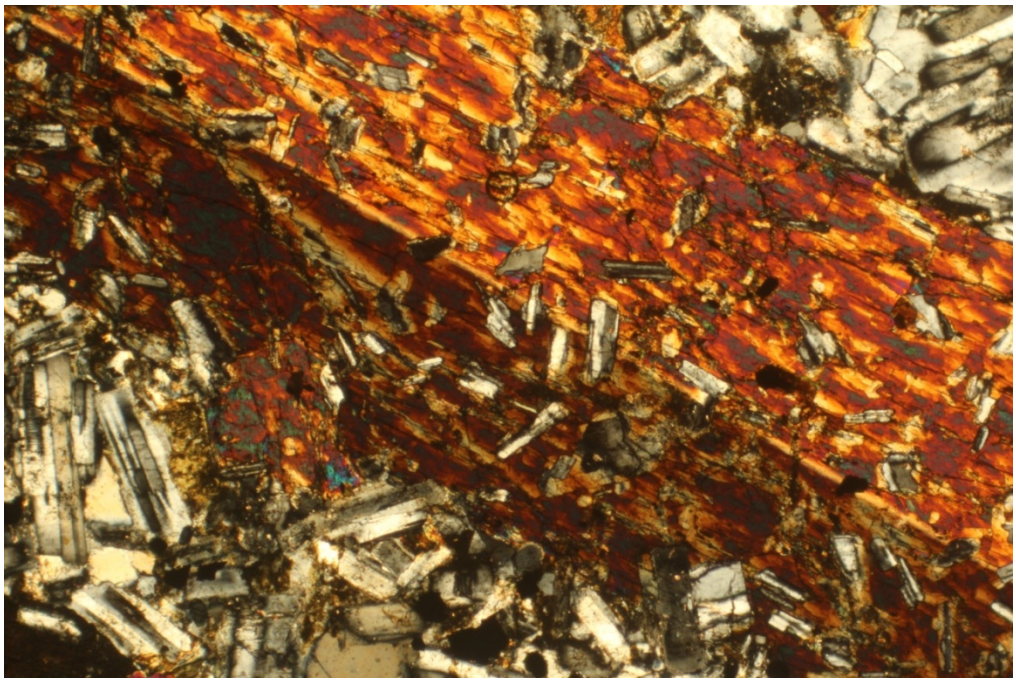

Figure A-15 – See caption at beginning of Appendix A.

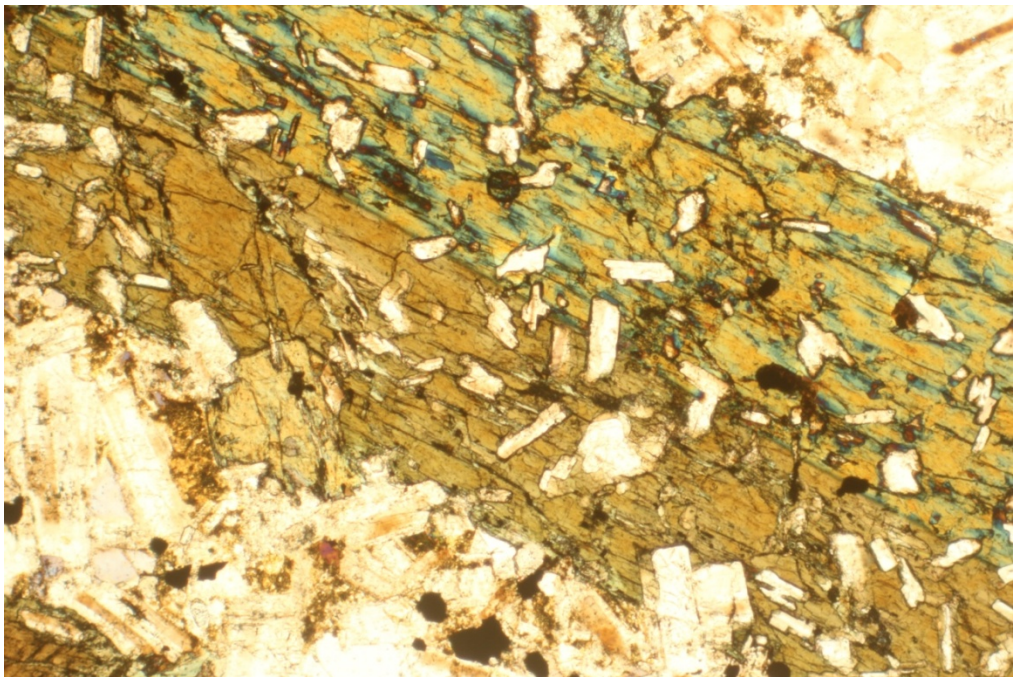

Figure A-16 – See caption at beginning of Appendix A.

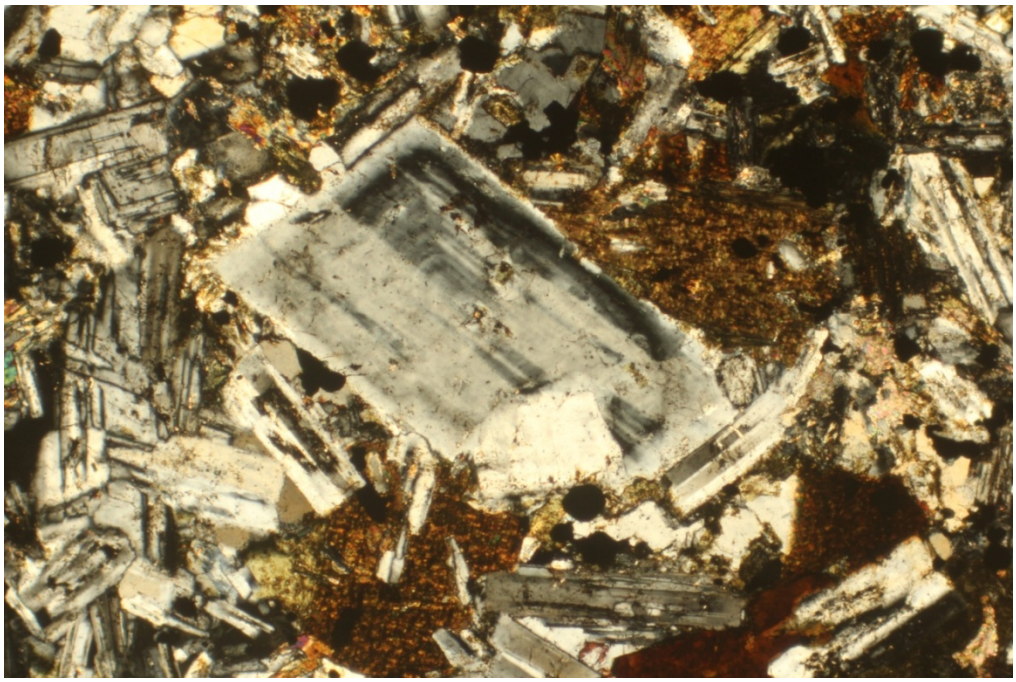

Figure A-17 – See caption at beginning of Appendix A.

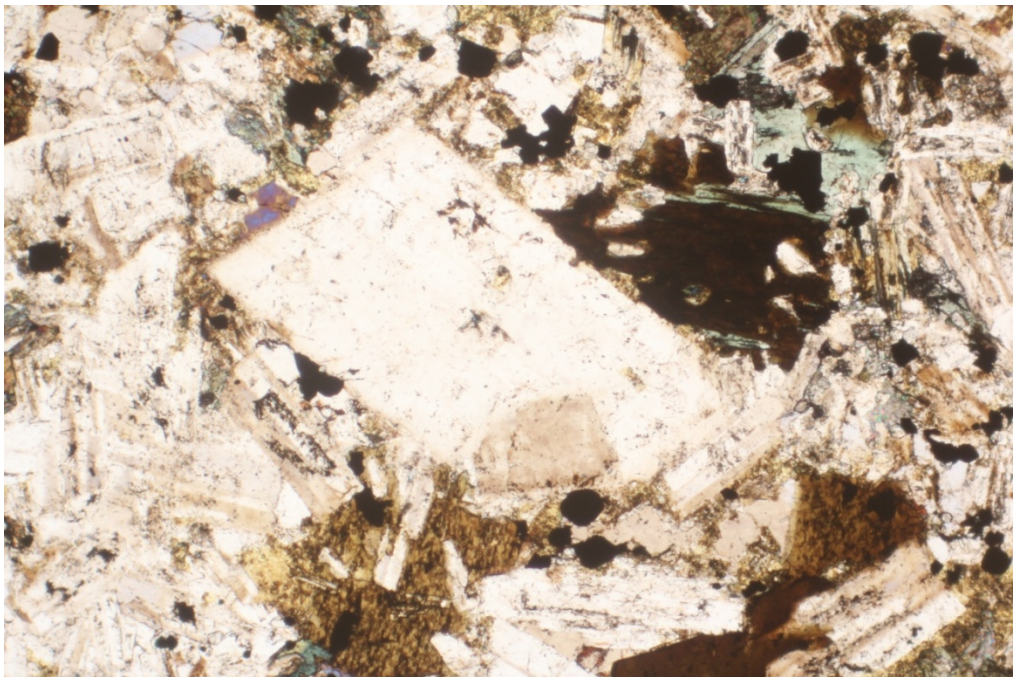

Figure A-18 – See caption at beginning of Appendix A.

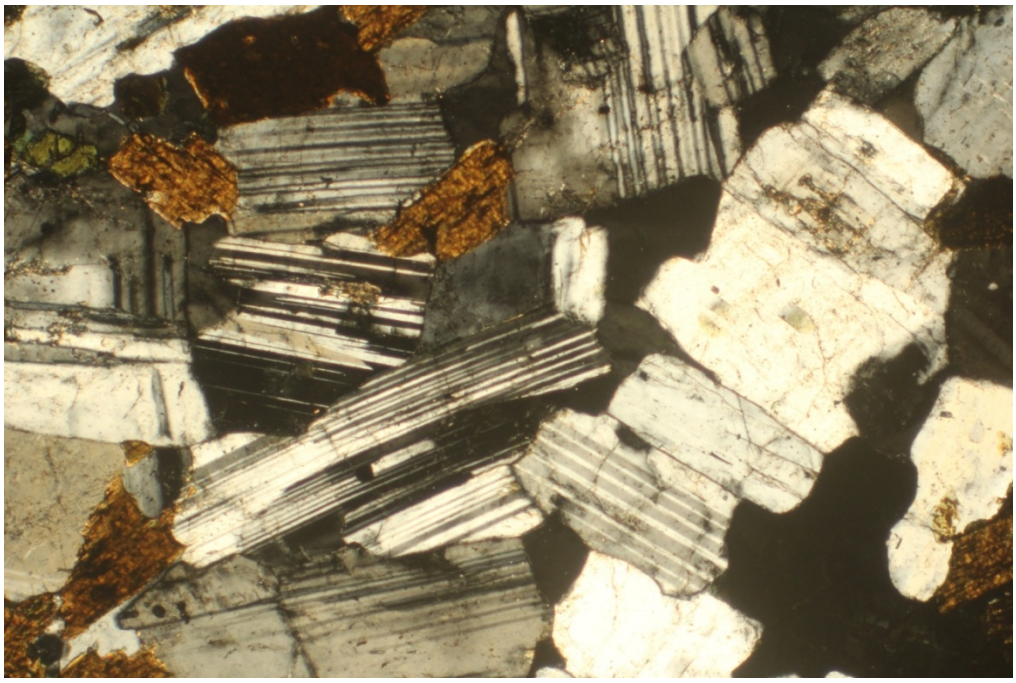

Figure A-19 – See caption at beginning of Appendix A.

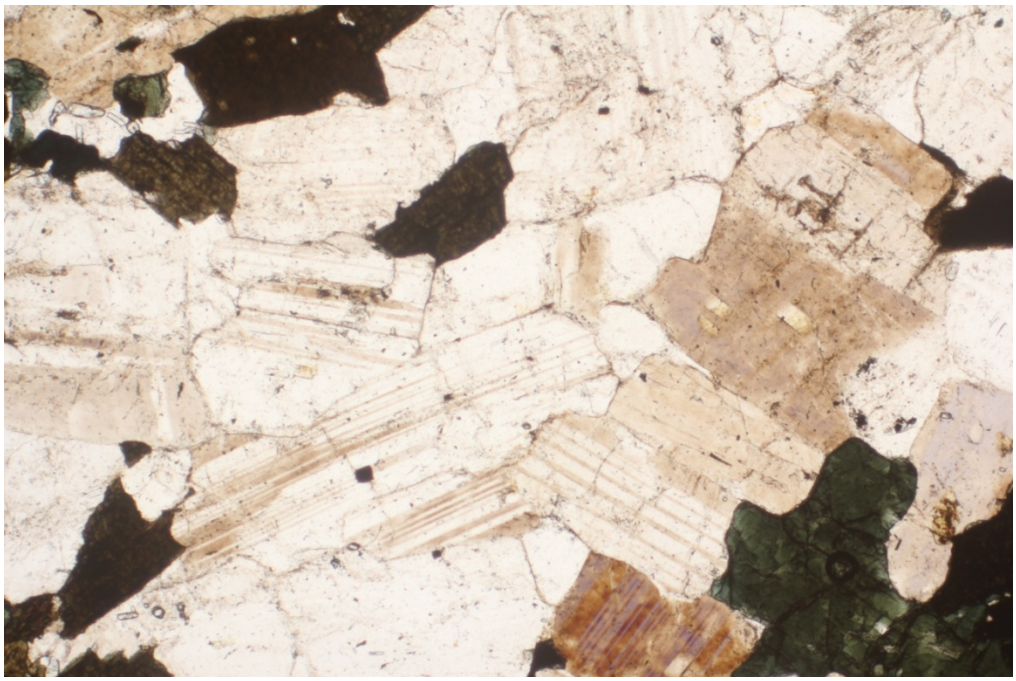

Figure A-20 – See caption at beginning of Appendix A.

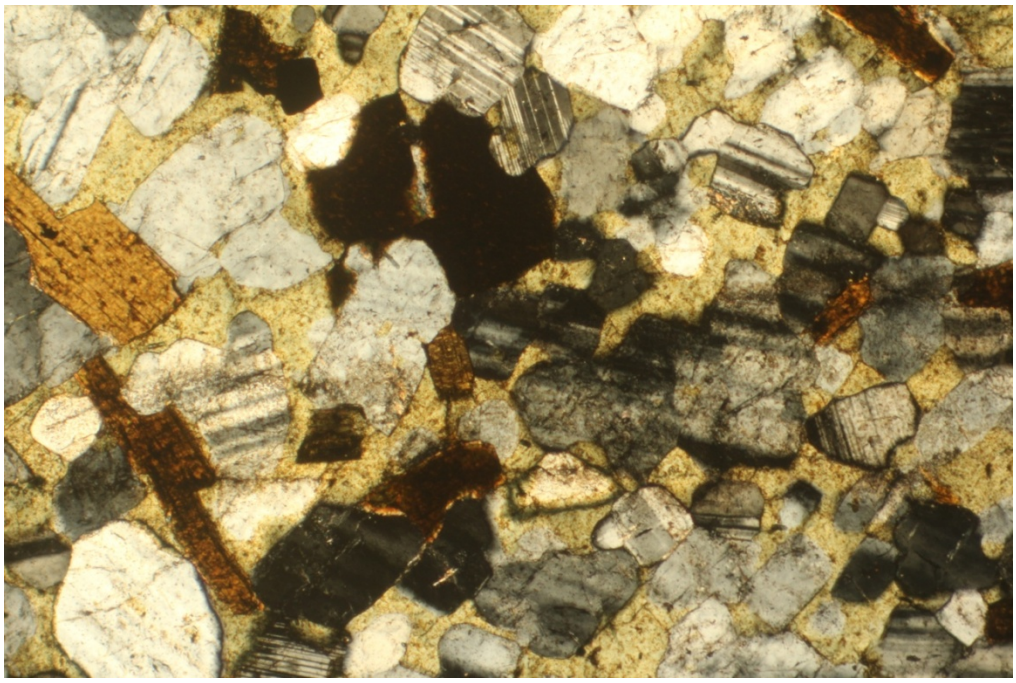

Figure A-21 – See caption at beginning of Appendix A.

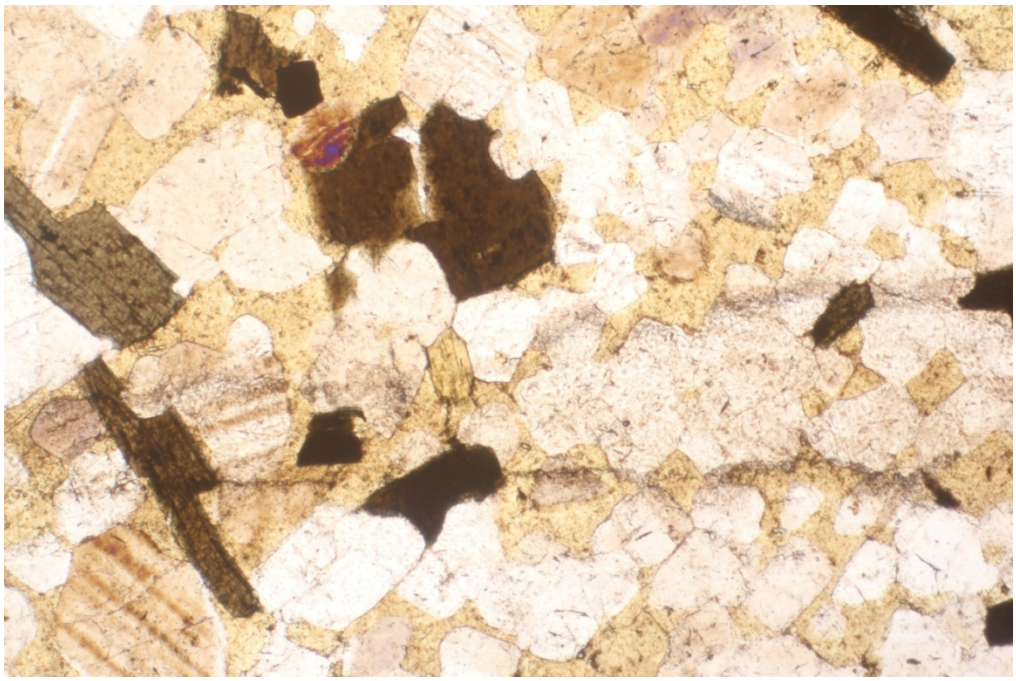

Figure A-22 – See caption at beginning of Appendix A.

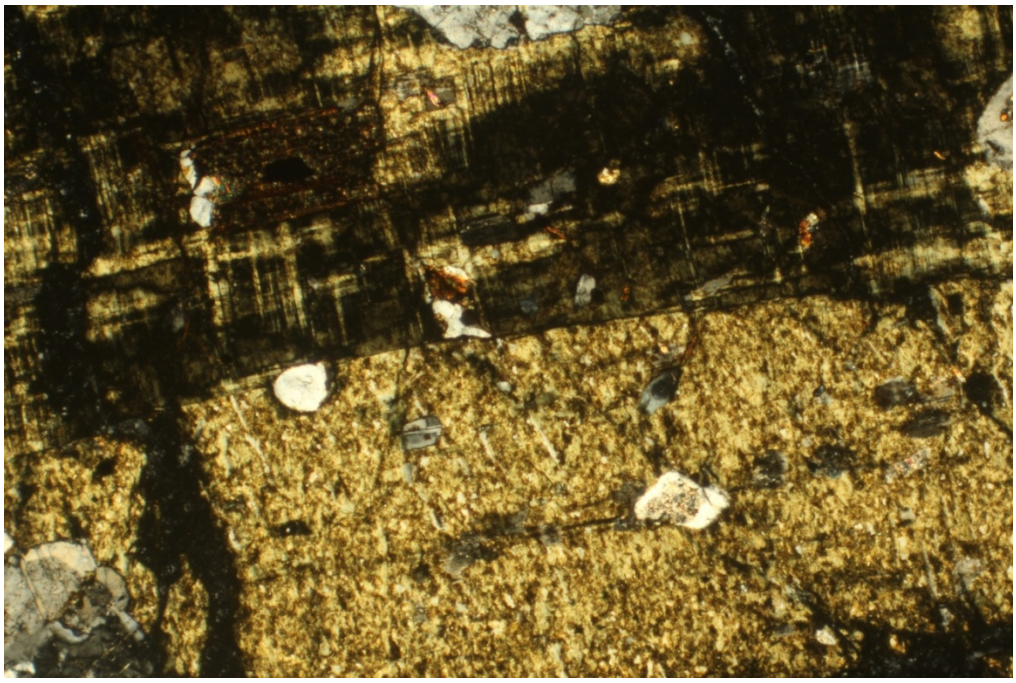

Figure A-23 – See caption at beginning of Appendix A.

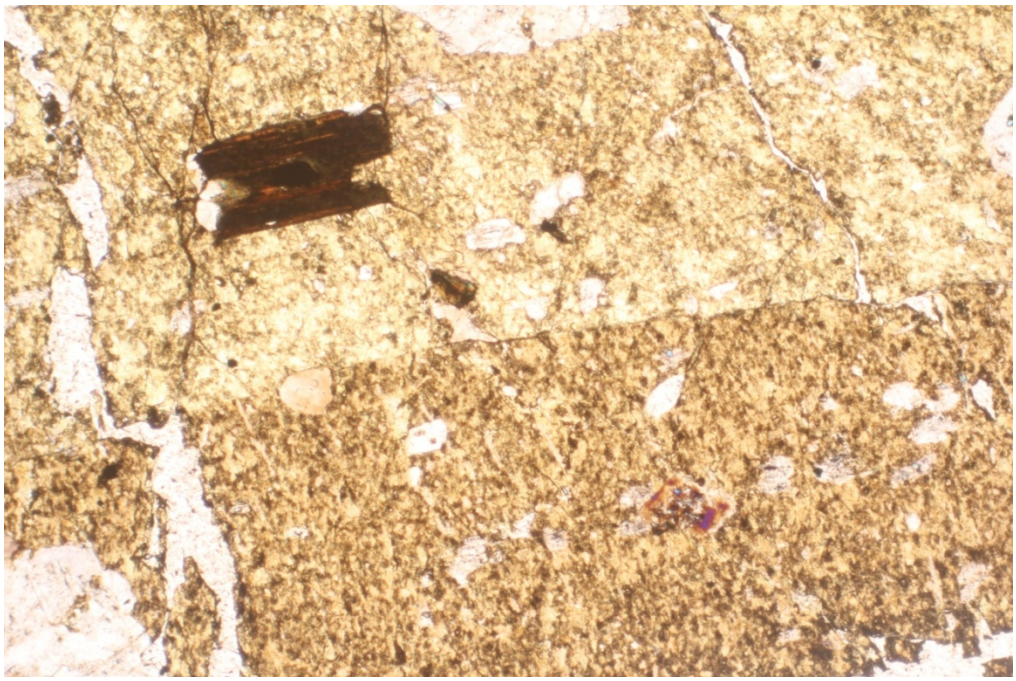

Figure A-24 – See caption at beginning of Appendix A.

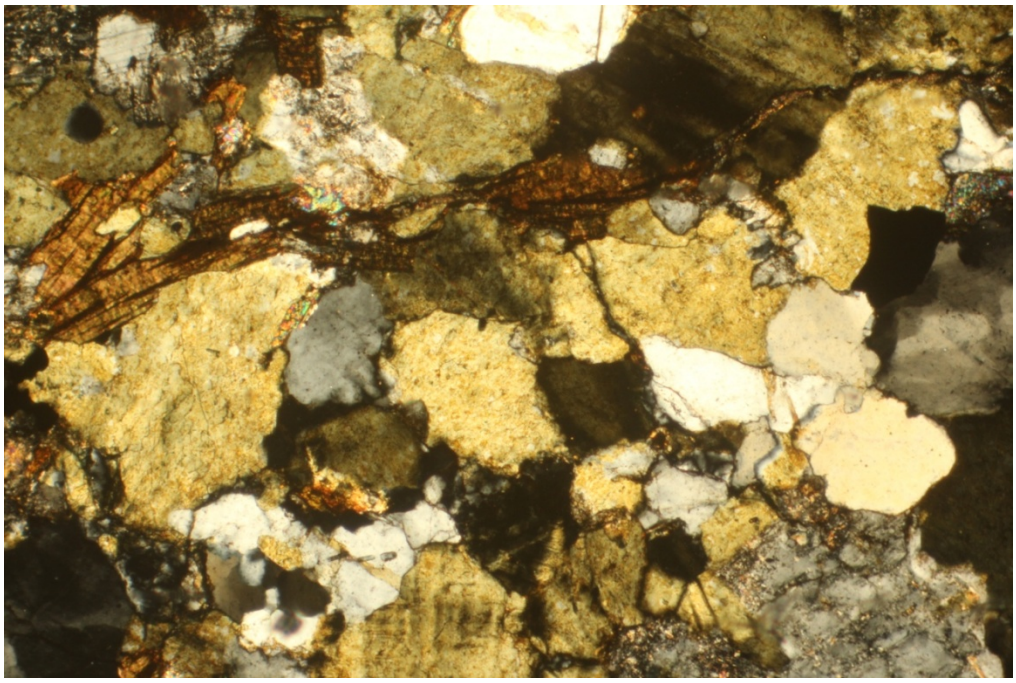

Figure A-25 – See caption at beginning of Appendix A.

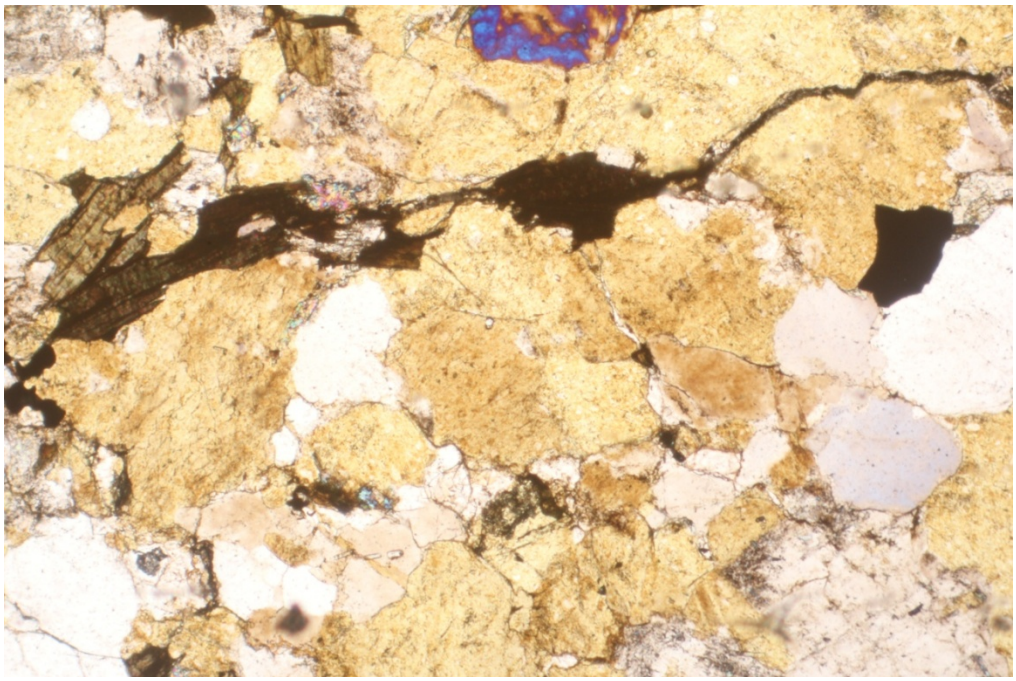

Figure A-26 – See caption at beginning of Appendix A.

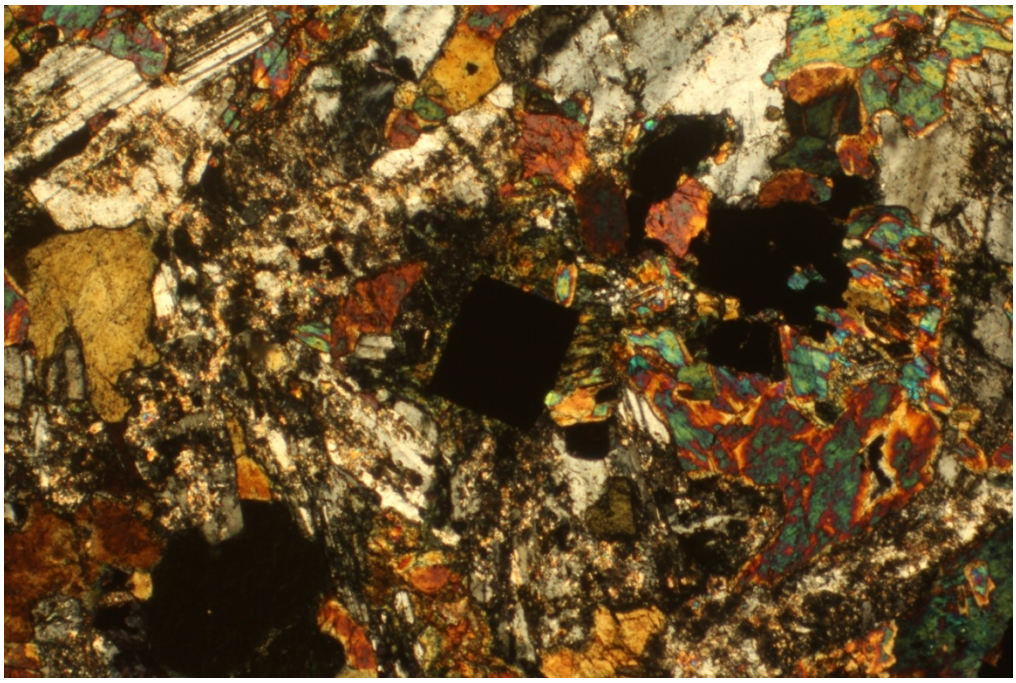

Figure A-27 – See caption at beginning of Appendix A.

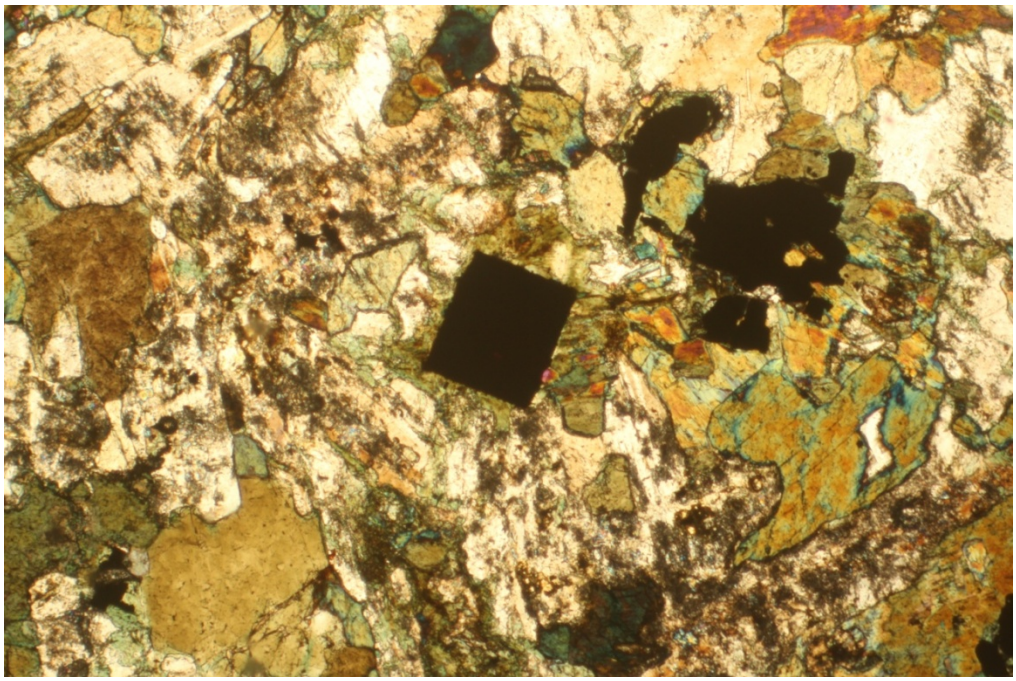

Figure A-28 – See caption at beginning of Appendix A.

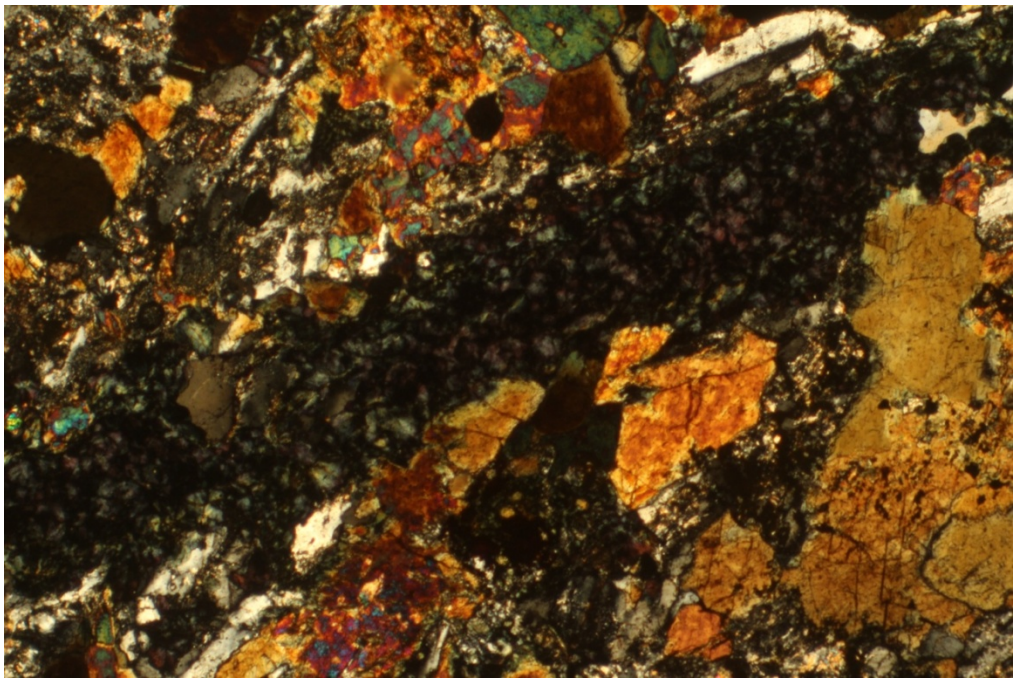

Figure A-29 – See caption at beginning of Appendix A.

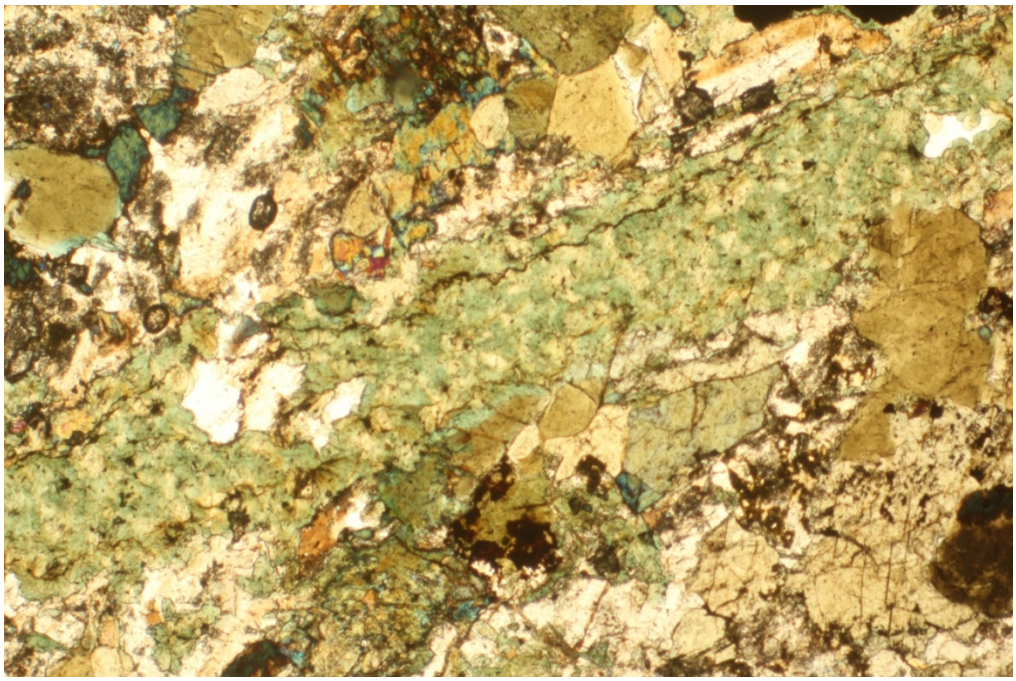

Figure A-30 – See caption at beginning of Appendix A.

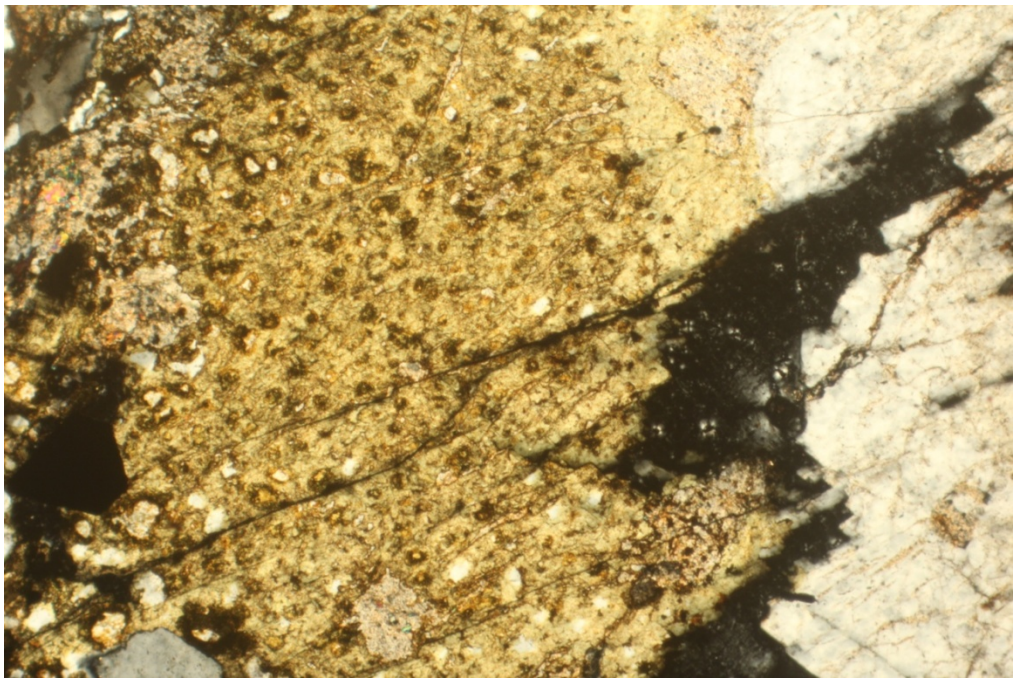

Figure A-31 – See caption at beginning of Appendix A.

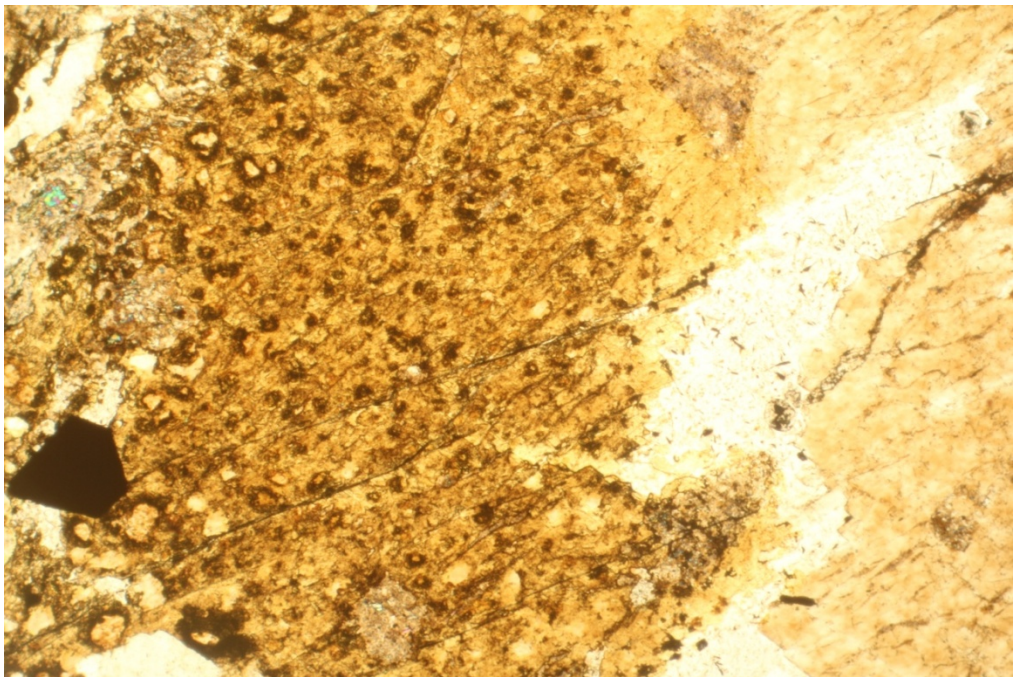

Figure A-32 – See caption at beginning of Appendix A.

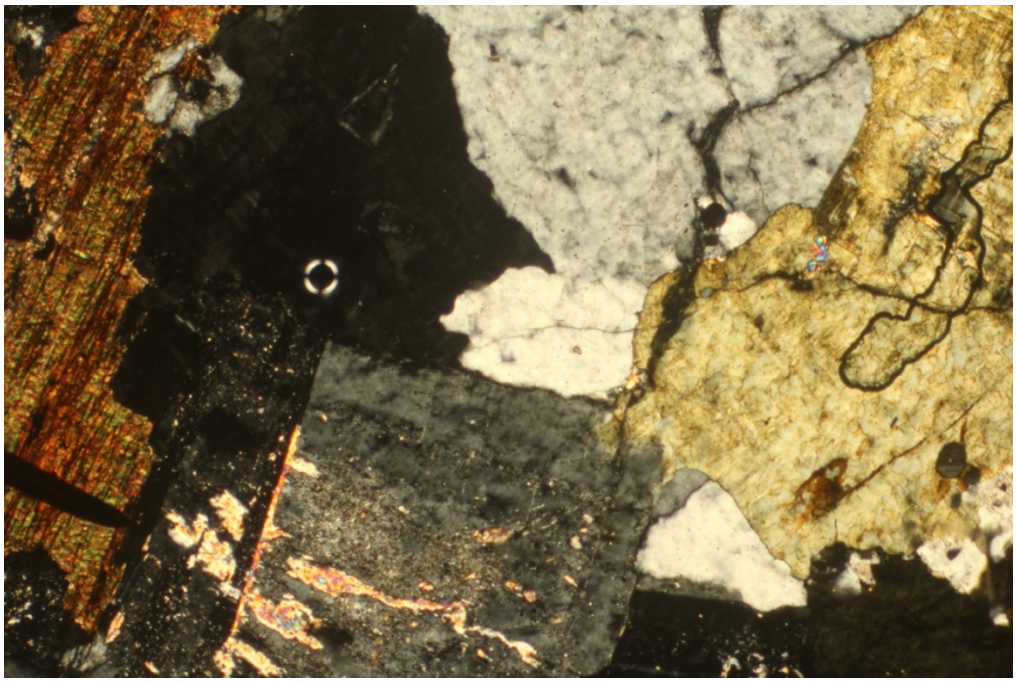

Figure A-33 – See caption at beginning of Appendix A.

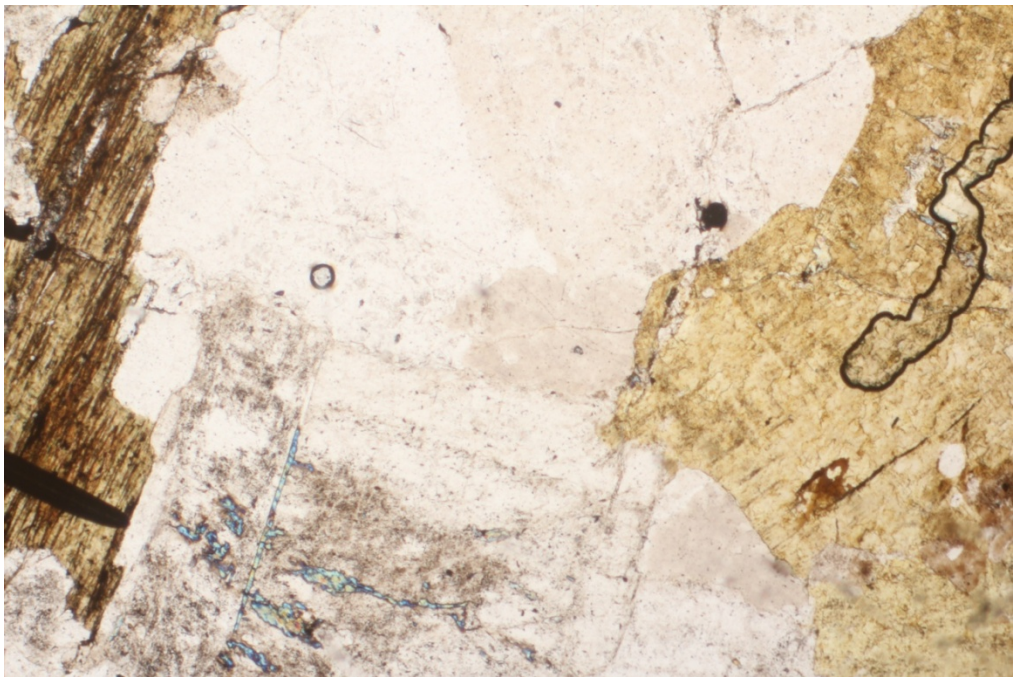

Figure A-34 – See caption at beginning of Appendix A.

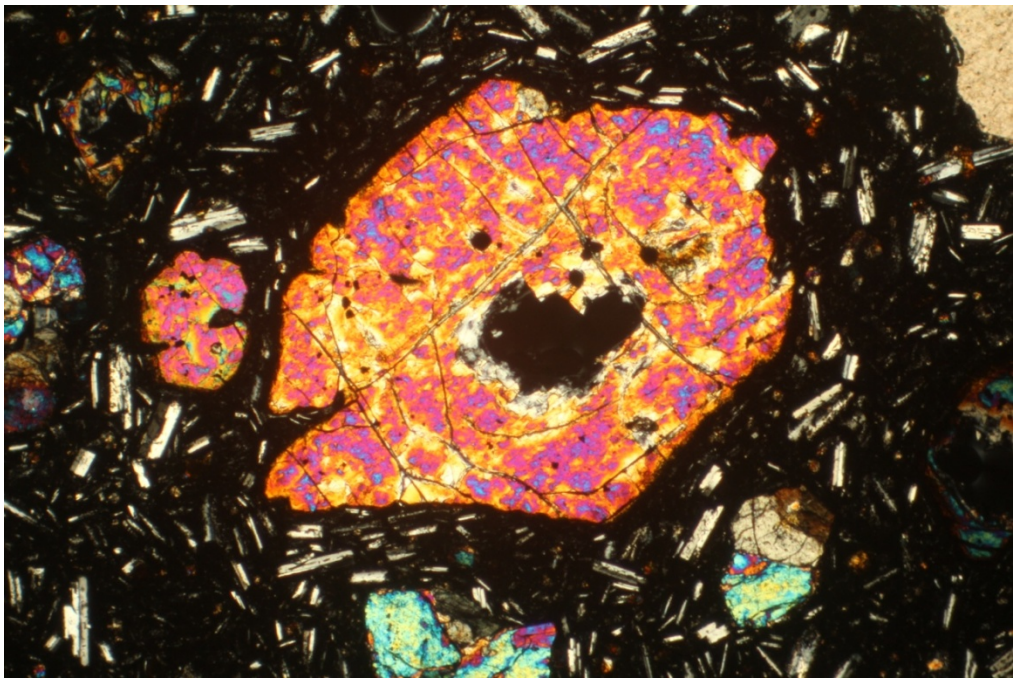

Figure A-35 – See caption at beginning of Appendix A.

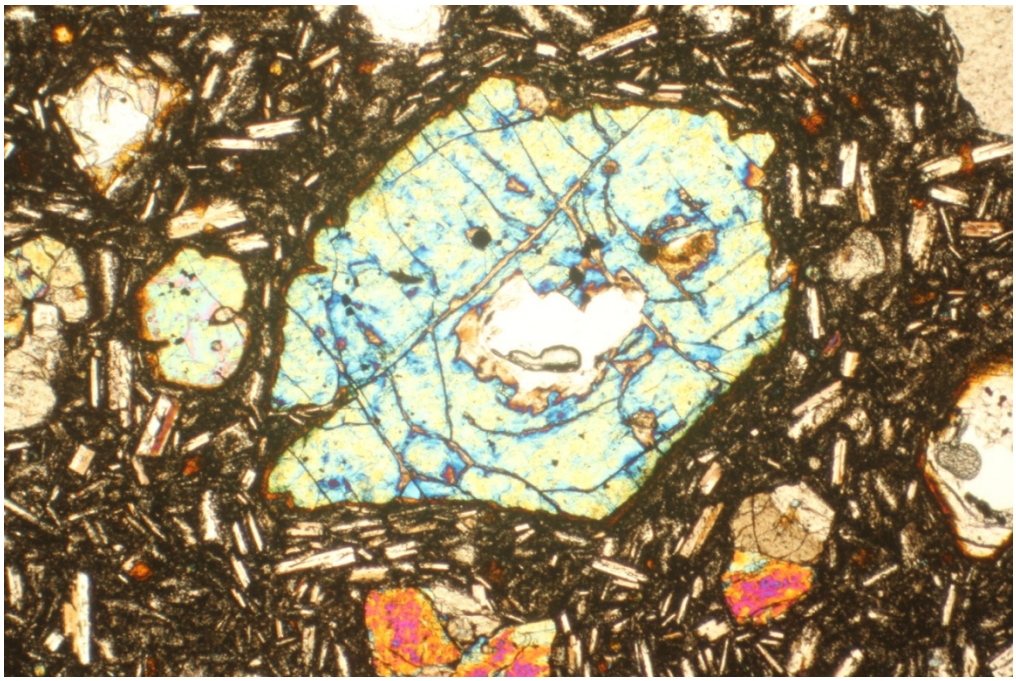

Figure A-36 – See caption at beginning of Appendix A.

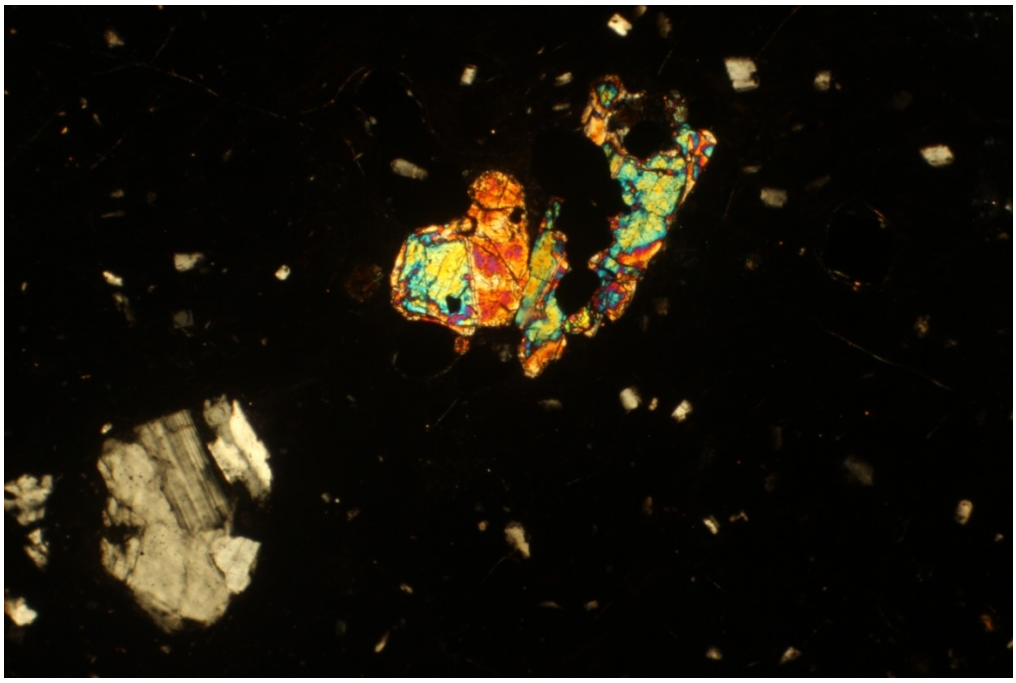

Figure A-37 – See caption at beginning of Appendix A.

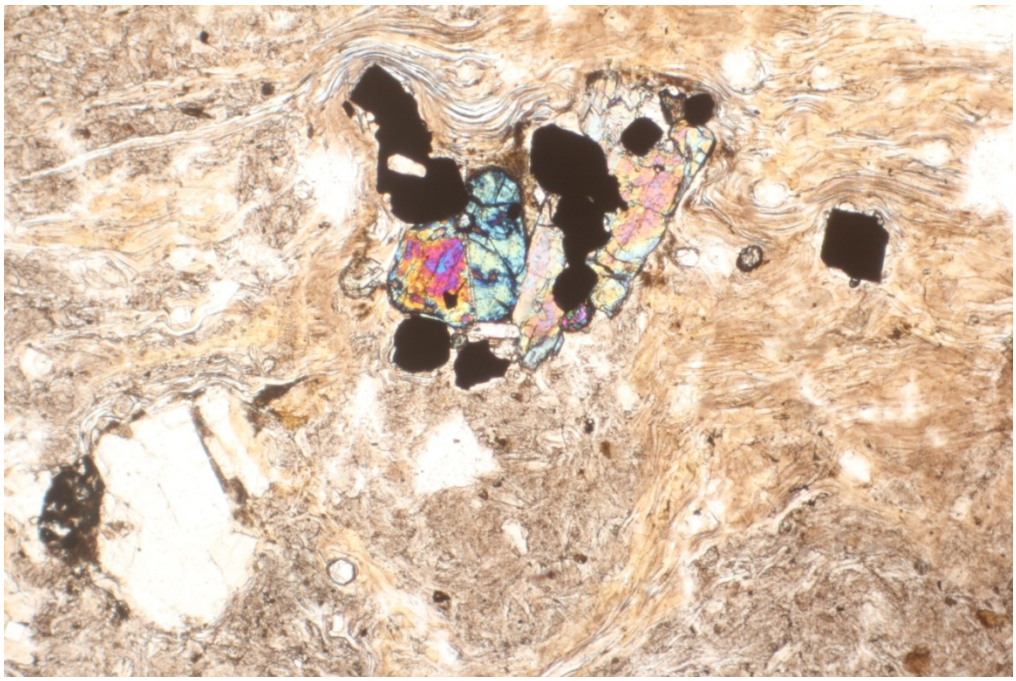

Figure A-38 – See caption at beginning of Appendix A.

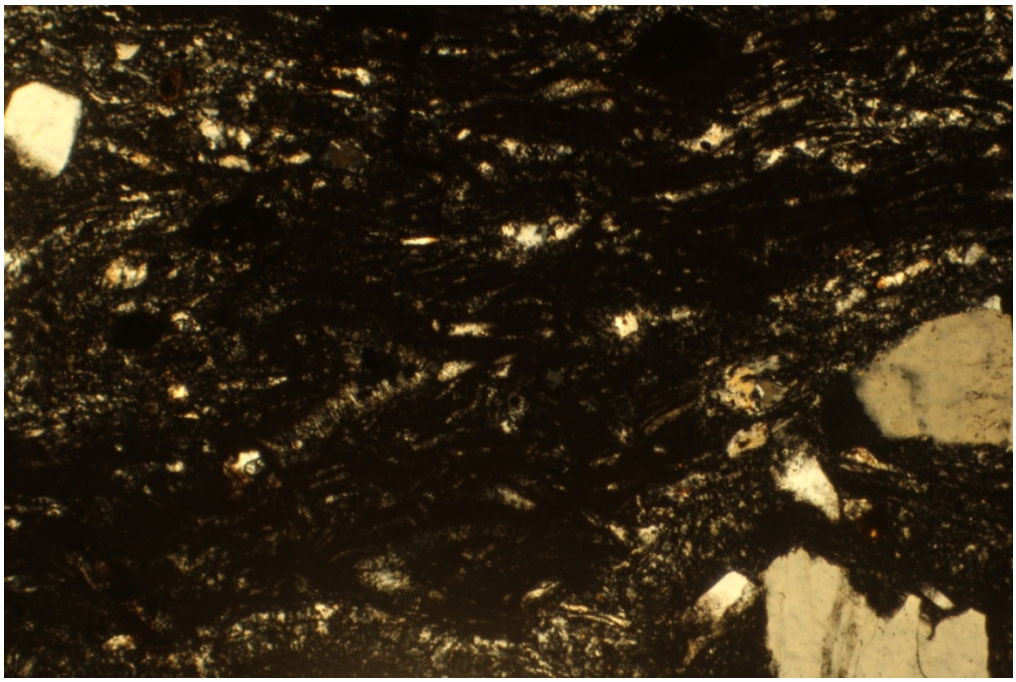

Figure A-39 – See caption at beginning of Appendix A.

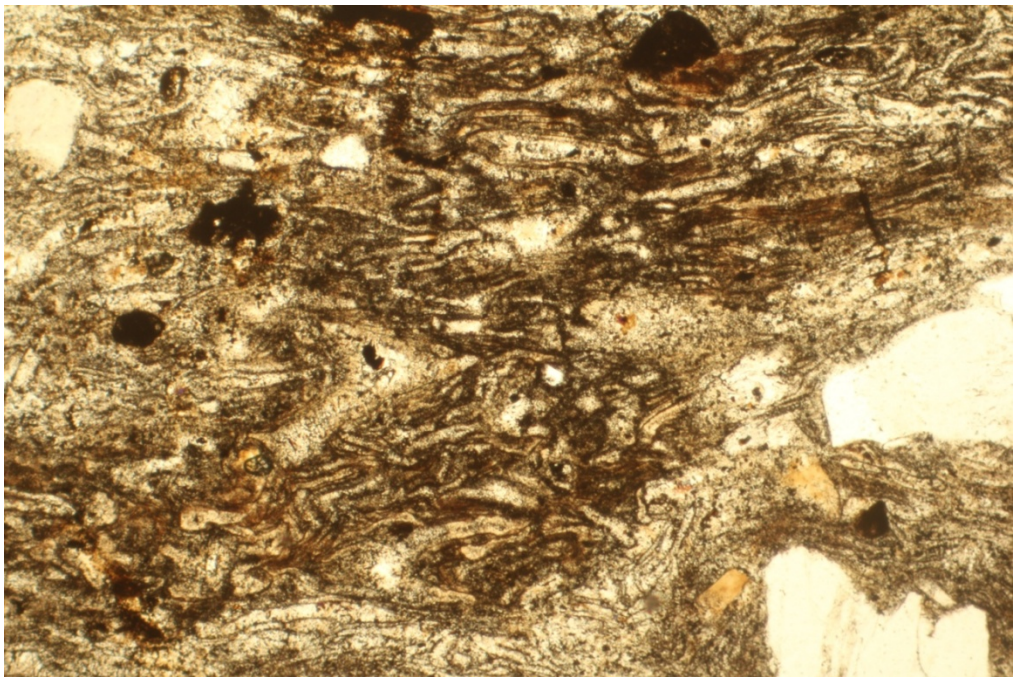

Figure A-40 – See caption at beginning of Appendix A.

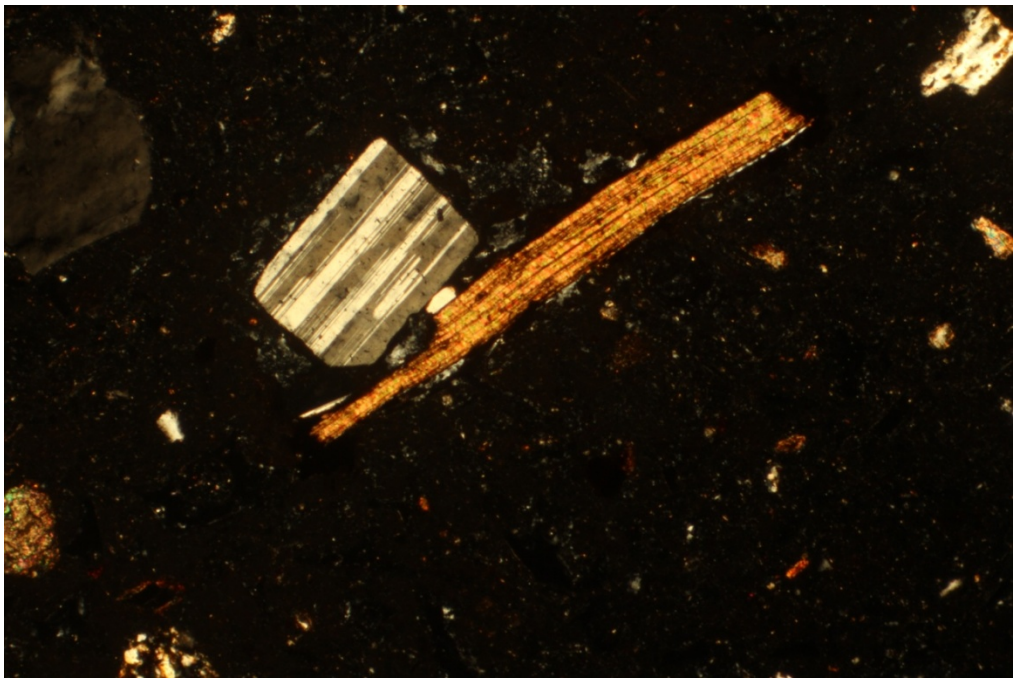

Figure A-41 – See caption at beginning of Appendix A.

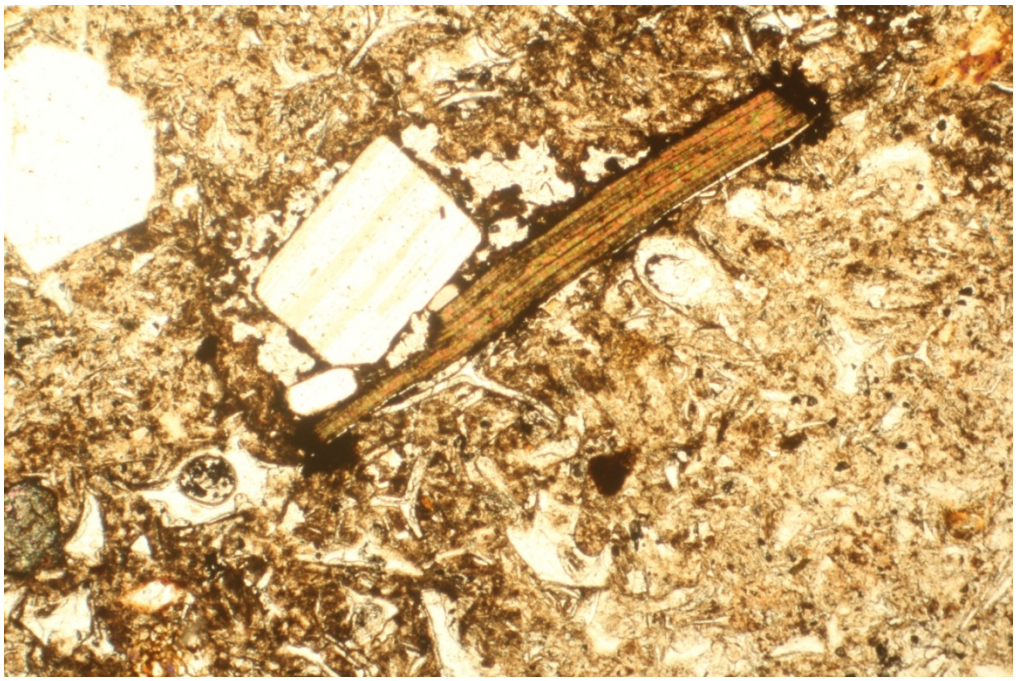

Figure A-42 – See caption at beginning of Appendix A.

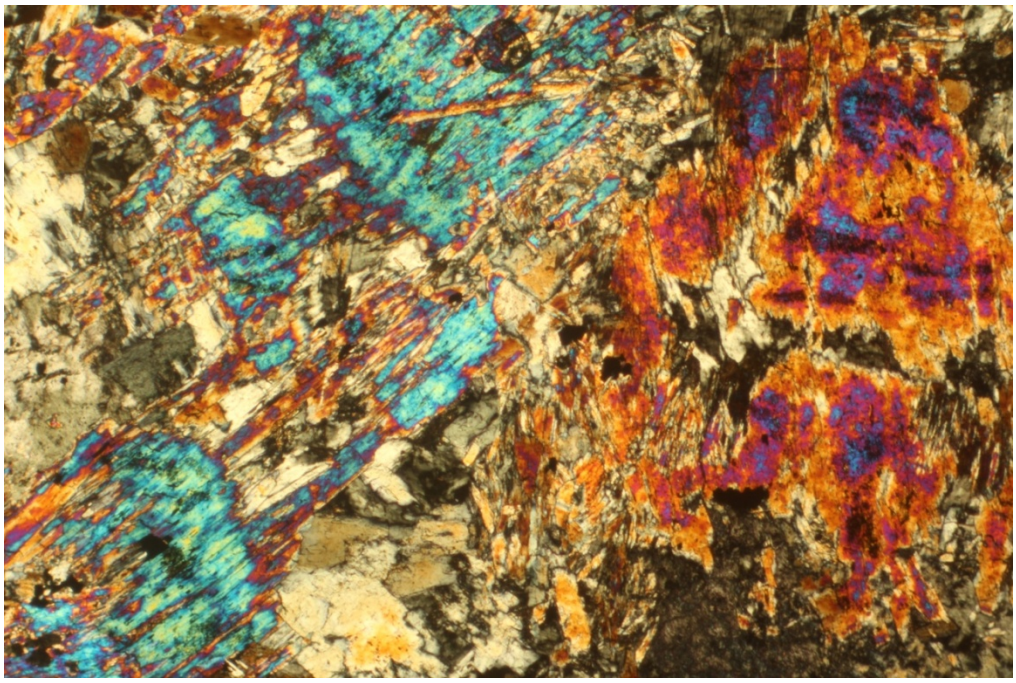

Figure A-43 – See caption at beginning of Appendix A.

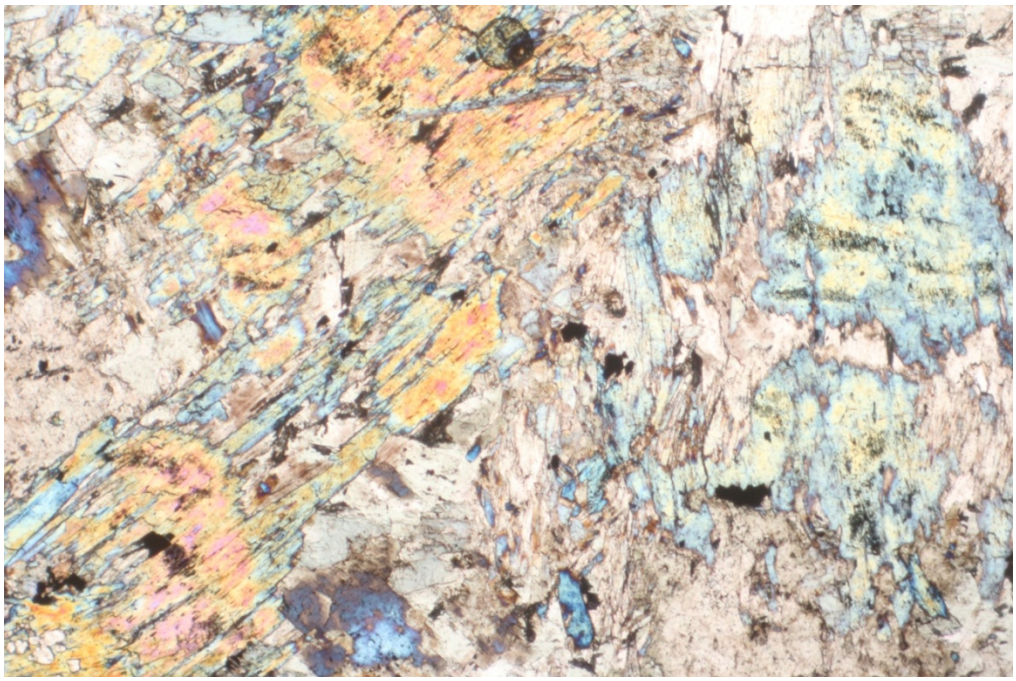

Figure A-44 – See caption at beginning of Appendix A.

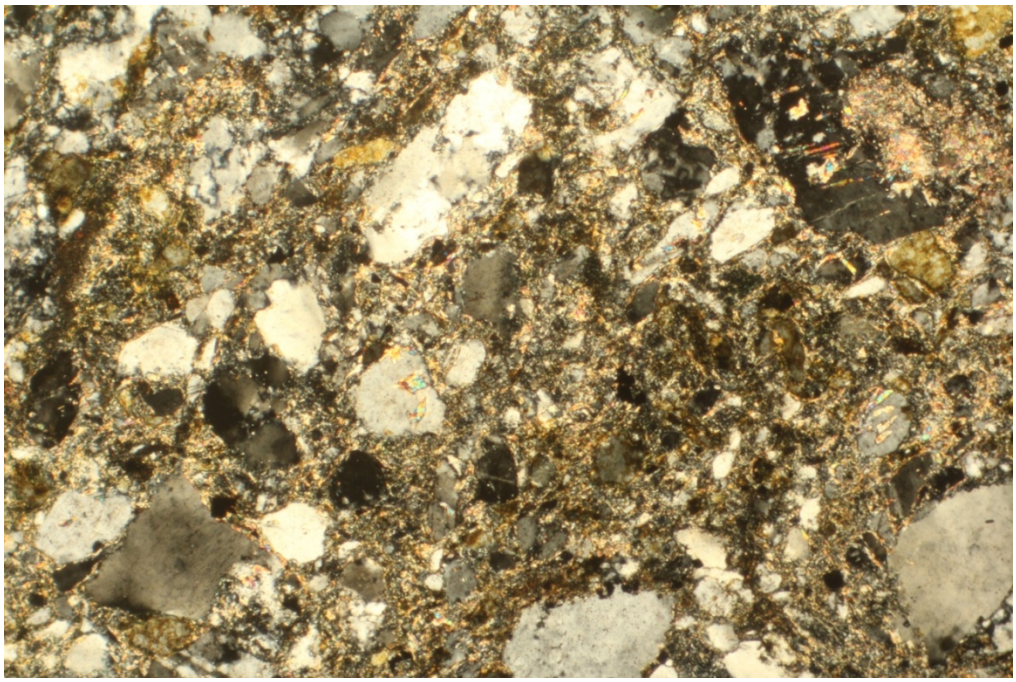

Figure A-45 – See caption at beginning of Appendix A.

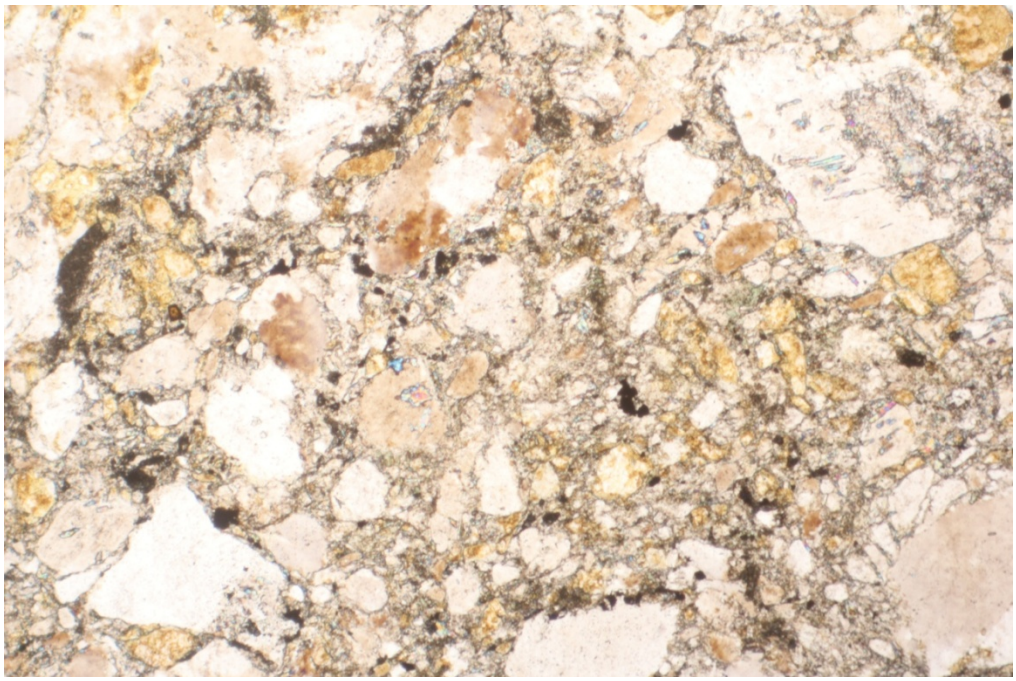

Figure A-46 – See caption at beginning of Appendix A.

# APPENDIX B

# U-PB ANALYSIS DATA

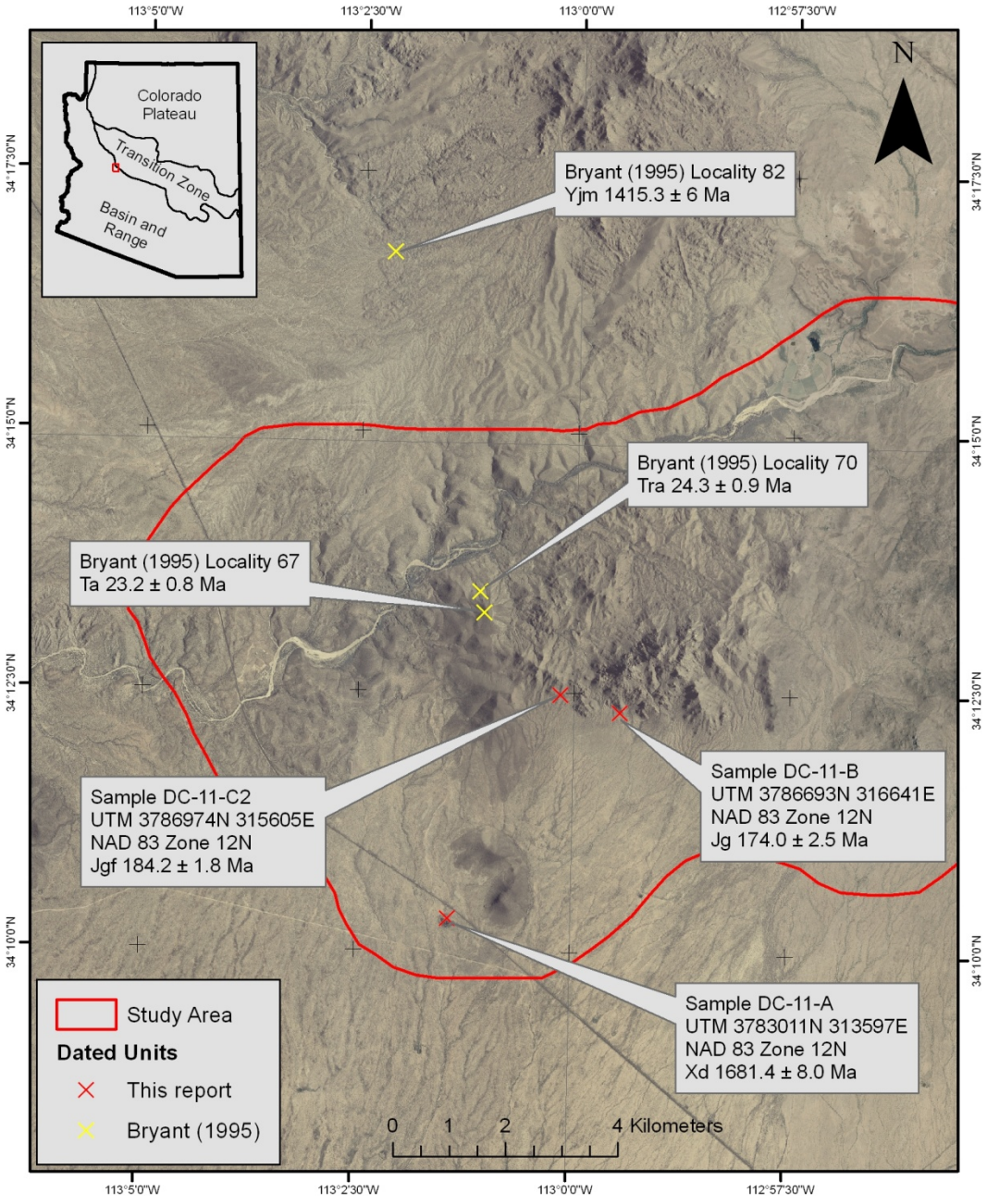


Figure B-1 – DOQQs of part of the study area showing locations of dated samples done for this study and data available from previous work.

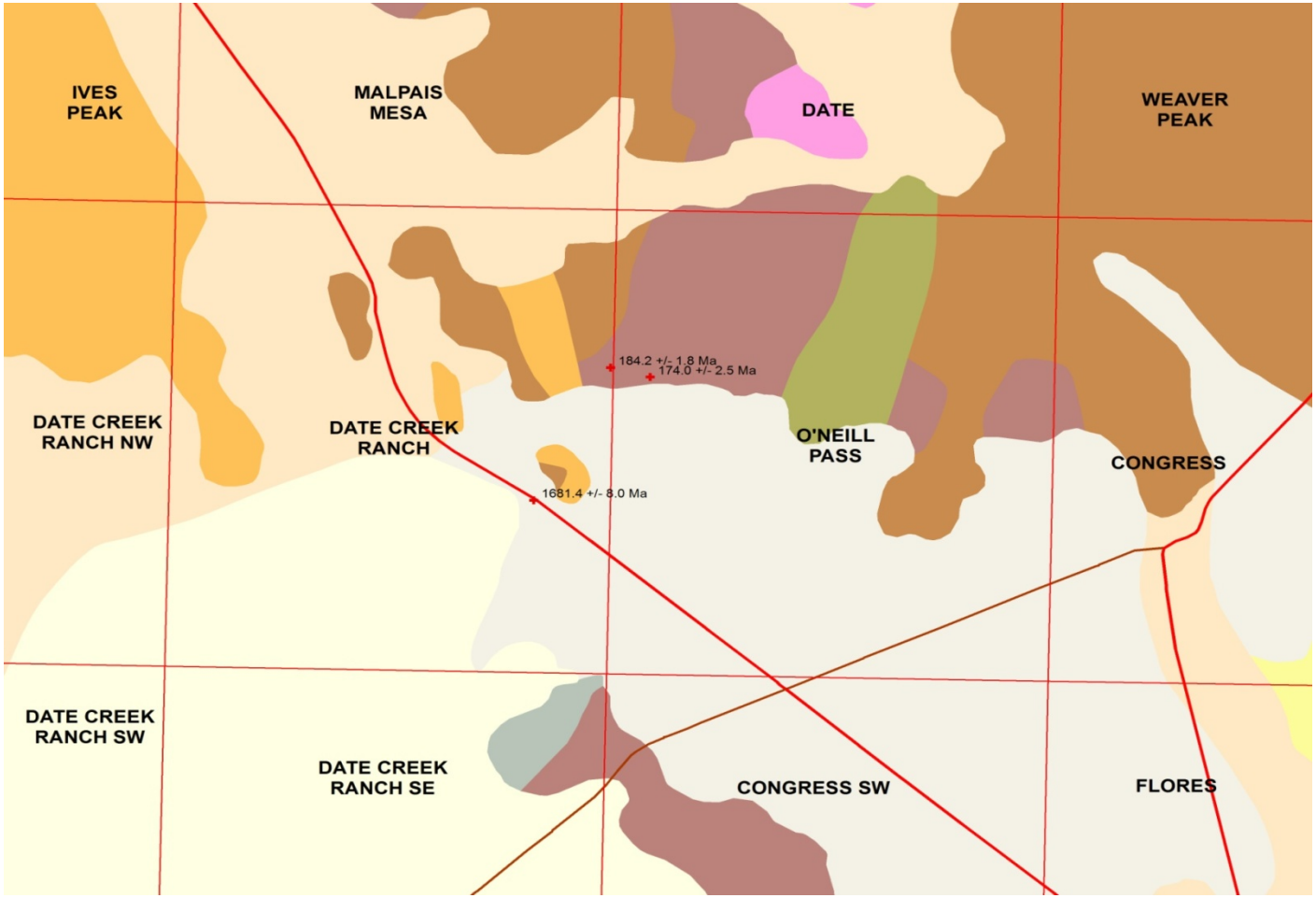


Figure B-2 – Map showing sample locations and analysis results. Samples are DC11A is 1681.4 ± 8.0, DC11B is 174.0 ± 2.5, and DC11C2 is 184.2 ± 1.8.

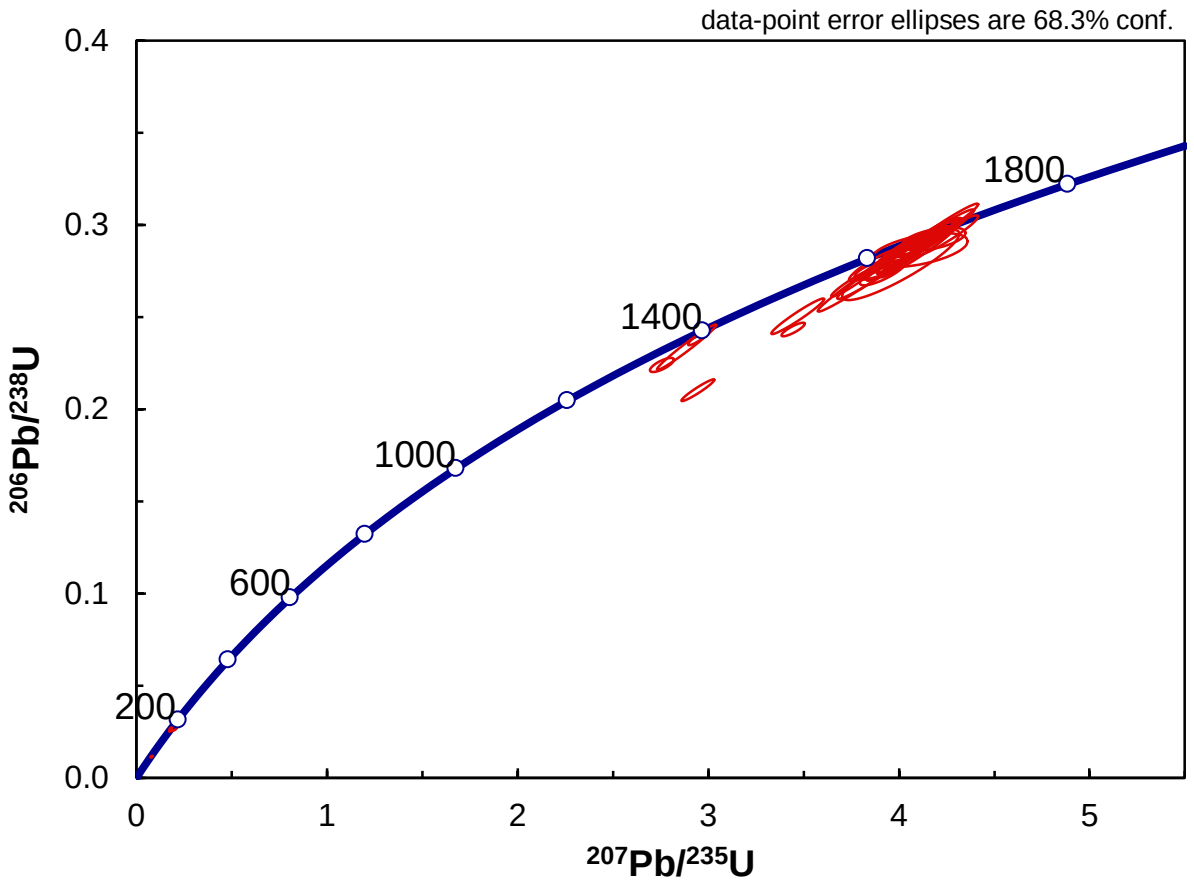


Figure B-3 – Concordia plot for sample DC11A.

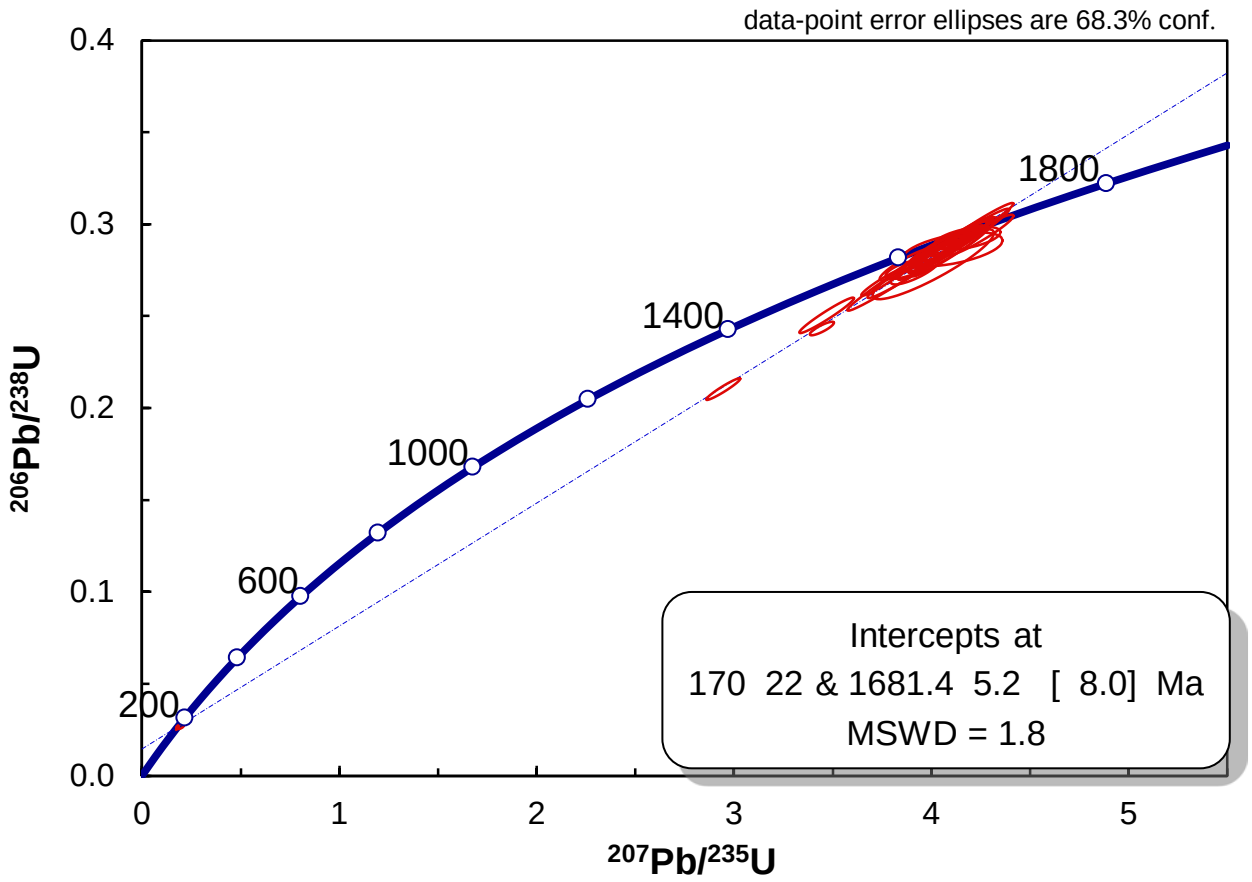


Figure B-4 – Concordia plot for sample DC11A.

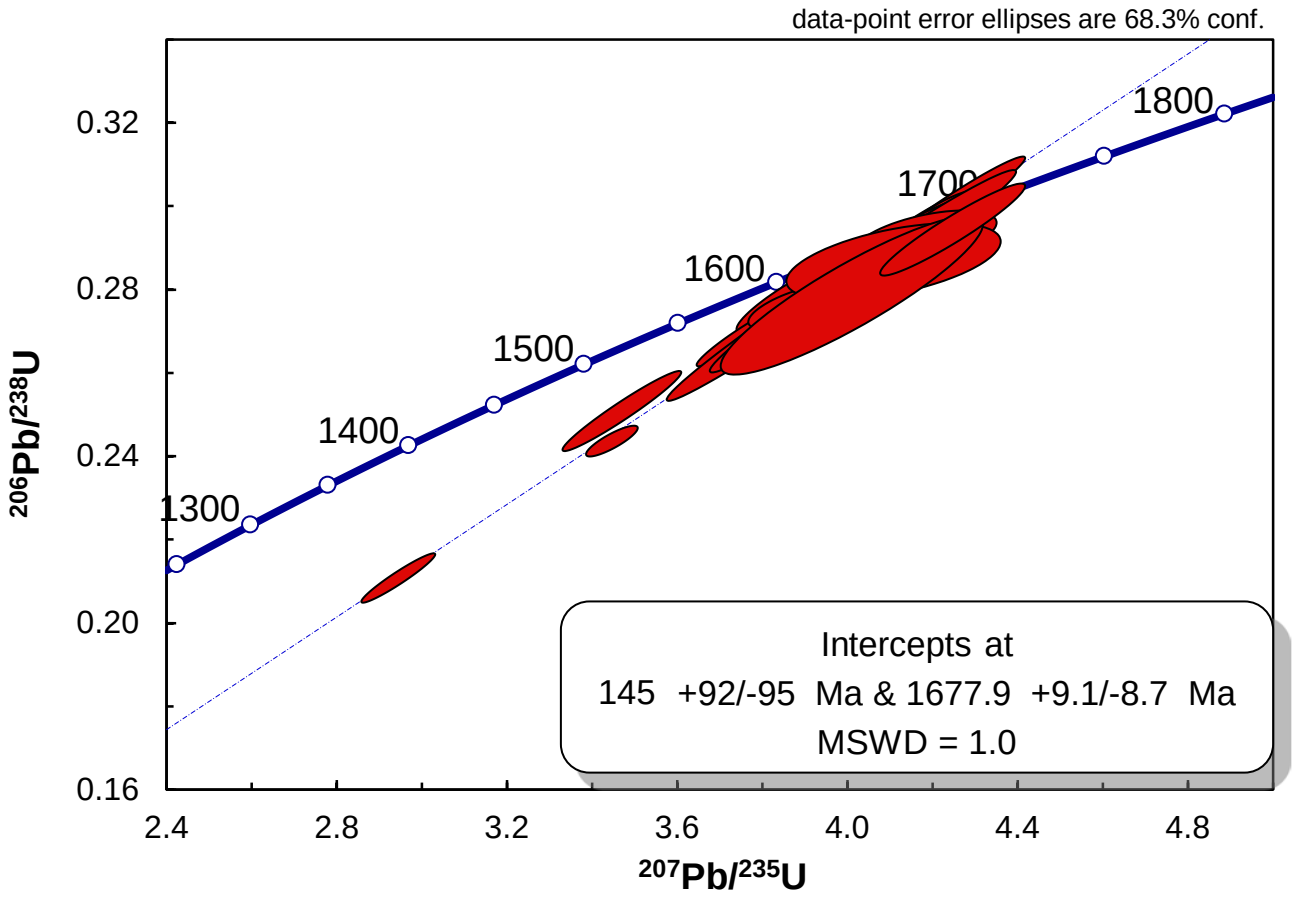


Figure B-5 – Concordia plot for sample DC11A.

Table _____. U-Pb geochronologic analyses.

| | | | | | | | Isotope ratios | | | | | | Apparent ages (Ma) | | | | | | |
|---|---|---|---|---|---|---|---|---|---|---|---|---|---|---|---|---|---|---|---|
| Analysis | U | 206Pb | U/Th | 206Pb* | ± | 207Pb* | ± | 206Pb* | ± | error | 206Pb* | ± | 207Pb* | ± | 206Pb* | ± | Best age | ± | Conc |
| | (ppm) | 204Pb | | 207Pb* | (%) | 235U* | (%) | 238U | (%) | corr. | 238U* | (Ma) | 235U | (Ma) | 207Pb* | (Ma) | (Ma) | (Ma) | (%) |
| DC-11-A-17C | 89 | 3246 | 0.6 | 19.8703 | 3.3 | 0.0798 | 4.2 | 0.0115 | 2.6 | 0.61 | 73.7 | 1.9 | 77.9 | 3.2 | 210.1 | 77.5 | 73.7 | 1.9 | NA |
| DC-11-A-17R | 210 | 13547 | 0.5 | 20.4172 | 2.1 | 0.0777 | 2.7 | 0.0115 | 1.6 | 0.60 | 73.7 | 1.2 | 76.0 | 1.9 | 146.8 | 50.1 | 73.7 | 1.2 | NA |
| DC-11-A-13C | 310 | 169800 | 0.9 | 19.9273 | 0.8 | 0.1786 | 2.3 | 0.0258 | 2.1 | 0.94 | 164.3 | 3.5 | 166.9 | 3.5 | 203.5 | 17.5 | 164.3 | 3.5 | NA |
| DC-11-A-13R | 603 | 61048 | 2.7 | 20.1877 | 0.7 | 0.1765 | 1.3 | 0.0258 | 1.1 | 0.86 | 164.5 | 1.9 | 165.0 | 2.0 | 173.2 | 15.7 | 164.5 | 1.9 | NA |
| DC-11-A-6C | 456 | 44979 | 1.0 | 19.1335 | 5.8 | 0.1927 | 6.7 | 0.0267 | 3.3 | 0.49 | 170.1 | 5.5 | 178.9 | 10.9 | 297.0 | 133.0 | 170.1 | 5.5 | NA |
| DC-11-A-20R | 256 | 33859 | 3.2 | 19.7622 | 1.0 | 0.1998 | 1.9 | 0.0286 | 1.5 | 0.83 | 182.0 | 2.8 | 184.9 | 3.1 | 222.7 | 23.7 | 182.0 | 2.8 | NA |
| DC-11-A-6R | 306 | 49093 | 1.4 | 20.0149 | 0.6 | 0.1978 | 1.6 | 0.0287 | 1.5 | 0.94 | 182.4 | 2.7 | 183.2 | 2.7 | 193.3 | 13.4 | 182.4 | 2.7 | NA |
| DC-11-A-22C | 290 | 506726 | 7.9 | 11.2058 | 1.0 | 2.7565 | 1.5 | 0.2240 | 1.1 | 0.75 | 1303.1 | 13.3 | 1343.9 | 11.2 | 1409.3 | 19.1 | 1409.3 | 19.1 | 92.5 |
| DC-11-A-21R | 90 | 139384 | 2.0 | 11.1647 | 0.5 | 2.9501 | 1.3 | 0.2389 | 1.1 | 0.90 | 1380.9 | 14.2 | 1394.9 | 9.6 | 1416.3 | 10.5 | 1416.3 | 10.5 | 97.5 |
| DC-11-A-21C | 101 | 194136 | 1.4 | 11.1645 | 0.7 | 2.8859 | 3.6 | 0.2337 | 3.5 | 0.98 | 1353.7 | 42.5 | 1378.2 | 26.8 | 1416.4 | 13.7 | 1416.4 | 13.7 | 95.6 |
| DC-11-A-11R | 120 | 258420 | 2.1 | 9.9541 | 0.7 | 3.4690 | 2.6 | 0.2504 | 2.5 | 0.97 | 1440.8 | 32.9 | 1520.2 | 20.8 | 1632.6 | 12.8 | 1632.6 | 12.8 | 88.2 |
| DC-11-A-10R | 84 | 96002 | 0.9 | 9.9020 | 1.0 | 3.8722 | 2.3 | 0.2781 | 2.1 | 0.90 | 1581.7 | 29.0 | 1607.9 | 18.5 | 1642.4 | 18.5 | 1642.4 | 18.5 | 96.3 |
| DC-11-A-10C | 47 | 72135 | 1.1 | 9.8655 | 0.6 | 3.7515 | 1.9 | 0.2684 | 1.8 | 0.95 | 1532.8 | 24.5 | 1582.4 | 15.1 | 1649.2 | 10.4 | 1649.2 | 10.4 | 92.9 |
| DC-11-A-19C | 43 | 57290 | 1.9 | 9.8613 | 0.6 | 3.9977 | 1.9 | 0.2859 | 1.8 | 0.94 | 1621.1 | 25.2 | 1633.7 | 15.2 | 1650.0 | 11.8 | 1650.0 | 11.8 | 98.2 |
| DC-11-A-23C | 112 | 119664 | 0.9 | 9.8466 | 0.6 | 2.9450 | 1.9 | 0.2103 | 1.8 | 0.96 | 1230.5 | 20.7 | 1393.6 | 14.7 | 1652.8 | 10.5 | 1652.8 | 10.5 | 74.4 |
| DC-11-A-15R | 210 | 492924 | 1.3 | 9.8015 | 1.3 | 3.8754 | 1.8 | 0.2755 | 1.2 | 0.68 | 1568.6 | 17.4 | 1608.6 | 14.8 | 1661.3 | 25.0 | 1661.3 | 25.0 | 94.4 |
| DC-11-A-12R | 190 | 188200 | 1.4 | 9.7571 | 1.2 | 4.0717 | 1.8 | 0.2881 | 1.3 | 0.71 | 1632.2 | 18.2 | 1648.7 | 14.5 | 1669.7 | 23.1 | 1669.7 | 23.1 | 97.8 |
| DC-11-A-4C | 168 | 343736 | 2.3 | 9.7474 | 0.9 | 3.8949 | 5.5 | 0.2753 | 5.4 | 0.99 | 1567.9 | 74.8 | 1612.6 | 44.1 | 1671.5 | 16.8 | 1671.5 | 16.8 | 93.8 |
| DC-11-A-8R | 117 | 191217 | 1.0 | 9.7463 | 0.7 | 4.1750 | 2.0 | 0.2951 | 1.8 | 0.93 | 1667.0 | 27.0 | 1669.1 | 16.2 | 1671.7 | 13.6 | 1671.7 | 13.6 | 99.7 |
| DC-11-A-18C | 71 | 169167 | 1.5 | 9.7402 | 0.6 | 4.2127 | 1.5 | 0.2976 | 1.4 | 0.92 | 1679.4 | 20.1 | 1676.5 | 12.2 | 1672.9 | 10.8 | 1672.9 | 10.8 | 100.4 |
| DC-11-A-9R | 92 | 103442 | 1.3 | 9.7401 | 0.7 | 4.2330 | 2.9 | 0.2990 | 2.8 | 0.97 | 1686.5 | 41.1 | 1680.4 | 23.4 | 1672.9 | 12.4 | 1672.9 | 12.4 | 100.8 |
| DC-11-A-16R | 48 | 68929 | 1.3 | 9.7367 | 0.6 | 3.4449 | 1.2 | 0.2433 | 1.0 | 0.85 | 1403.7 | 12.6 | 1514.7 | 9.2 | 1673.5 | 11.3 | 1673.5 | 11.3 | 83.9 |
| DC-11-A-3C | 117 | 100265 | 2.1 | 9.7366 | 0.8 | 4.0403 | 2.0 | 0.2853 | 1.8 | 0.91 | 1618.1 | 25.6 | 1642.4 | 16.0 | 1673.6 | 15.3 | 1673.6 | 15.3 | 96.7 |
| DC-11-A-14C | 36 | 52278 | 1.1 | 9.7309 | 0.9 | 3.9535 | 4.6 | 0.2790 | 4.5 | 0.98 | 1586.4 | 63.9 | 1624.7 | 37.6 | 1674.6 | 17.4 | 1674.6 | 17.4 | 94.7 |
| DC-11-A-18R | 121 | 116098 | 1.0 | 9.7285 | 0.9 | 4.0523 | 2.8 | 0.2859 | 2.7 | 0.95 | 1621.1 | 38.5 | 1644.8 | 23.1 | 1675.1 | 16.8 | 1675.1 | 16.8 | 96.8 |
| DC-11-A-14R | 54 | 70283 | 1.3 | 9.7261 | 0.6 | 4.1610 | 2.3 | 0.2935 | 2.3 | 0.97 | 1659.1 | 33.2 | 1666.4 | 19.2 | 1675.5 | 10.8 | 1675.5 | 10.8 | 99.0 |
| DC-11-A-19R | 69 | 63685 | 1.0 | 9.7246 | 0.6 | 4.1874 | 1.5 | 0.2953 | 1.4 | 0.93 | 1668.1 | 20.5 | 1671.6 | 12.3 | 1675.8 | 10.2 | 1675.8 | 10.2 | 99.5 |
| DC-11-A-12C | 127 | 163608 | 1.4 | 9.7208 | 0.9 | 4.0548 | 2.1 | 0.2859 | 1.8 | 0.90 | 1620.9 | 26.4 | 1645.3 | 16.7 | 1676.6 | 16.8 | 1676.6 | 16.8 | 96.7 |
| DC-11-A-2R | 114 | 113784 | 1.3 | 9.7146 | 0.8 | 4.1281 | 2.9 | 0.2909 | 2.8 | 0.96 | 1645.8 | 40.8 | 1659.9 | 23.8 | 1677.7 | 14.5 | 1677.7 | 14.5 | 98.1 |
| DC-11-A-11C | 33 | 81643 | 1.1 | 9.7089 | 0.8 | 4.1559 | 1.2 | 0.2926 | 0.9 | 0.77 | 1654.7 | 13.4 | 1665.4 | 9.8 | 1678.8 | 14.1 | 1678.8 | 14.1 | 98.6 |
| DC-11-A-24R | 144 | 311682 | 1.3 | 9.7078 | 0.9 | 4.0560 | 1.6 | 0.2856 | 1.3 | 0.84 | 1619.4 | 19.1 | 1645.5 | 12.9 | 1679.0 | 16.0 | 1679.0 | 16.0 | 96.4 |
| DC-11-A-4R | 239 | 466321 | 1.9 | 9.7071 | 0.8 | 4.2498 | 1.3 | 0.2992 | 1.0 | 0.78 | 1687.3 | 15.1 | 1683.7 | 10.8 | 1679.2 | 15.3 | 1679.2 | 15.3 | 100.5 |
| DC-11-A-7R | 133 | 159668 | 1.5 | 9.7035 | 0.9 | 4.1467 | 1.9 | 0.2918 | 1.7 | 0.88 | 1650.7 | 24.9 | 1663.6 | 15.9 | 1679.9 | 17.1 | 1679.9 | 17.1 | 98.3 |

| | | | | | | | | | | | | | | | | | | | |
|---|---|---|---|---|---|---|---|---|---|---|---|---|---|---|---|---|---|---|---|
| DC-11-A-23R | 384 | 253216 | 2.1 | 9.7001 | 1.4 | 4.0685 | 4.0 | 0.2862 | 3.7 | 0.93 | 1622.7 | 53.3 | 1648.0 | 32.4 | 1680.5 | 26.1 | 1680.5 | 26.1 | 96.6 |
| DC-11-A-16C | 188 | 408147 | 2.4 | 9.7000 | 1.0 | 4.0247 | 1.9 | 0.2831 | 1.6 | 0.85 | 1607.2 | 23.0 | 1639.2 | 15.5 | 1680.5 | 18.4 | 1680.5 | 18.4 | 95.6 |
| DC-11-A-22R | 59 | 100287 | 0.9 | 9.6961 | 0.6 | 4.0135 | 2.1 | 0.2822 | 2.1 | 0.96 | 1602.6 | 29.1 | 1636.9 | 17.4 | 1681.3 | 11.2 | 1681.3 | 11.2 | 95.3 |
| DC-11-A-3R | 111 | 91929 | 1.3 | 9.6956 | 0.5 | 4.2178 | 0.7 | 0.2966 | 0.6 | 0.74 | 1674.4 | 8.1 | 1677.5 | 6.1 | 1681.4 | 9.3 | 1681.4 | 9.3 | 99.6 |
| DC-11-A-1C | 50 | 64765 | 1.0 | 9.6919 | 0.9 | 4.1126 | 4.5 | 0.2891 | 4.4 | 0.98 | 1636.9 | 64.0 | 1656.8 | 37.0 | 1682.1 | 17.4 | 1682.1 | 17.4 | 97.3 |
| DC-11-A-1R | 270 | 216242 | 1.6 | 9.6539 | 1.2 | 3.9156 | 2.0 | 0.2742 | 1.7 | 0.81 | 1561.9 | 23.1 | 1616.9 | 16.5 | 1689.3 | 21.9 | 1689.3 | 21.9 | 92.5 |
| DC-11-A-7C | 63 | 43078 | 0.9 | 9.6392 | 2.2 | 4.1824 | 2.6 | 0.2924 | 1.4 | 0.53 | 1653.5 | 20.6 | 1670.6 | 21.6 | 1692.1 | 41.2 | 1692.1 | 41.2 | 97.7 |
| DC-11-A-20C | 186 | 1708420 | 1.5 | 9.6125 | 3.5 | 4.1075 | 4.1 | 0.2864 | 2.1 | 0.52 | 1623.3 | 30.5 | 1655.8 | 33.2 | 1697.2 | 63.9 | 1697.2 | 63.9 | 95.6 |
| DC-11-A-5R | 25 | 67130 | 1.5 | 9.5816 | 0.6 | 4.0801 | 2.8 | 0.2835 | 2.8 | 0.97 | 1609.1 | 39.4 | 1650.3 | 23.2 | 1703.2 | 11.9 | 1703.2 | 11.9 | 94.5 |
| DC-11-A-2C | 57 | 43489 | 1.2 | 9.5696 | 2.3 | 4.0094 | 5.1 | 0.2783 | 4.5 | 0.89 | 1582.6 | 63.4 | 1636.1 | 41.1 | 1705.5 | 42.0 | 1705.5 | 42.0 | 92.8 |
| DC-11-A-9C | 31 | 30442 | 1.3 | 9.5493 | 0.9 | 4.2463 | 2.6 | 0.2941 | 2.5 | 0.95 | 1661.9 | 36.5 | 1683.0 | 21.6 | 1709.4 | 15.7 | 1709.4 | 15.7 | 97.2 |

Table B-1 – U-Pb analysis data for sample DC11A.

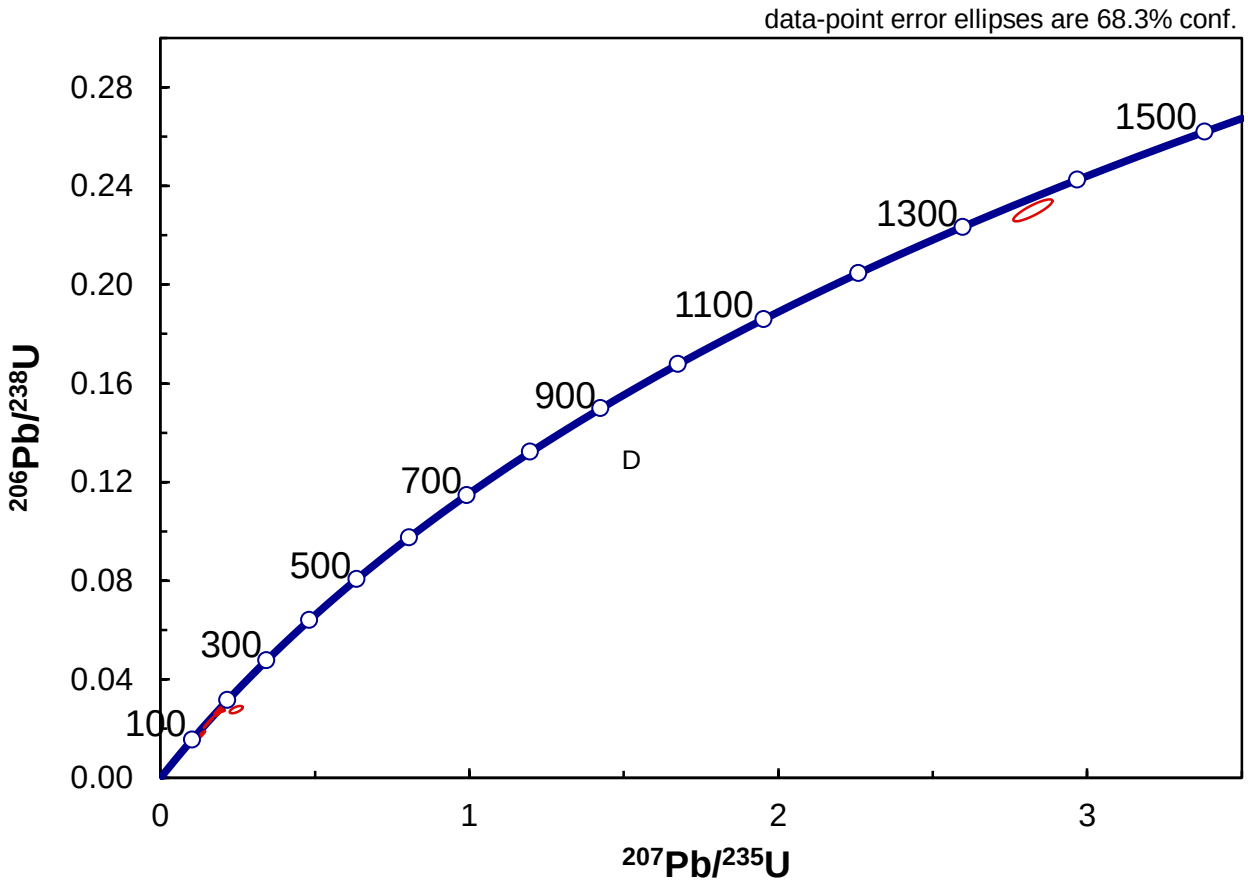


Figure B-6 – Concordia plot for sample DC11B.

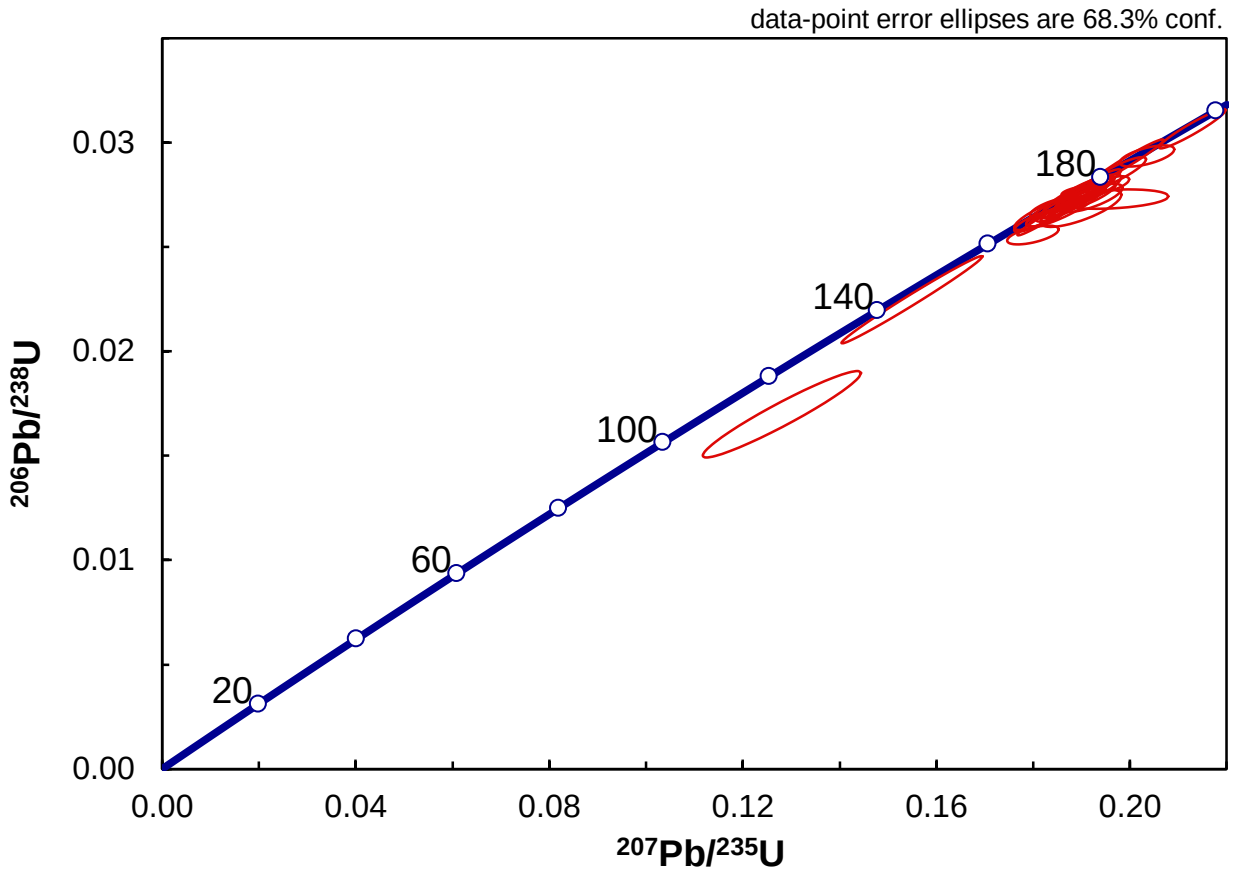


Figure B-7 – Concordia plot for sample DC11B

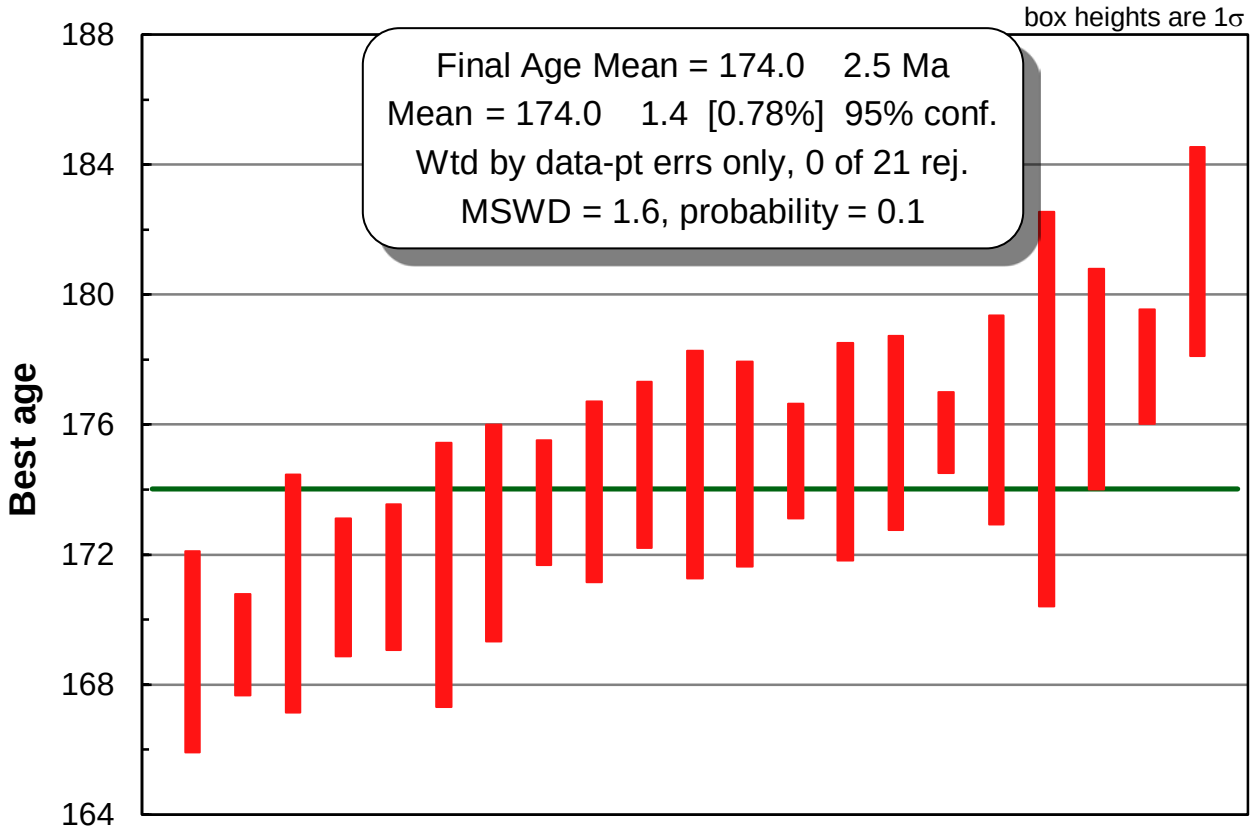


Figure B-8 – Average plot for sample DC11B.

Table _____. U-Pb geochronologic analyses.

| | | | | | | | Isotope ratios | | | | | | Apparent ages (Ma) | | | | | | |
|---|---|---|---|---|---|---|---|---|---|---|---|---|---|---|---|---|---|---|---|
| Analysis | U | 206Pb | U/Th | 206Pb* | ± | 207Pb* | ± | 206Pb* | ± | error | 206Pb* | ± | 207Pb* | ± | 206Pb* | ± | Best age | ± | Conc |
| | (ppm) | 204Pb | | 207Pb* | (%) | 235U* | (%) | 238U | (%) | corr. | 238U* | (Ma) | 235U | (Ma) | 207Pb* | (Ma) | (Ma) | (Ma) | (%) |
| DC-11-B-11R | 1288 | 16516 | 1.5 | 18.2888 | 2.5 | 0.1281 | 8.4 | 0.0170 | 8.0 | 0.95 | 108.6 | 8.7 | 122.4 | 9.7 | 399.1 | 56.4 | 108.6 | 8.7 | NA |
| DC-11-B-15R | 520 | 45885 | 1.4 | 20.0005 | 0.9 | 0.1549 | 6.2 | 0.0225 | 6.2 | 0.99 | 143.3 | 8.7 | 146.3 | 8.5 | 195.0 | 20.3 | 143.3 | 8.7 | NA |
| DC-11-B-9C | 305 | 21245 | 1.1 | 19.5965 | 1.6 | 0.1799 | 2.0 | 0.0256 | 1.2 | 0.59 | 162.8 | 1.9 | 168.0 | 3.0 | 242.2 | 36.1 | 162.8 | 1.9 | NA |
| DC-11-B-16R | 470 | 34155 | 0.9 | 20.0660 | 0.9 | 0.1803 | 1.5 | 0.0262 | 1.3 | 0.83 | 166.9 | 2.1 | 168.3 | 2.4 | 187.3 | 20.0 | 166.9 | 2.1 | NA |
| DC-11-B-14R | 477 | 47217 | 0.9 | 19.9220 | 0.5 | 0.1824 | 2.1 | 0.0264 | 2.0 | 0.97 | 167.7 | 3.3 | 170.1 | 3.2 | 204.0 | 11.7 | 167.7 | 3.3 | NA |
| DC-11-B-3R | 574 | 295750 | 0.8 | 19.9481 | 0.9 | 0.1822 | 1.3 | 0.0264 | 0.9 | 0.71 | 167.7 | 1.6 | 169.9 | 2.1 | 201.0 | 21.7 | 167.7 | 1.6 | NA |
| DC-11-B-12R | 869 | 101514 | 0.6 | 19.9121 | 0.8 | 0.1829 | 1.4 | 0.0264 | 1.1 | 0.81 | 168.1 | 1.8 | 170.6 | 2.1 | 205.2 | 18.7 | 168.1 | 1.8 | NA |
| DC-11-B-4C | 844 | 73160 | 1.4 | 20.1018 | 1.2 | 0.1822 | 2.2 | 0.0266 | 1.9 | 0.84 | 169.0 | 3.1 | 170.0 | 3.5 | 183.2 | 28.4 | 169.0 | 3.1 | NA |
| DC-11-B-3C | 295 | 111686 | 1.0 | 19.9457 | 0.7 | 0.1839 | 1.2 | 0.0266 | 0.9 | 0.81 | 169.2 | 1.6 | 171.4 | 1.8 | 201.3 | 15.6 | 169.2 | 1.6 | NA |
| DC-11-B-18R | 125 | 18067 | 2.3 | 19.4957 | 1.9 | 0.1899 | 2.9 | 0.0268 | 2.2 | 0.75 | 170.8 | 3.7 | 176.5 | 4.7 | 254.0 | 44.5 | 170.8 | 3.7 | NA |
| DC-11-B-4R | 670 | 107859 | 1.7 | 20.0948 | 1.3 | 0.1844 | 1.8 | 0.0269 | 1.3 | 0.69 | 171.0 | 2.1 | 171.9 | 2.9 | 184.0 | 30.8 | 171.0 | 2.1 | NA |
| DC-11-B-16C | 361 | 40875 | 0.8 | 20.0548 | 0.6 | 0.1851 | 1.5 | 0.0269 | 1.3 | 0.91 | 171.3 | 2.2 | 172.5 | 2.3 | 188.6 | 14.4 | 171.3 | 2.2 | NA |
| DC-11-B-2R | 334 | 66254 | 1.1 | 19.9228 | 1.4 | 0.1864 | 2.8 | 0.0269 | 2.4 | 0.86 | 171.4 | 4.1 | 173.6 | 4.5 | 204.0 | 32.9 | 171.4 | 4.1 | NA |
| DC-11-B-8R | 288 | 32025 | 1.1 | 19.8224 | 0.7 | 0.1888 | 2.1 | 0.0271 | 2.0 | 0.94 | 172.6 | 3.3 | 175.6 | 3.4 | 215.7 | 16.4 | 172.6 | 3.3 | NA |
| DC-11-B-5C | 421 | 18380 | 0.4 | 19.1712 | 3.7 | 0.1963 | 3.9 | 0.0273 | 1.1 | 0.29 | 173.6 | 1.9 | 182.0 | 6.5 | 292.5 | 85.5 | 173.6 | 1.9 | NA |
| DC-11-B-18C | 144 | 31898 | 1.8 | 19.6476 | 1.5 | 0.1919 | 2.2 | 0.0273 | 1.6 | 0.72 | 173.9 | 2.8 | 178.3 | 3.7 | 236.2 | 35.7 | 173.9 | 2.8 | NA |
| DC-11-B-1C | 158 | 38306 | 1.5 | 19.7403 | 1.0 | 0.1919 | 1.8 | 0.0275 | 1.5 | 0.83 | 174.7 | 2.6 | 178.3 | 2.9 | 225.3 | 22.7 | 174.7 | 2.6 | NA |
| DC-11-B-19R | 398 | 134274 | 0.8 | 20.0942 | 0.9 | 0.1886 | 2.2 | 0.0275 | 2.0 | 0.91 | 174.8 | 3.5 | 175.4 | 3.6 | 184.0 | 21.8 | 174.8 | 3.5 | NA |
| DC-11-B-1R | 355 | 45116 | 1.1 | 19.9255 | 0.9 | 0.1902 | 2.0 | 0.0275 | 1.8 | 0.90 | 174.8 | 3.2 | 176.8 | 3.3 | 203.6 | 21.1 | 174.8 | 3.2 | NA |
| DC-11-B-6R | 331 | 25466 | 0.8 | 20.0123 | 0.6 | 0.1895 | 1.2 | 0.0275 | 1.0 | 0.87 | 174.9 | 1.8 | 176.2 | 1.9 | 193.6 | 13.7 | 174.9 | 1.8 | NA |
| DC-11-B-5R | 495 | 72845 | 0.4 | 19.9591 | 0.7 | 0.1903 | 2.1 | 0.0275 | 1.9 | 0.93 | 175.2 | 3.4 | 176.9 | 3.4 | 199.8 | 17.2 | 175.2 | 3.4 | NA |
| DC-11-B-2C | 412 | 47186 | 1.6 | 19.9188 | 0.8 | 0.1913 | 1.9 | 0.0276 | 1.7 | 0.91 | 175.7 | 3.0 | 177.7 | 3.1 | 204.5 | 18.4 | 175.7 | 3.0 | NA |
| DC-11-B-21R | 227 | 23105 | 1.2 | 20.0137 | 1.4 | 0.1904 | 1.6 | 0.0276 | 0.7 | 0.45 | 175.7 | 1.2 | 177.0 | 2.6 | 193.4 | 32.8 | 175.7 | 1.2 | NA |
| DC-11-B-13C | 280 | 52189 | 1.5 | 19.9275 | 1.3 | 0.1917 | 2.3 | 0.0277 | 1.9 | 0.82 | 176.1 | 3.2 | 178.0 | 3.7 | 203.4 | 29.7 | 176.1 | 3.2 | NA |
| DC-11-B-11C | 540 | 7536 | 1.6 | 15.5966 | 4.4 | 0.2454 | 5.6 | 0.0278 | 3.5 | 0.62 | 176.5 | 6.1 | 222.8 | 11.2 | 745.5 | 93.1 | 176.5 | 6.1 | NA |
| DC-11-B-6C | 446 | 82942 | 0.8 | 20.0304 | 0.8 | 0.1920 | 2.1 | 0.0279 | 1.9 | 0.93 | 177.4 | 3.4 | 178.4 | 3.4 | 191.5 | 18.3 | 177.4 | 3.4 | NA |

| | | | | | | | | | | | | | | | | | | | |
|---|---|---|---|---|---|---|---|---|---|---|---|---|---|---|---|---|---|---|---|
| DC-11-B-20C | 768 | 184141 | 1.0 | 19.7435 | 1.2 | 0.1953 | 1.5 | 0.0280 | 1.0 | 0.65 | 177.8 | 1.8 | 181.1 | 2.6 | 224.9 | 27.0 | 177.8 | 1.8 | NA |
| DC-11-B-9R | 293 | 42457 | 1.8 | 19.9494 | 1.0 | 0.1972 | 2.1 | 0.0285 | 1.8 | 0.87 | 181.3 | 3.2 | 182.7 | 3.4 | 200.9 | 23.3 | 181.3 | 3.2 | NA |
| DC-11-B-17R | 803 | 73041 | 1.6 | 20.1119 | 0.6 | 0.1994 | 2.5 | 0.0291 | 2.4 | 0.97 | 184.8 | 4.4 | 184.6 | 4.2 | 182.0 | 13.9 | 184.8 | 4.4 | NA |
| DC-11-B-13R | 131 | 24185 | 2.5 | 19.8907 | 1.4 | 0.2035 | 1.8 | 0.0294 | 1.1 | 0.62 | 186.5 | 2.1 | 188.1 | 3.1 | 207.7 | 33.1 | 186.5 | 2.1 | NA |
| DC-11-B-20R | 289 | 74540 | 1.8 | 19.8605 | 0.7 | 0.2129 | 2.1 | 0.0307 | 2.0 | 0.95 | 194.7 | 3.9 | 196.0 | 3.8 | 211.2 | 15.5 | 194.7 | 3.9 | NA |
| DC-11-B-10R | 76 | 121859 | 2.1 | 11.2349 | 0.8 | 2.8241 | 1.5 | 0.2301 | 1.3 | 0.86 | 1335.1 | 15.4 | 1362.0 | 11.1 | 1404.3 | 14.4 | 1404.3 | 14.4 | 95.1 |

Table B-2 - U-Pb analysis data for sample DC11B.

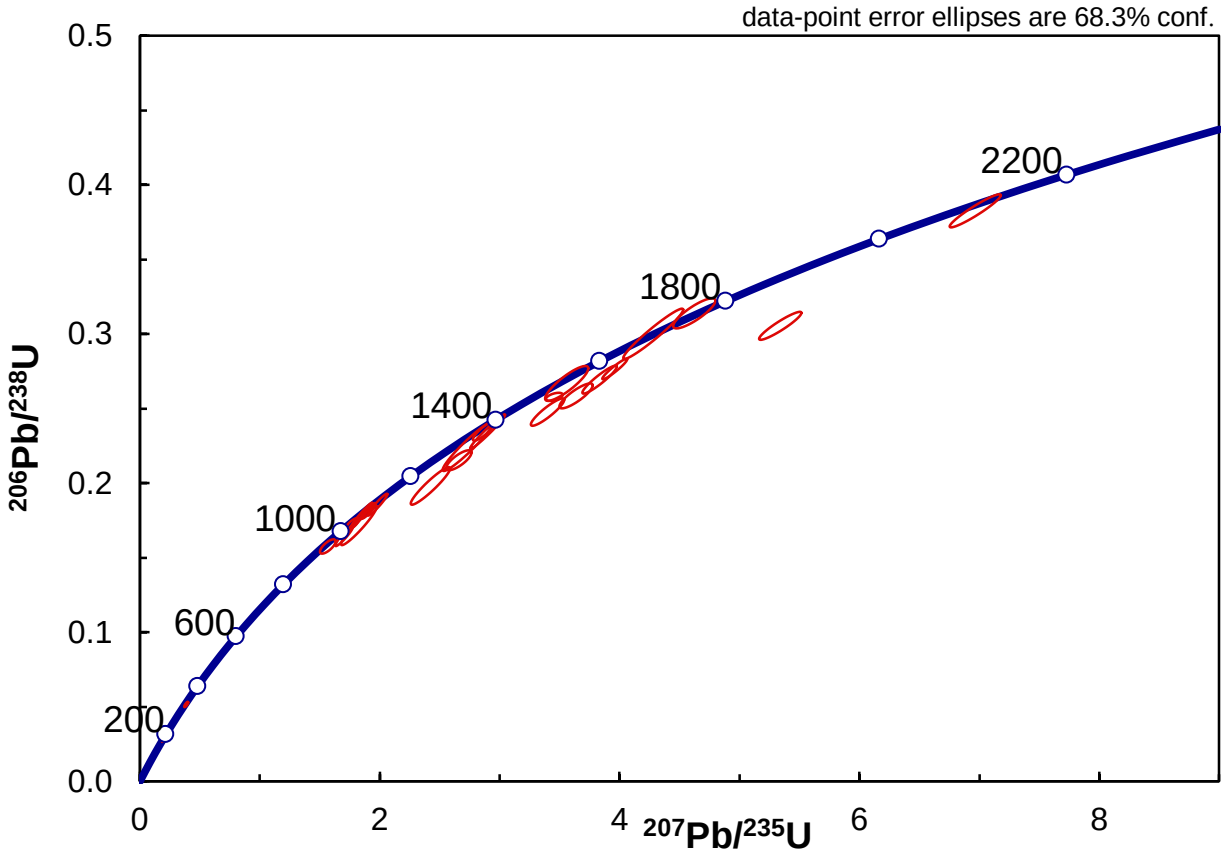


Figure B-9 – Concordia plot for sample DC11C2.

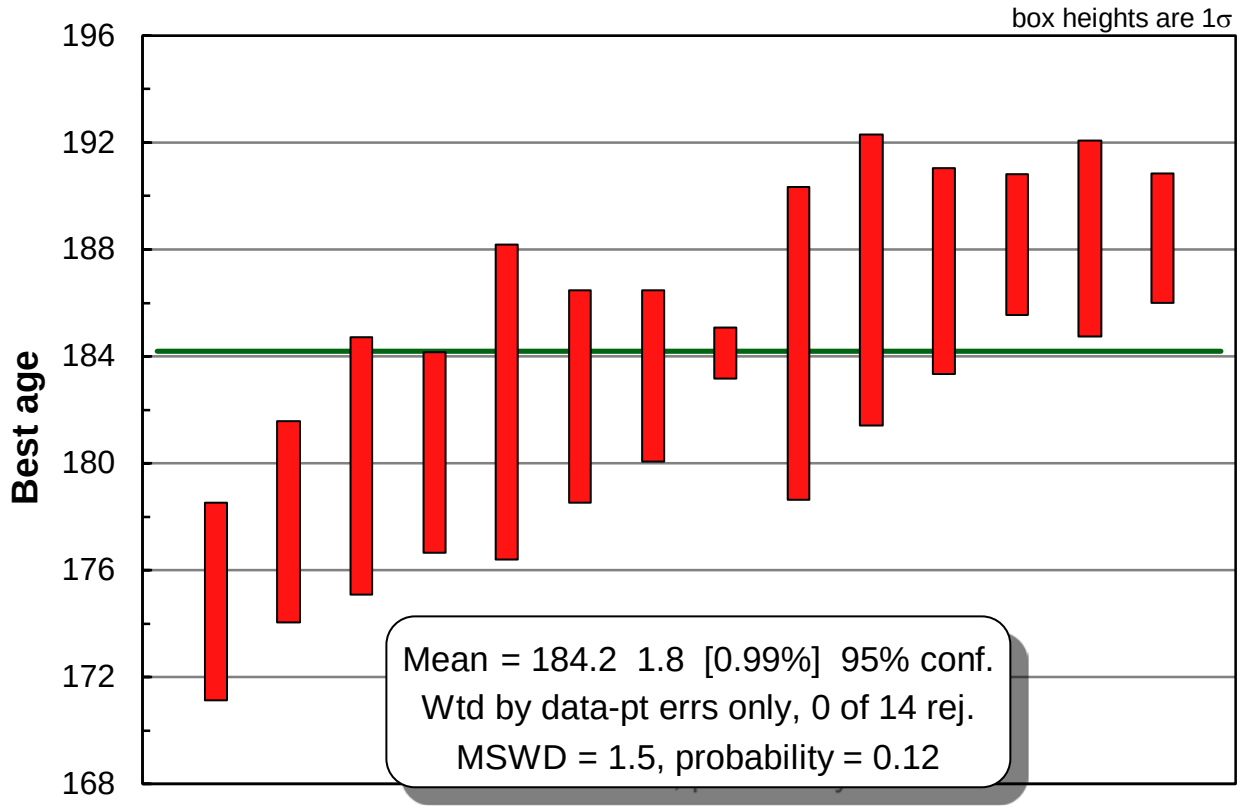


Figure B-10 – Average plot for sample DC11C2.

| Table _____. U-Pb geochronologic analyses. | | | | | | | | | | | | | | | | | | | |
|---|---|---|---|---|---|---|---|---|---|---|---|---|---|---|---|---|---|---|---|
| | | | | | | | Isotope ratios | | | | | | Apparent ages (Ma) | | | | | | |
| Analysis | U | 206Pb | U/Th | 206Pb* | ± | 207Pb* | ± | 206Pb* | ± | error | 206Pb* | ± | 207Pb* | ± | 206Pb* | ± | Best age | ± | Conc |
| | (ppm) | 204Pb | | 207Pb* | (%) | 235U* | (%) | 238U | (%) | corr. | 238U* | (Ma) | 235U | (Ma) | 207Pb* | (Ma) | (Ma) | (Ma) | (%) |
| DC11C2-34R | 347 | 38997 | 3.6 | 19.7172 | 0.8 | 0.1922 | 2.3 | 0.0275 | 2.1 | 0.94 | 174.8 | 3.7 | 178.5 | 3.8 | 228.0 | 18.7 | 174.8 | 3.7 | NA |
| DC11C2-24R | 188 | 21500 | 1.9 | 19.5529 | 1.0 | 0.1972 | 2.4 | 0.0280 | 2.1 | 0.91 | 177.8 | 3.8 | 182.7 | 4.0 | 247.3 | 23.0 | 177.8 | 3.8 | NA |
| DC11C2-16R | 404 | 67644 | 2.3 | 19.6638 | 0.8 | 0.1984 | 2.8 | 0.0283 | 2.7 | 0.96 | 179.9 | 4.8 | 183.8 | 4.8 | 234.3 | 19.0 | 179.9 | 4.8 | NA |
| DC11C2-14R | 293 | 45707 | 10.0 | 19.4216 | 1.2 | 0.2015 | 2.4 | 0.0284 | 2.1 | 0.87 | 180.4 | 3.8 | 186.4 | 4.1 | 262.8 | 27.3 | 180.4 | 3.8 | NA |
| DC11C2-29R | 336 | 37224 | 2.1 | 19.7461 | 1.6 | 0.2003 | 3.6 | 0.0287 | 3.3 | 0.90 | 182.3 | 5.9 | 185.4 | 6.2 | 224.6 | 36.6 | 182.3 | 5.9 | NA |
| DC11C2-15R | 386 | 35849 | 2.4 | 19.3795 | 1.2 | 0.2043 | 2.5 | 0.0287 | 2.2 | 0.88 | 182.5 | 4.0 | 188.8 | 4.3 | 267.7 | 26.9 | 182.5 | 4.0 | NA |
| 11DC11C2-6C | 166 | 16530 | 2.0 | 19.6722 | 1.7 | 0.2021 | 2.4 | 0.0288 | 1.8 | 0.73 | 183.3 | 3.2 | 186.9 | 4.1 | 233.3 | 38.2 | 183.3 | 3.2 | NA |
| DC11C2-11R | 699 | 121807 | 1.5 | 19.8345 | 0.7 | 0.2014 | 0.9 | 0.0290 | 0.5 | 0.62 | 184.1 | 1.0 | 186.3 | 1.5 | 214.3 | 15.6 | 184.1 | 1.0 | NA |
| DC11C2-11C | 379 | 44406 | 1.0 | 19.7692 | 0.8 | 0.2025 | 3.3 | 0.0290 | 3.2 | 0.97 | 184.5 | 5.9 | 187.2 | 5.7 | 221.9 | 19.2 | 184.5 | 5.9 | NA |
| DC11C2-27R | 345 | 49298 | 4.2 | 19.6194 | 0.8 | 0.2067 | 3.1 | 0.0294 | 3.0 | 0.96 | 186.9 | 5.5 | 190.8 | 5.3 | 239.5 | 18.7 | 186.9 | 5.5 | NA |
| 11DC11C2-6R | 394 | 68855 | 2.9 | 19.4542 | 0.6 | 0.2088 | 2.2 | 0.0295 | 2.1 | 0.96 | 187.2 | 3.9 | 192.6 | 3.8 | 258.9 | 14.5 | 187.2 | 3.9 | NA |
| 11DC11C2-2C | 93 | 11336 | 1.1 | 18.1509 | 6.6 | 0.2250 | 6.8 | 0.0296 | 1.4 | 0.21 | 188.2 | 2.6 | 206.1 | 12.7 | 416.0 | 148.4 | 188.2 | 2.6 | NA |
| DC11C2-12R | 260 | 23441 | 2.6 | 19.6875 | 1.2 | 0.2077 | 2.3 | 0.0297 | 2.0 | 0.86 | 188.4 | 3.7 | 191.6 | 4.0 | 231.4 | 27.4 | 188.4 | 3.7 | NA |
| 11DC11C2-2R | 662 | 141908 | 2.1 | 20.0278 | 0.8 | 0.2042 | 1.5 | 0.0297 | 1.3 | 0.86 | 188.4 | 2.4 | 188.7 | 2.6 | 191.8 | 17.8 | 188.4 | 2.4 | NA |
| 11DC11C2-1R | 226 | 31994 | 5.7 | 20.1536 | 1.2 | 0.2128 | 1.5 | 0.0311 | 1.0 | 0.65 | 197.4 | 1.9 | 195.9 | 2.7 | 177.2 | 26.9 | 197.4 | 1.9 | NA |
| DC11C2-19R | 224 | 62009 | 1.6 | 18.4437 | 1.6 | 0.3863 | 2.8 | 0.0517 | 2.3 | 0.82 | 324.7 | 7.2 | 331.6 | 7.8 | 380.1 | 35.8 | 324.7 | 7.2 | NA |
| DC11C2-19R2 | 221 | 75363 | 1.5 | 18.2925 | 0.9 | 0.3905 | 1.8 | 0.0518 | 1.6 | 0.87 | 325.6 | 5.1 | 334.8 | 5.2 | 398.6 | 20.3 | 325.6 | 5.1 | NA |
| DC11C2-26R | 367 | 45834 | 8.2 | 18.3822 | 0.6 | 0.4690 | 1.1 | 0.0625 | 0.9 | 0.81 | 391.0 | 3.3 | 390.5 | 3.5 | 387.6 | 14.0 | 391.0 | 3.3 | NA |
| DC11C2-22R | 129 | 22640 | 1.2 | 17.9256 | 1.1 | 0.4917 | 2.0 | 0.0639 | 1.7 | 0.85 | 399.4 | 6.7 | 406.1 | 6.8 | 443.8 | 24.0 | 399.4 | 6.7 | NA |
| DC11C2-28R | 404 | 165194 | 25.8 | 13.8623 | 1.9 | 1.5674 | 2.8 | 0.1576 | 2.0 | 0.73 | 943.3 | 17.6 | 957.4 | 17.1 | 989.8 | 38.2 | 989.8 | 38.2 | 95.3 |
| DC11C2-32R | 221 | 168850 | 3.2 | 13.4331 | 1.3 | 1.7716 | 2.0 | 0.1726 | 1.5 | 0.76 | 1026.4 | 14.5 | 1035.1 | 13.1 | 1053.5 | 26.6 | 1053.5 | 26.6 | 97.4 |
| DC11C2-35R | 231 | 205323 | 9.8 | 13.3168 | 1.0 | 1.7039 | 2.9 | 0.1646 | 2.7 | 0.94 | 982.1 | 24.5 | 1010.0 | 18.4 | 1071.0 | 19.8 | 1071.0 | 19.8 | 91.7 |
| 11DC11C2-3 | 84 | 101866 | 1.8 | 13.3128 | 0.8 | 1.8453 | 3.3 | 0.1782 | 3.2 | 0.97 | 1057.0 | 31.7 | 1061.7 | 22.0 | 1071.6 | 15.6 | 1071.6 | 15.6 | 98.6 |
| DC11C2-13R | 100 | 70671 | 1.8 | 13.1340 | 0.9 | 1.9043 | 2.1 | 0.1814 | 1.9 | 0.90 | 1074.6 | 19.0 | 1082.6 | 14.3 | 1098.7 | 19.0 | 1098.7 | 19.0 | 97.8 |
| DC11C2-25R | 95 | 72835 | 3.7 | 12.9661 | 1.8 | 1.8266 | 5.4 | 0.1718 | 5.1 | 0.95 | 1021.9 | 48.2 | 1055.1 | 35.4 | 1124.4 | 35.1 | 1124.4 | 35.1 | 90.9 |
| DC11C2-20R | 260 | 132614 | 6.2 | 12.9099 | 0.8 | 1.9824 | 2.7 | 0.1856 | 2.6 | 0.96 | 1097.6 | 26.3 | 1109.5 | 18.4 | 1133.1 | 15.8 | 1133.1 | 15.8 | 96.9 |
| DC11C2-31R | 315 | 297317 | 4.8 | 11.3270 | 1.5 | 2.7336 | 5.0 | 0.2246 | 4.8 | 0.95 | 1306.0 | 56.9 | 1337.6 | 37.5 | 1388.7 | 28.7 | 1388.7 | 28.7 | 94.0 |
| 11DC11C2-9C | 157 | 266723 | 1.6 | 11.2958 | 1.0 | 2.8663 | 2.1 | 0.2348 | 1.8 | 0.87 | 1359.7 | 22.0 | 1373.1 | 15.5 | 1394.0 | 19.2 | 1394.0 | 19.2 | 97.5 |
| 11DC11C2-1C | 645 | 1135357 | 9.4 | 11.2757 | 1.6 | 2.4233 | 4.5 | 0.1982 | 4.2 | 0.94 | 1165.5 | 44.7 | 1249.5 | 32.2 | 1397.4 | 30.0 | 1397.4 | 30.0 | 83.4 |
| 11DC11C2-5R | 507 | 449596 | 41.2 | 11.1639 | 1.6 | 2.6601 | 2.6 | 0.2154 | 2.0 | 0.78 | 1257.4 | 23.4 | 1317.5 | 19.3 | 1416.5 | 31.3 | 1416.5 | 31.3 | 88.8 |

| | | | | | | | | | | | | | | | | | | | |
|---|---|---|---|---|---|---|---|---|---|---|---|---|---|---|---|---|---|---|---|
| DC11C2-30R | 154 | 110250 | 7.0 | 11.1550 | 0.7 | 2.8996 | 3.3 | 0.2346 | 3.2 | 0.98 | 1358.5 | 39.6 | 1381.8 | 25.0 | 1418.0 | 13.8 | 1418.0 | 13.8 | 95.8 |
| DC11C2-17R | 547 | 582817 | 6.1 | 10.3388 | 1.7 | 3.5592 | 3.3 | 0.2669 | 2.9 | 0.87 | 1525.0 | 39.3 | 1540.5 | 26.5 | 1561.8 | 31.3 | 1561.8 | 31.3 | 97.6 |
| 11DC11C2-7C | 99 | 127779 | 1.9 | 10.2881 | 1.1 | 3.4562 | 1.3 | 0.2579 | 0.7 | 0.52 | 1479.0 | 9.1 | 1517.3 | 10.5 | 1571.0 | 21.4 | 1571.0 | 21.4 | 94.1 |
| 11DC11C2-10C | 262 | 643068 | 81.1 | 10.0445 | 1.2 | 3.3997 | 2.7 | 0.2477 | 2.4 | 0.90 | 1426.4 | 31.2 | 1504.3 | 21.2 | 1615.8 | 21.6 | 1615.8 | 21.6 | 88.3 |
| 11DC11C2-7R | 540 | 595198 | 2.3 | 9.7997 | 1.3 | 3.6375 | 2.5 | 0.2585 | 2.1 | 0.85 | 1482.3 | 28.2 | 1557.8 | 20.1 | 1661.6 | 24.8 | 1661.6 | 24.8 | 89.2 |
| DC11C2-33R | 137 | 193620 | 3.3 | 9.6913 | 0.9 | 3.8335 | 2.5 | 0.2695 | 2.3 | 0.93 | 1538.0 | 31.5 | 1599.8 | 19.9 | 1682.2 | 16.8 | 1682.2 | 16.8 | 91.4 |
| 11DC11C2-5C | 126 | 280526 | 2.1 | 9.6674 | 1.1 | 4.2809 | 3.9 | 0.3002 | 3.7 | 0.96 | 1692.1 | 55.2 | 1689.7 | 31.8 | 1686.7 | 19.5 | 1686.7 | 19.5 | 100.3 |
| DC11C2-21R | 87 | 59392 | 2.3 | 9.6292 | 0.6 | 3.9597 | 1.7 | 0.2765 | 1.6 | 0.95 | 1573.9 | 22.9 | 1626.0 | 14.0 | 1694.0 | 10.2 | 1694.0 | 10.2 | 92.9 |
| 11DC11C2-4 | 163 | 443415 | 3.3 | 9.3605 | 1.3 | 4.6232 | 2.5 | 0.3139 | 2.1 | 0.84 | 1759.7 | 32.7 | 1753.5 | 21.0 | 1746.0 | 24.7 | 1746.0 | 24.7 | 100.8 |
| DC11C2-23R | 61 | 86174 | 1.5 | 7.8880 | 0.8 | 5.3401 | 2.2 | 0.3055 | 2.0 | 0.93 | 1718.5 | 30.6 | 1875.3 | 18.7 | 2053.7 | 14.4 | 2053.7 | 14.4 | 83.7 |
| DC11C2-18R | 67 | 121932 | 2.5 | 7.5730 | 0.7 | 6.9659 | 2.0 | 0.3826 | 1.9 | 0.95 | 2088.4 | 34.1 | 2107.1 | 18.0 | 2125.4 | 11.6 | 2125.4 | 11.6 | 98.3 |

Table B-3 - U-Pb analysis data for sample DC11C2.

# Geology of the Western Park of the Date Creek Mountains, Yavapai County, Arizona

by David L. Eddy

**Plate 1**

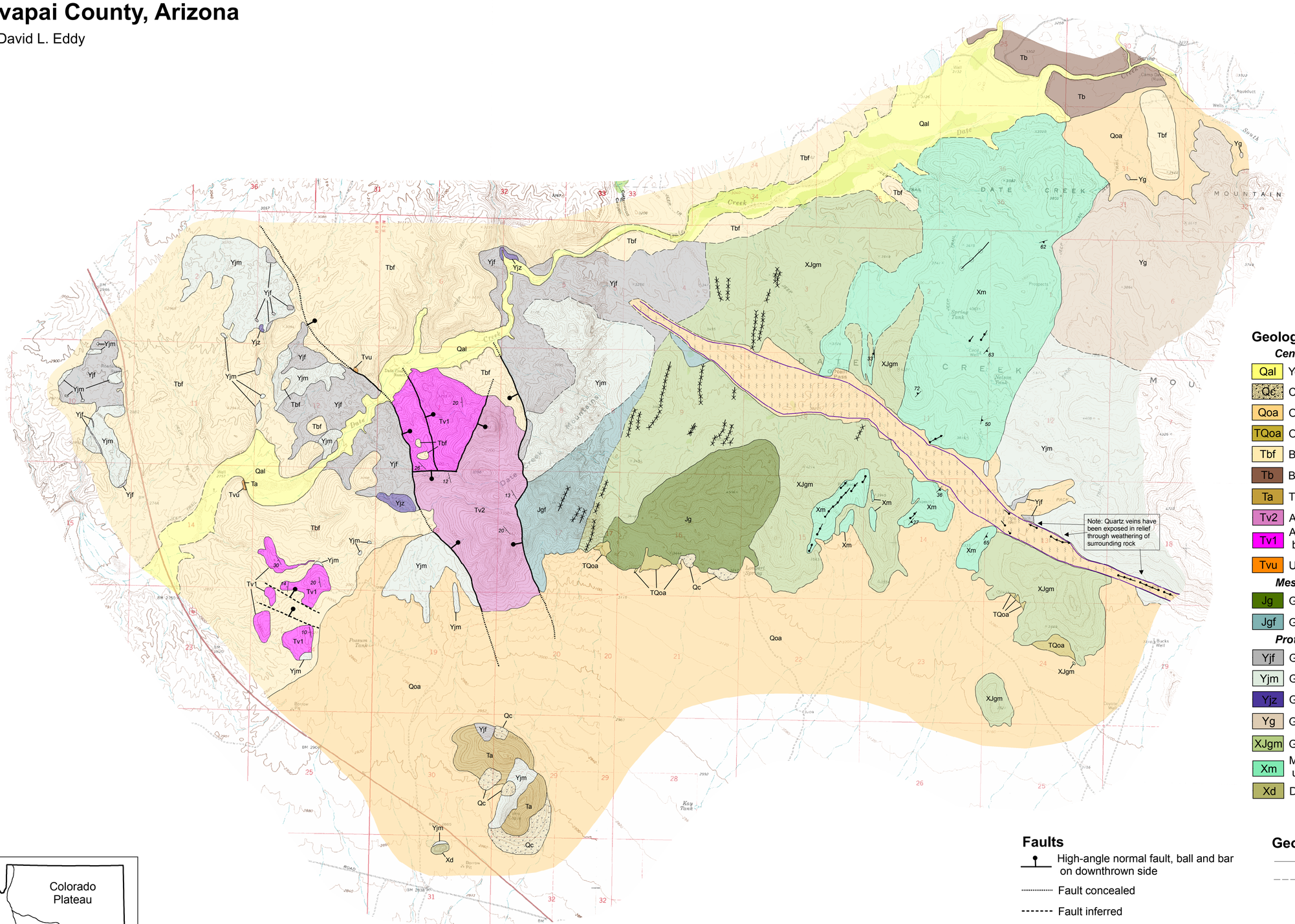


## Geologic Map Units

***Cenozoic***

- Qal — Young alluvium in active fluvial environments
- Qc — Colluvium
- Qoa — Older alluvium
- TQoa — Older moderately indurated alluvium
- Tbf — Basin fill
- Tb — Basalt flows
- Ta — Trachyandesitic to basaltic lava flows
- Tv2 — Ash-fall tuff, andesitic to basaltic lava flows
- Tv1 — Ash-fall tuff, vitrophyre, welded tuff, and basaltic lava flows
- Tvu — Undifferentiated volcanics

***Mesozoic***

- Jg — Granite, medium grained
- Jgf — Granite, fine-grained

***Proterozoic***

- Yjf — Granite of Joshua Tree Parkway, fine-grained
- Yjm — Granite of Joshua Tree Parkway, megacrystic
- Yjz — Granite of Joshua Tree Parkway, mafic
- Yg — Granite, medium-grained, porphyritic
- XJgm — Granite, megacrystic (may be Jurassic)
- Xm — Metasedimentary and metavolcanic rocks undifferentiated
- Xd — Diorite

## Faults

- High-angle normal fault, ball and bar on downthrown side
- Fault concealed
- Fault inferred
- Fault zone

## Bedding & Foliation

- 33 — Strike and dip of foliation
- 33 — Strike and dip of bedding

## Geologic Contacts

- Contact
- Contact approximate

## Dikes and Veins

- Felsic dike
- Pegmatite dike
- Massive quartz vein

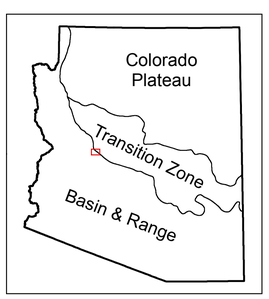


SCALE 1:24,000

1 0.5 0 1 Mile

1 0.5 0 1 Kilometer

2012